Bioorganic Chemistry 156 (2025) 108155

Contents lists available at ScienceDirect

Bioorganic Chemistry

journal homepage: www.elsevier.com/locate/bioorg

Design, synthesis, *in-vitro* and *in-silico* studies of novel *N*-heterocycle based hydrazones as α-glucosidase inhibitors

Rehmatullah Farooqi [a,b], Saeed Ullah [c], Ajmal Khan [c,i], Shailesh S. Gurav [d], Suraj N. Mali [e], Hina Aftab [a], Mohammad Khalid Al-Sadoon [f], Ming-Hua Hsu [b], Parham Taslimi [g], Ahmed Al-Harrasi [c,*], Zahid Shafiq [a,*], Silvia Schenone [h,*]

[a] Institute of Chemical Sciences, Bahauddin Zakariya University, Multan 60800 Pakistan
[b] National Changhua University of Education, Changhua 50007 Taiwan
[c] Natural and Medical Sciences Research Centre, University of Nizwa, P.O. Box 33, PC 616, Birkat Al Mauz, Nizwa, Oman
[d] Department of Chemistry, VIVA College, Virar (W)-401303, Maharashtra, India
[e] School of Pharmacy, DY Patil Deemed to Be University, Navi Mumbai, India
[f] Department of Zoology, College of Science, King Saud University, PO Box 2455, Riyadh 11451, Saudi Arabia
[g] Department of Biotechnology, Faculty of Science, Bartin University, 74110 Bartin, Turkey
[h] Department of Pharmacy, University of Genoa, Viale Benedetto XV, 3, Genoa 16132, Italy
[i] Department of Chemical and Biological Engineering, College of Engineering, Korea University, 145 Anam-ro, Seongbuk-gu, Seoul 02841, Republic of Korea

ARTICLE INFO

Keywords:
Hydrazones
α-Glucosidase
α-Amylase
Diabetes mellitus
Molecular docking
QSAR

ABSTRACT

Diabetes mellitus has dominated the globe as a chronic health condition and has become a major global health concern. The inhibition of the key metabolic enzymes of carbohydrates digestion including α-amylase and α-glucosidase are the promising targets for the treatment of diabetes *via* delaying glucose absorption. Therefore, nitrogen containing saturated heterocycle (pyrrolidinyl, piperidinyl and *N*-methylpiperazinyl) based hydrazones derivatives **5**–**23** were synthesized through two step reactions and evaluated for their anti-diabetic potential. All compounds exhibited potent α-glucosidase inhibitory capability ranging (IC_{50} = 10.26–47.35 μM), as compared to acarbose (IC_{50} = 871.40 ± 1.24 μM). Interestingly these derivatives also exhibited significant inhibitory capability against α-amylase with IC_{50} values in the range 25.81–76.05 μM. Mechanistic study on the most potent compound indicated a competitive type of inhibition with a K_i value of 8.30 ± 0.0076 μM. Molecular docking was performed to predict binding interactions between receptor proteins and moiety. In QSAR analysis, through use of QSARINS different 1D and 2D descriptors were used to generate different models that enabled further identification of structural requirements that contributed to activity. pIC_{50} values were also predicted by QSAR model. Furthermore, *in-silico* ADMET and BOILED-egg model analysis showed that all analogues exhibited passive GI absorption, and all showed BBB penetration.

1. Introduction

Diabetes mellitus (DM), a disorder that imposes serious complications to human health (*viz.* coronary micro and macro vascular diseases, diabetic nephropathy, retinopathy) and is one of the most prevailing ailments around the globe [1]. A latest report issued by IDF (International Diabetes Federation) states that, by 2045, about 700 million people are expected to be affected from diabetes [2]. Irregularities in insulin's action and secretion raises blood sugar level which, basically, is the root cause of DM that has a few categories of which type-II Diabetes Mellitus (TIIDM) accounts for 75–85 % of diabetic cases [3].

The concentration of glucose in blood is very critical for DM and must be maintained within 70–100 mg/dl [4]. An enzyme, named, α-glucosidase (EC3.2.1.20) discovered in lining of intestinal tract (brush borders), causes the lysis of non-absorbable carbohydrates to absorbable α-D-glucose that gets into blood stream and hence raising postprandial blood glucose level resulting in the origin of DM [5]. Thus, one of the most effective and recent approaches, very fascinating approach for pharmaceutical industries indeed that combats many diseases including diabetics, hepatitis, viral infections and cancers [6–8], is hampering of

* Corresponding authors.
E-mail addresses: aharrasi@unizwa.edu.om (A. Al-Harrasi), zahidshafiq@bzu.edu.pk (Z. Shafiq), silvia.schenone@unige.it (S. Schenone).

https://doi.org/10.1016/j.bioorg.2025.108155
Received 17 September 2024; Received in revised form 4 January 2025; Accepted 8 January 2025
Available online 10 January 2025

α-glucosidase that manages levels of postprandial glucose and represses post-prandial hyperglycemia [9,10].

During the metabolism of glycoproteins, α-glucosidase plays a vital role. This enzyme, part of the hydrolase family, is found in the gut. As a result, α-glucosidase inhibitors have various therapeutic applications, including in the treatment of diabetes, metastatic cancer, AIDS, antimicrobial infections, and lysosomal storage disorders.

α-amylase is a calcium-dependent metalloenzyme that facilitates digestion by breaking down polysaccharides into smaller molecules, such as glucose and maltose. Furthermore, the enzyme contributes to postprandial hyperglycemia, leading to elevated blood glucose levels. As a result, inhibition of α-amylase is a recognized therapeutic target for managing and controlling postprandial blood glucose. Inhibitors of α-amylase and α-glucosidase have been demonstrated to slow the breakdown of starch and oligosaccharides, thereby delaying glucose absorption and reducing postprandial blood glucose levels [11–13].

Inhibitors of α-glucosidase lowers plasma glucose level by reversibly and competitively inhibiting abdominal α-glucosidase and hence impeding secretion of glucose from non-absorbable carbohydrates and complex starch. This whole mode of action is an insulin independent hypoglycemic action of α-glucosidase inhibitors and is safer, potent and non-toxic [14,15]. Acarbose, nojirimycin, castanospermine, emiglitate, and voglibose are some carbohydrate mimics that are extensively being used clinically to control blood glucose level in diabetic patients [15–19]. Due to a number of side effects associated with these inhibitors (for instance, meteorism, diarrhea and abdominal distension) and absorptivity complications [20], medicinal chemists across the globe are targeting to design & synthesize new potent, safer and effective non-glycosidic based α-glucosidase inhibitors [21,22].

On top of that, eradication of monosaccharides from viral glycoproteins is also one of the jobs of α-glucosidase, consequently, virus identification by cells and alteration of cell to cell signals could be the role of its inhibitors that leads to its use as medication for cancer and viral diseases [23,24]. Saturated heterocyclic compounds, which contain one heteroatom in their ring structure, are found in several crucial biomolecules such as heme, chlorophyll and nucleotides, highlighting their importance and effectiveness [25]. The heterocyclic core is a key structural element in many widely used drugs for anti-Alzheimer's disease, cancer and anti-human immunodeficiency virus (HIV) [26–28]. These compounds have also provided a foundation for creating new and effective lead compounds and biologically active drugs across various fields [29].

Nitrogen(s) containing saturated heterocycles like pyrrolidine, piperidine and piperazine are important pharmacophores in numerous pharmaceutically active drugs and exhibit a number of biological activities. For instance, *N*-methylmicrocosamine B **I** [30], *α*-methylene-*γ*-lactam **II** [31], *α*-1-C-butyl-LAB **II** [32], and benzimidazole derivative **III** [33] having piperidine, pyrrolidine and piperazine rings, respectively, possessed considerable *α*-glucosidase inhibition (Fig. 1). Furthermore, these moieties add up to advantages of drug design due to unconstrained ring conformation that can be locked and tuned with different substituents [34] and on incorporation into hybrid molecular structures, they show remarkable pharmacological properties. Due to these reasons, medicinal chemists intend to study these heterocycles as lead molecules for the treatment of different ailments.

The scaffolds that can be prepared through non-toxic promoters/catalysts and simple synthetic routes are highly regarded in medicinal chemistry. Synthesis of hydrazones fulfils the aforementioned criterion. Hydrazones, due to azomethine functionality, exhibit a number of biological activities, for instance, antiviral [35], antitumor [36], antimicrobial [37] and antioxidant [38]. Previously, phenyl acetohydrazide **IV**, benzene sulfonamide **V**, thiadiazole based hydrazone **VI**, dichloro benzo hydrazide **VII** and flavone hydrazone **VIII** (having azomethine functionality) possessed *α*-glucosidase inhibitory activity [39,4,40–42] (Fig. 1). In our previous work, various series of hydrazones as potential α-glucosidase inhibitors were synthesized [40,41,43,44]. But synthesis

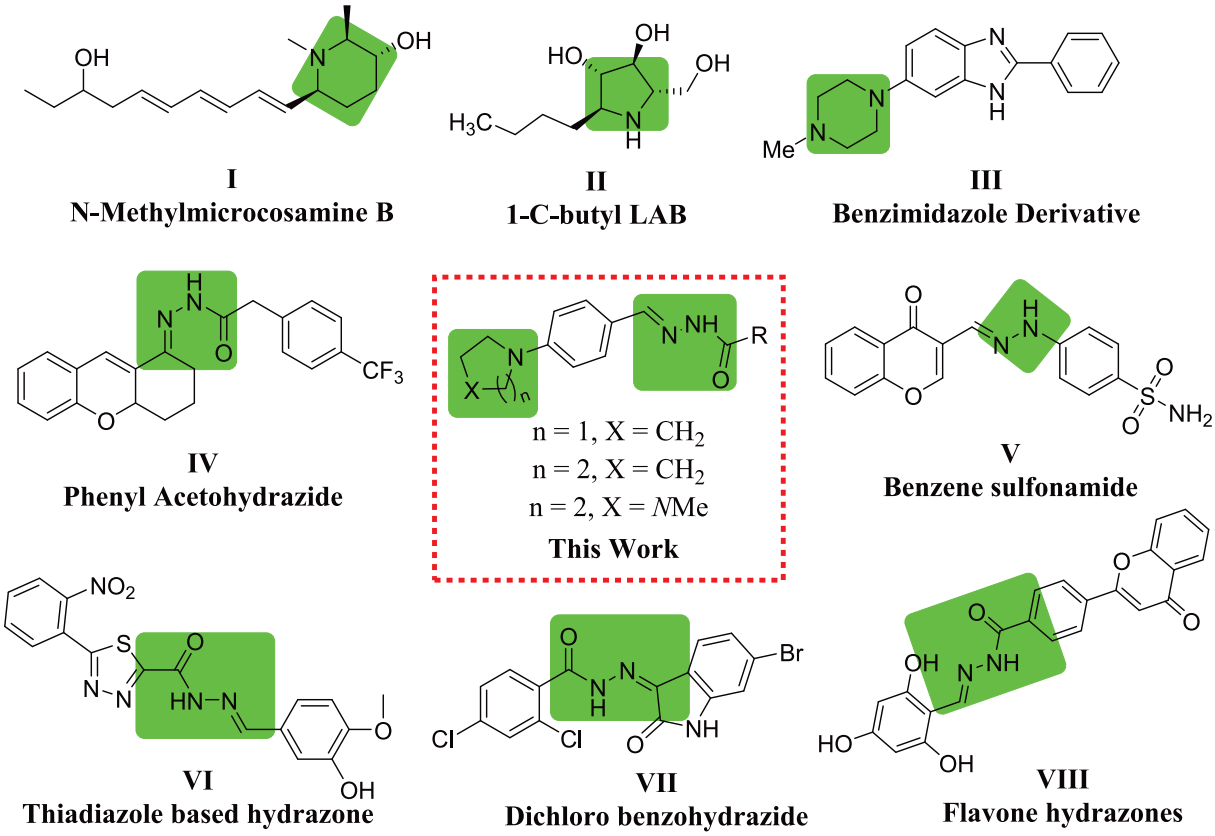

Fig. 1. *N*-Heterocycle and hydrazone based *α*-glucosidase inhibitors [4,30,32,33,39–42] and our approach.

of 5 and 6 membered nitrogen(s) containing saturated heterocyclic based-hydrazones and their pharmaceutical application as α-glucosidase inhibitors have not been reported till date. Hybridization is an emerging concept in drug discovery that has recently garnered significant attention in the scientific community as a strategy to overcome serious drug resistance [45]. Building on the results mentioned above and our ongoing efforts, we aim to synthesize a heterocyclic nucleus with high biological relevance that incorporates a hybrid structure [46]. In our current work, molecular hybridization approach is being used that furnishes new hybrid molecules that are very crucial α-glucosidase and α-amylase inhibitors. *In-vitro & In-silico* studies of compounds **5**–**23** were conducted as well.

2. Result and discussion

2.1. Chemistry

The title derivatives were generated by route as depicted in Scheme 1. The pyrrolidinyl, piperidinyl, *N*-methylpiperazinyl based novel hydrazones **5**–**23 (Table-1)** were formed through reaction of benzaldehydes substituted at *p*-position with (1-pyrrolidinyl) **3a**, (1-piperidinyl) **3b**, and (4-methylpiperazin-1-yl) **3c** with various hydrazides **4a-k** promoted by AcOH, a single step acid-catalyzed reaction, giving the corresponding products **5**–**23** in moderate to excellent (60–93 %) yields. Aldehydes **3a-c**, vital precursors for formation of target derivatives **5**–**23**, were generated through a single step reaction as well, as reported by Baseer and co-workers [47,48]. At the very beginning, nitrogen containing bases, i.e. pyrrolidine, piperidine, and *N*-methyl piperazine **2a-c** undergo nucleophilic aromatic substitution reaction (S_NAr) with 4-fluorobenzaldehyde **1** using K_2CO_3 in DMF to give aldehydes **3a-c** in 70–80 % yields. The structures of respective novel products **5**–**23** were established through various characterization techniques i.e. FT-IR, ^{1}H NMR, ^{13}C NMR and HRMS. (See Scheme 2).

In the IR spectra, C═O vibrational stretching of hydrazine-hydrazone moiety appeared between 1640–1672 cm^{-1}, while the narrow N − H band was observed in the range of 3227 to 3468 cm^{-1}, both characteristic of hydrazones. Additionally, a broad –OH band from naphthol derivatives appeared at 3420–34270 cm^{-1}, and the Ar-H stretch along with overtones of the phenyl rings were noted between 1800–2000 cm^{-1}.

In the ^{1}H NMR spectra of compounds **5**–**12**, the protons of pyrrolidinyl ring resonated between δ_H 1.93 and 3.4 ppm, with triplet for the $2CH_2$ near to nitrogen appearing downfield, while the other triplet for $2CH_2$ farther from nitrogen appeared upfield. For compounds **13**–**18**, multiplets for the piperidinyl ring protons resonated from δ_H 1.51 to 3.29 ppm, with the peak for $3CH_2$ near the nitrogen appeared upfield, and the peak of $2CH_2$ away from nitrogen appearing downfield. In the ^{1}H NMR spectra for compounds **19**–**23**, the singlet of *N*-methyl group was observed at δ_H 2.18–2.2 ppm, and the 8H of *N*-methyl piperazinyl ring resonated in the range of δ_H 2.39–3.29 ppm. The phenyl protons of each derivative resonated in aromatic region (δ_H 6.5 to 8.0 ppm) as doublets and multiplets. For compounds **5**,**8**,**9**,**14**,**15**,**20**,**23**, double sets of resonances for NH-CO were attributed to amide-iminol tautomerism, with singlets appearing in the range δ 11.06–11.60 ppm, and the methine (CH=N-) proton resonated from δ 7.83 to 8.28 ppm. Based on the double signal splitting, it is concluded that a mixture of E/Z isomers of hydrazones may have formed in the DMSO-d_6 solution due to restricted rotation around amide bond. The resonance for NH protons of the Z-isomers appear downfield relative to same protons' signals in the E-isomers [49,50].

In the ^{13}C NMR spectra of compounds **5**–**12**, signals appeared from δ 25.40 to 47.69 ppm, confirming the presence of pyrrolidine ring. In compounds **13**–**18**, three signals for the piperidinyl ring were found in the range of δ 24.38 − 48.81 ppm, while in compounds **19**–**23**, C-13 peak was noted at δ 54.82 ppm. Moreover, the imine carbon signal (NH − N = C) in ^{13}C NMR above δ 155 ppm also confirms its presence. High-resolution Mass Spectrometry (HRMS, ESI +) further validated that the molecular ion peaks of each derivative matched the calculated molecular weights.

2.2. In-vitro α-glucosidase and α-amylase inhibitory evaluation

To assess the medicinal use of synthesized compounds, all the compounds **5**–**23** were subjected to the *in-vitro* inhibitory assay of α-glucosidase and α-amylase. Interestingly, inhibitory activities of **5**–**23** derivatives were found to be in the range 10.26 ± 0.17–47.35 ± 1.24μ M, relative to standard acarbose (IC_{50} = 871.40 ± 1.24μ M) (Table 1). The inhibitory capability of these compounds against α-amylase was also impressive ranging from 25.81 − 76.05μ M. The most potent derivatives among the series are compounds **6** (IC_{50} = 10.26 ± 0.17μ M), **20** (IC_{50} = 12.10 ± 0.15μ M), **13** (IC_{50} = 13.25 ± 0.27μ M) and **11** (IC_{50} = 14.25 ± 0.30μ M), while other derivatives showed slight variations in their potency through strong or weak interactions due to different substituents (**Table-1**). The same derivatives **6**, **20**, **13** and **11** exhibited good inhibitory capability against α-amylase with IC_{50} values of 66.91 ± 3.42, 25.81 ± 2.48, 45.77 ± 3.83 and 51.98 ± 6.78μ M, respectively. Generally, electron poor substituents on benzene ring increased the potency of derivatives while the opposite is true for electron rich substituents. For instance, compound **9** with *o*-trifluoromethyl group on benzyl ring is more potent (IC_{50} = 17.49 ± 0.26μ M) relative to compound **5** having no substituent on benzyl ring. Interestingly, compound **9** also exhibited significant inhibitory effect against α-amylase (IC_{50} = 28.02 ± 3.08 μM). Likewise, compound **13** with *m*-chloro substituent showed greater activity than compound **7** with *p*-methoxy substituent. Compound **7** was found to be inactive against α-amylase and compound **13** exhibited weak inhibition. Compound **6** also exhibited a decrease in the anti α-amylase activity (IC_{50} = 66.91 ± 3.42 μM). On the contrary, compound **5** displayed a slight increase in the α-amylase inhibitory activity (IC_{50} = 58.02 ± 6.24 μM), as compared to compound **6**. The similar pattern of inhibitory capability was followed by compounds **8**, **9** against α-amylase and exhibited further increase in the α-amylase inhibition with IC_{50} values 31.88 ± 4.60 and 28.02 ± 3.08 μM respectively. Compounds **10** and **11** exhibited the opposite inhibitory effect against α-amylase with IC_{50} values 56.92 ± 4.57 and 51.98 ± 6.78 μM, respectively. Compounds **13**–**15** displayed favorable effect of the

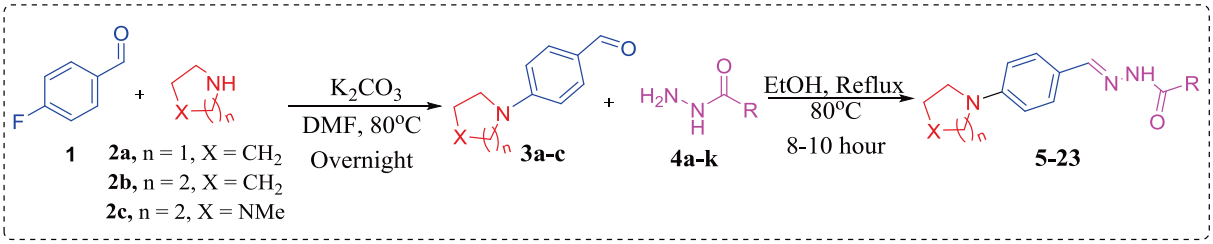

Scheme 1. Synthetic route to novel hydrazones **5**–**23.**

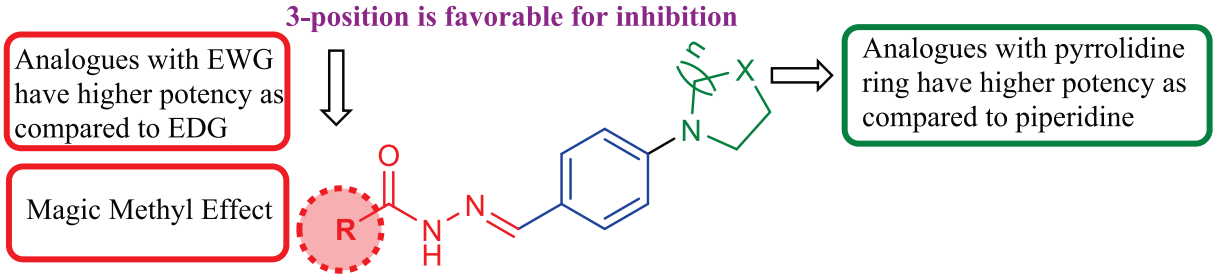

Scheme 2. Pictorial presentation of SAR.

Table 1
Structures of derivatives **5**–**23** and their *in-vitro* *α*-glucosidase and α-amylase inhibition values.

Code	n	X	R	Yield (%)	*α*-glucosidase		*α*-amylase	
					% Inhibition (0.5 mM)	IC_{50} (μM ± SEM*)	% Inhibition (0.5 mM)	IC_{50} (μM ± SEM*)
5	1	CH_2	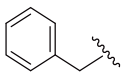	75	84.59	30.51 ± 0.57	59.21	58.02 ± 6.24
6	1	CH_2	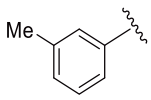	70	90.50	10.26 ± 0.17	52.04	66.91 ± 3.42
7	1	CH_2	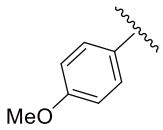	75	86.96	27.44 ± 0.53	14.08	> 100
8	1	CH_2	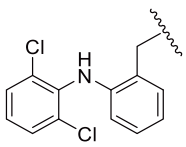	93	87.51	36.11 ± 0.67	73.27	31.88 ± 4.60
9	1	CH_2	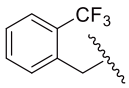	62	88.57	21.70 ± 0.39	77.36	28.02 ± 3.08
10	1	CH_2	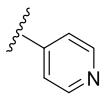	65	80.42	47.35 ± 1.24	60.01	56.92 ± 4.57
11	1	CH_2	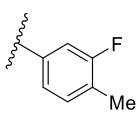	69	90	14.25 ± 0.30	63.36	51.98 ± 6.78

(*continued on next page*)

Table 1 (*continued*)

Code	n	X	R	Yield (%)	α-glucosidase		α-amylase	
					% Inhibition (0.5 mM)	IC_{50} (μM ± SEM*)	% Inhibition (0.5 mM)	IC_{50} (μM ± SEM*)
12	1	CH_2	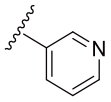	65	78.49	42.67 ± 1.36	21.07	> 100
13	2	CH_2	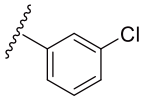	60	90.73	13.25 ± 0.27	66.84	45.77 ± 3.83
14	2	CH_2	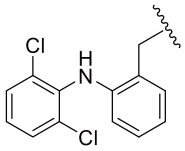	79	79.85	36.70 ± 0.85	72.43	33.51 ± 5.22
15	2	CH_2	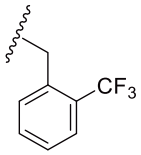	78	90.07	17.49 ± 0.26	80.87	30.67 ± 4.78
16	2	CH_2	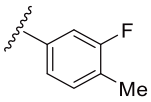	84	89.26	19.24 ± 0.37	63.68	42.48 ± 7.98
17	2	CH_2	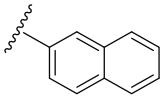	63	76.34	32.11 ± 0.72	32.65	76.05 ± 8.31
18	2	CH_2	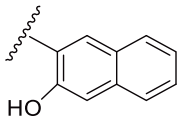	77	86.79	24.33 ± 0.27	65.46	45.66 ± 5.10
19	2	*N*-Me	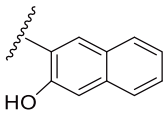	80	85.40	26.15 ± 0.31	68.78	43.13 ± 5.07
20	2	*N*-Me	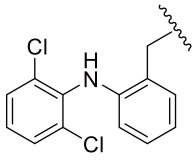	86	91.26	12.10 ± 0.15	83.46	25.81 ± 2.48

(*continued on next page*)

Table 1 (*continued*)

Code	n	X	R	Yield (%)	α-glucosidase		α-amylase	
					% Inhibition (0.5 mM)	IC_{50} (μM ± SEM*)	% Inhibition (0.5 mM)	IC_{50} (μM ± SEM*)
21	2	*N*-Me	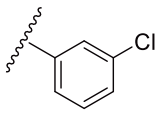	67	89.76	18.64 ± 0.37	78.04	33.57 ± 5.01
22	2	*N*-Me	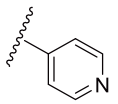	66	77.50	37.22 ± 0.89	28.31	> 100
23	2	*N*-Me	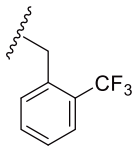	67	89.46	19.53 ± 0.34	79.02	30.42 ± 4.72
Acarbose					873.34 ± 1.67		68.40	60.73 ± 5.98

*SEM = Standard error of mean.

α-amylase inhibition and exhibited gradual increase in the α-amylase inhibitory activity with IC_{50} values 45.77 ± 3.83, 33.51 ± 5.22, 30.67 ± 4.78 μM respectively. Compounds **16**, **18** and **19** exhibited almost similar anti α-amylase effect with IC_{50} values 42.48 ± 7.98, 45.66 ± 5.10, 43.13 ± 5.07 μM, respectively. On the other hand, compound **17** exhibited drastic decrease in the α-amylase inhibitory capability and was found to be the least active compound (IC_{50} = 76.0 5 ± 8.31 μM). Compound **20** exhibited excellent activity against α-amylase and was the most active compound (IC_{50} = 25.81 ± 2.48 μM). Similarly compounds **21** and also exhibited excellent activity against α-amylase with IC_{50} values 33.57 ± 5.01 and 30.42 ± 4.72 μM respectively. The activity of various derivatives can be co-related by some other factors: *viz.* the excellent potency of **6**, having ortho methyl substitution on aromatic ring, is due to appreciable hydrogen bonding with enzyme active site and magic methyl effect (the effect that enhances binding affinity of

Table 2
Docking score (kcal/mol) of compounds against α-glucosidase target protein 3A4A.

Comp Id/ Std	Binding/Interaction energies (kcal/mol)	Comp Id	Binding/Interaction energies (kcal/mol)
	3A4A		3A4A
	α-glucosidase		*α-glucosidase*
5	−8.6	**14**	−9.7
6	**−10.5**	**15**	−9.9
7	−8.4	**16**	−8.7
8	−9.7	**17**	−9.0
9	−9.6	**18**	−9.7
10	−7.7	**19**	−9.4
11	−9.8	**20**	**−10.5**
12	−8.5	**21**	−8.2
13	−10.0	**22**	−7.8
Acarbose	−8.2	**23**	−9.1

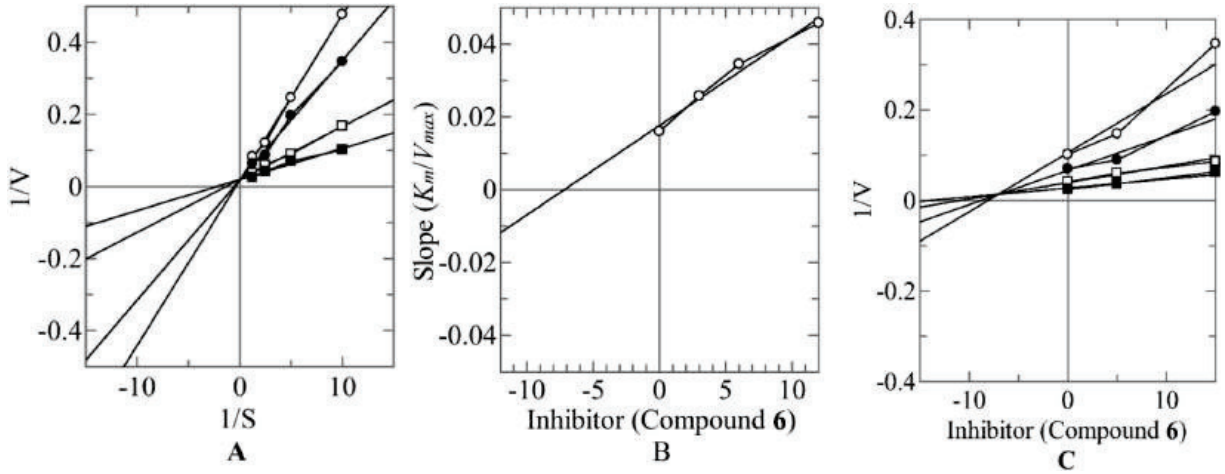

Fig. 2. α-Glucosidase inhibition via compound **6** (A) Line weaver-Burk graph of reciprocal of velocities (1/V) versus reciprocal of p-nitro phenyl-α-D-glucopyranoside substrate (1/S) in the presence of 5 μM (□), 10 (●), and 20 (○) and in the absence (■) of compound **6**. (B) Secondary replot of Line weaver-Burk plot between the slopes of each line on-Line weaver-Burk plot vs various concentrations of **6**. (C) Dixon graph of reciprocal of velocities vs various concentrations of **6**.

Table 3
The interactions and binding residues of some highly docked compounds with α-glucosidase target protein 3A4A.

Most docked comp. Id	Docking score (kcal/mol)	Interactions & binding residues [residue code (Interaction type)]
6	−10.5	LEU A:313 (**H-bond**); LYS A:156 (π-alkyl); SER A:240 (π-donor H-bond); TYR A:158 ($\pi-\pi$ *T*-shaped, π-alkyl); ARG A:315, HIS A:280 (π-alkyl).
11	−9.8	PRO A:312 (**H-bond**); ASP A:242 (π-anion); SER A:240 (π-donor H-bond); TYR A:158 (π-alkyl, $\pi-\pi$ *T*-shaped & π-sigma,); GLU A:411 (C—H bond); ARG A:315 (π-alkyl).
13	−10.0	ASN A:259 (**H-bond**); GLU A:296 (**H-bond, H-bond**); ALA A:292 (π-sigma); VAL A:266, ARG A:263 (alkyl).
20	−10.5	PRO A:312 (**H-bond**, π-sigma, π-alkyl); ASP A307 (attractive charge, C—H bond); SER A304, THR A:310 (C—H bond); ASP A:242 (π-anion); ARG A:315 (π-alkyl); TYR A:158 (($\pi-\pi$ *T*-stacked).

synthesized analogues with enzymes [51,52]). Structure activity relationship (SAR) among **8**, **14**, and **20**, with diclofenac moiety, also suggest that **20** is most potent among these three derivatives and 2nd most potent among all derivative which could be due to magic methyl effect (exhibited by *N*-Me in piperazinyl skeleton in **20** but **8** and **14** are void of such effect). Derivatives **11** and **16**, with 3-F and 4-Me substituents, exhibit different IC_{50} values, former has less value than later showing that pyrrolidine ring has strong interactions with enzyme active site rather than piperidine ring (the same is true for **8** and **14**). Derivatives **10**,**12**, and **22** bearing pyridinyl moiety (highly electron deficient) possess least IC_{50} values among all derivatives while among these 3 derivatives **22** is potent than other two (*N*-Me magic methyl effect could be the main cause [51,52]). Based on the discussion above, it is important to note that substituents at the 3-position of the phenyl ring, whether electron-withdrawing groups (EWG) or electron-donating groups (EDG), are more effective at enhancing inhibition compared to those at the 2- and 4- positions.

2.3. Mechanistic study

To precisely identify binding locations, modes of inhibition, and effects on enzyme kinetics, mechanistic research of enzyme inhibitors is crucial to comprehending how inhibitors interact with their targets. This study allows the design of more selective and potent inhibitors by revealing critical structural and chemical properties required for effective efficacy. Additionally, mechanistic insights aid in the prediction of resistance mechanisms and possible off-target consequences, which promotes the creation of safer and more efficient treatment medicines. This method guarantees that inhibitors interact with the enzyme in the intended manner under physiological settings and helps optimize lead compounds in drug discovery. The highly potent compound **6** was further proceeded for mechanistic study. Mechanism-based study identified compound **6** as concentration dependent type of competitive inhibitor with K_i 8.30 ± 0.0076 μM. In such inhibitory patterns, binding of inhibitor takes place at the active site of enzyme's residue, increased the K_m value while keeping V_{max} of the enzyme constant (Fig. 2). The type of inhibition was determined by Lineweaver-Burk plots, the reciprocal of the rate of the reaction was plotted against the reciprocal of substrate concentrations to monitor the effect of inhibitor on both K_m and V_{max}. It was observed from Lineweaver-Burk plots compound **6** clearly showed competitive inhibition Fig. 2**: A**. The secondary replots of Lineweaver-Burk plots were used to determine the K_i values. The *Ki* values were calculated by plotting the slope of each line in the Lineweaver-Burk plots against different concentrations of compounds **3**–**5** and **11** (Fig. 2**: B**). The K_i value was confirmed from Dixon plot by plotting the reciprocal of the rate of reaction against different concentrations of compounds **6** (Fig. 2**: C**).

2.4. Molecular docking Simulations

The diabetes-related enzymes, *viz.* dipeptidyl peptidase IV (DPP-IV), α-glucosidase and α-amylase, are crucial for digestion and blood sugar regulation. Among these, α-glucosidase is particularly significant in managing TIIDM, where reduced insulin sensitivity leads to hyperglycemia and raised blood glucose levels. Thus, inhibitors of α-glucosidase are a promising treatment for achieving precise blood sugar control in TIIDM patients. Previous commercial inhibitors, such as miglitol, voglibose and acarbose have been effective in stabilizing blood glucose

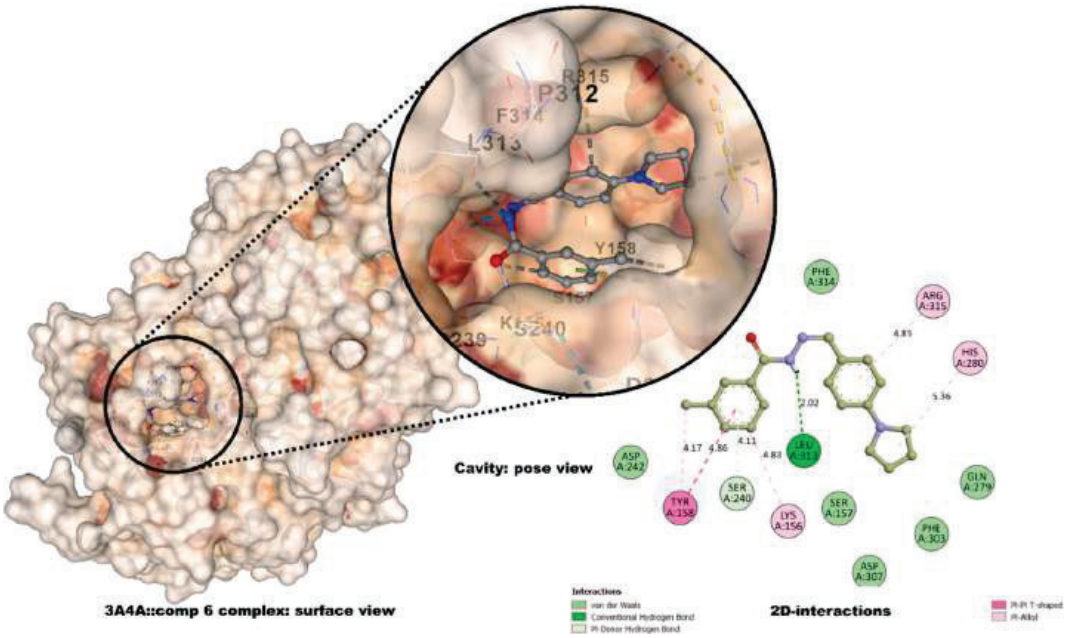

Fig. 3. Molecular docking of compound **6** with protein 3A4A: surface view, pose view, and 2D interactions.

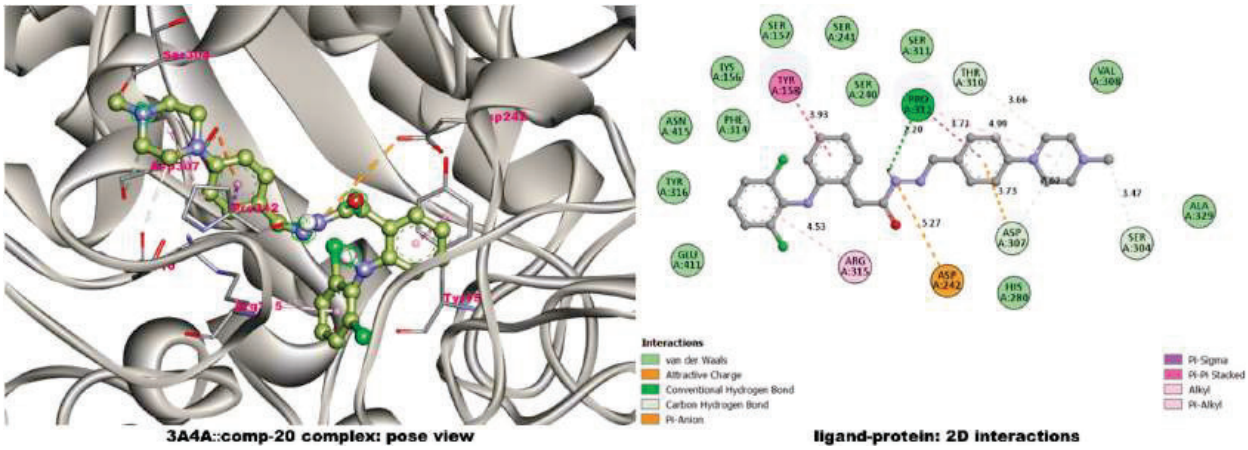

Fig. 4. *Two & three*-dimensional docking interactions of derivative **20** with target protein 3A4A.

levels in those with insulin resistance or insufficiency [53–56]. With these considerations in mind, an α-glucosidase target protein with PDB Id: 3A4A (crystal structure derived from Saccharomyces cerevisiae i.e. isomaltase) and α-amylase target protein PDB Id: 1B2Y (crystal structure of human pancreatic α-amylase complexed with the carbohydrate inhibitor acarbose) were selected for docking. Detailed docking methodology is provided in the supplementary information file. Re-docking is carried out to validate molecular docking studies, ensuring the accuracy of predicted ligand-receptor binding poses. The binding or interaction energies of derivatives **5**–**23** with the aforementioned protein 3A4A are demonstrated in Table 2. Compounds 6, 11, 13, 15 and 20 unveiled finest docking score of −10.5, −9.8, −10.0, −9.9, & −10.5 kcal/mol with protein 3A4A, respectively. A comprehensive overview of interaction energies between receptor protein and moiety are given in Table 3. The most docked (−10.5 kcal/mol) compound-6 exhibited multiple interactions with residues of amino acid, for instance, LEU A:313 (H-bond); LYS A:156 (*π*-alkyl); SER A:240 (*π*-donor H-bond); TRY A:158 (*π* −*π T*-shaped, *π*-alkyl); ARG A:315, HIS A:280 (*π* −alkyl). In the same way, interactions of second most docked compound-20 with 3A4A encompasses PRO A:312 (H-bond, *π*-sigma, *π*-alkyl); ASP A307 (attractive charge, C—H bond); SER A304, THR A:310 (C—H bond); ASP A:242 (*π*-anion); ARG A:315 (*π*-alkyl); TYR A:158 ((*π* −*π T*-stacked); whereas, next highly docked compound-13 involves ASN A:259 (H-bond); GLU A:296 (H-bond, H-bond); ALA A:292 (*π*-sigma); VAL A:266, ARG A:263 (alkyl) interactions. Further, compound-11, having −9.8 kcal/mol binding energy, exhibited PRO A:312 (H-bond); ASP A:242 (*π*-anion); SER A:240 (*π* −donor H-bond); TYR A:158 (*π*-alkyl, *π* −*π T*-shaped & *π*-sigma); GLU A:411 (C—H bond); ARG A:315 (*π*-alkyl) interactions. Interestingly, it was observed that all highly bound moieties have induced *π*-interactions and H-bonding which are crucial in influencing the inhibitory action of compounds. Figs. 3, 4, and 5 depict the images of interactions of derivatives **6**, **20** and standard acarbose with protein 3A4A**.** The images of interactions of derivatives **8**, **11**, **14**, **16**, and **18** with target protein 3A4A are provided in supplementary information file.

The best docked compound-**20** with α-amylase target protein 1B2Y exhibited docking score of −9.4 kcal/mol and revealed diverse binding interactions (Tables 4 and 5). The O-atom of acetohydrazide group of compound-**20** developed hydrogen bonding with pocket amino acid residue GLY A:306 at a distance of 2.46 Å. Further, *N*-atom of acetohydrazide group formed attractive charge interaction (5.54 Å) with residue GLU A:233. The π-electron density of middle amino-phenyl ring induced two crucial π-interactions including π-anion (3.60 Å) and π-π *T*-shaped (4.86 Å) with residues ASP A:300 and TYR A:62. Similarly, π-electron density of dichlorophenyl ring persuaded two π-interactions such as π-π stacked (5.77 Å) and π-alkyl (5.34 Å) with TRP A:59 and LEU A:165. Also, π-electrons of benzylidene ring produced π-π stacked (4.89 Å) and π-alkyl (4.90 Å) interactions with TYR A:151 and ILE A:235 whereas, methylpiperazine ring formed π-alkyl (5.39 Å) interactions with residue TYR A:151 (Fig. 6).

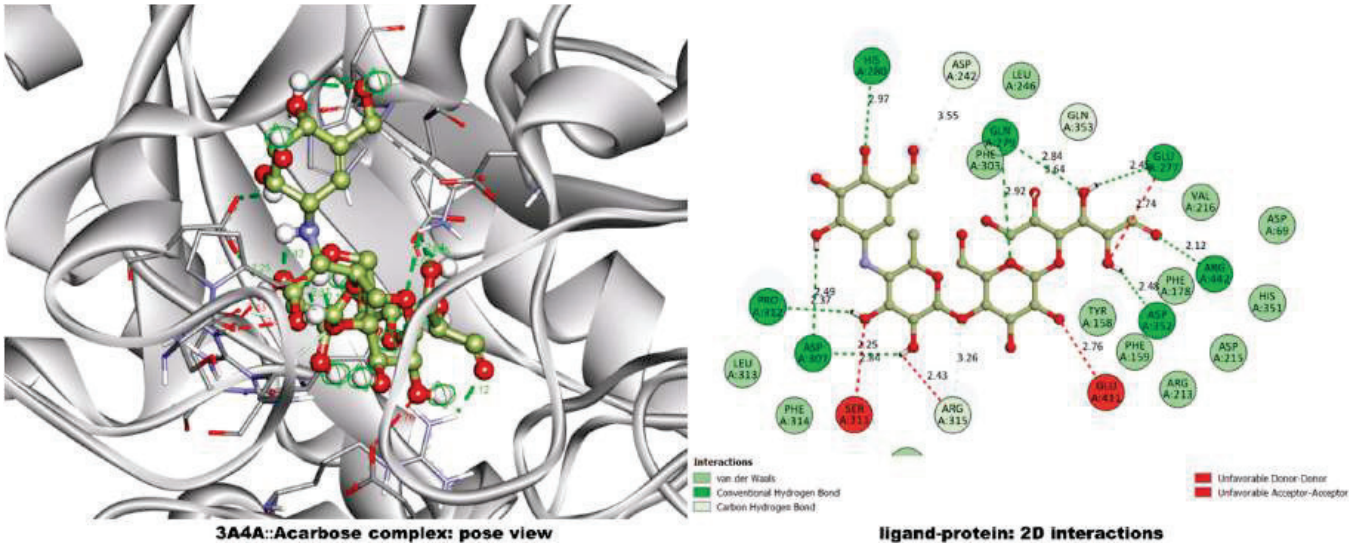

Fig. 5. *Two & three*-dimensional docking interactions of standard drug acarbose with target protein 3A4A.

Table 4
Docking score of compounds against target protein α-amylase (PDB ID: 1B2Y).

Comp Id/ Std	Binding/Interaction energies (kcal/mol)	Comp Id	Binding/Interaction energies (kcal/mol)
	1B2Y		1B2Y
	α-amylase		*α-amylase*
5	−7.4	**14**	−8.3
6	−7.6	**15**	−8.5
7	−6.9	**16**	−7.7
8	−8.7	**17**	−7.2
9	−8.9	**18**	−7.5
10	−7.5	**19**	−7.7
11	−7.9	**20**	**−9.4**
12	−6.7	**21**	−8.2
13	−7.8	**22**	−6.5
Acarbose	−10.8	**23**	−8.4

The standard drug acarbose exhibited docking score of −10.8 kcal/mol against target protein 1B2Y with assorted binding interactions including GLY A:306 (carbon-hydrogen bond); TRP A:59 (hydrogen bond); ASP A:300 (acceptor–acceptor); GLN A:63 (hydrogen bond); HIS A:305 (hydrogen bond); HIS A:201 (hydrogen bond); ALA A:198 (alkyl); and LEU A:162 (alkyl) interactions (Fig. 7). The image of interactions of derivative 9 with target protein 1B2Y is provided in supplementary information file.

Table 5
The interactions and binding residues of best docked compound and standard with α-amylase target protein 1B2Y.

Most docked comp. Id	Docking score (kcal/mol)	Interactions & binding residues [residue code (Interaction type)]
20	−9.4	GLY A:306 (**H-bond**); TRP A:59 (π-π stacked); ASP A:300 (π-anion); GLU A:233 (attractive charge); TYR A:62 (π-π *T*-shaped); TYR A:151 (π-π stacked, π-alkyl); LEU A:165 (π-alkyl); ILE A:235 (π-alkyl).
9	−8.9	ILE A: 235 (**H-bond,** π-sigma, alkyl); TRP A:59 (π-alkyl); ASP A:300 (attractive charge); GLU A:233 (halogen, attractive charge); ASP A:197 (attractive charge); ALA A:198 (halogen); LEU A:162 (π-alkyl); HIS A:201 (π-cation, π-alkyl); LYS A:200 (π-alkyl, alkyl)
Acarbose	−10.8	GLY A:306 (C—H bond); TRP A:59 (**H-bond**); ASP A:300 (acceptor–acceptor); GLN A:63 (**H-bond**); HIS A:305 (**H-bond**); HIS A:201 (**H-bond**); ALA A:198 (alkyl); LEU A:162 (alkyl).

2.5. *In silico ADME, pharmacokinetics, and drug-likeness studies*

The pharmacokinetic & ADME profiles of synthesized scaffolds help to predict the absorption, permeability, & bioavailability of potential drug candidates, and hence enabled the election of molecules with optimal absorption. Drug distribution is affected significantly by various factors like blood–brain barrier (BBB) permeability & gastrointestinal

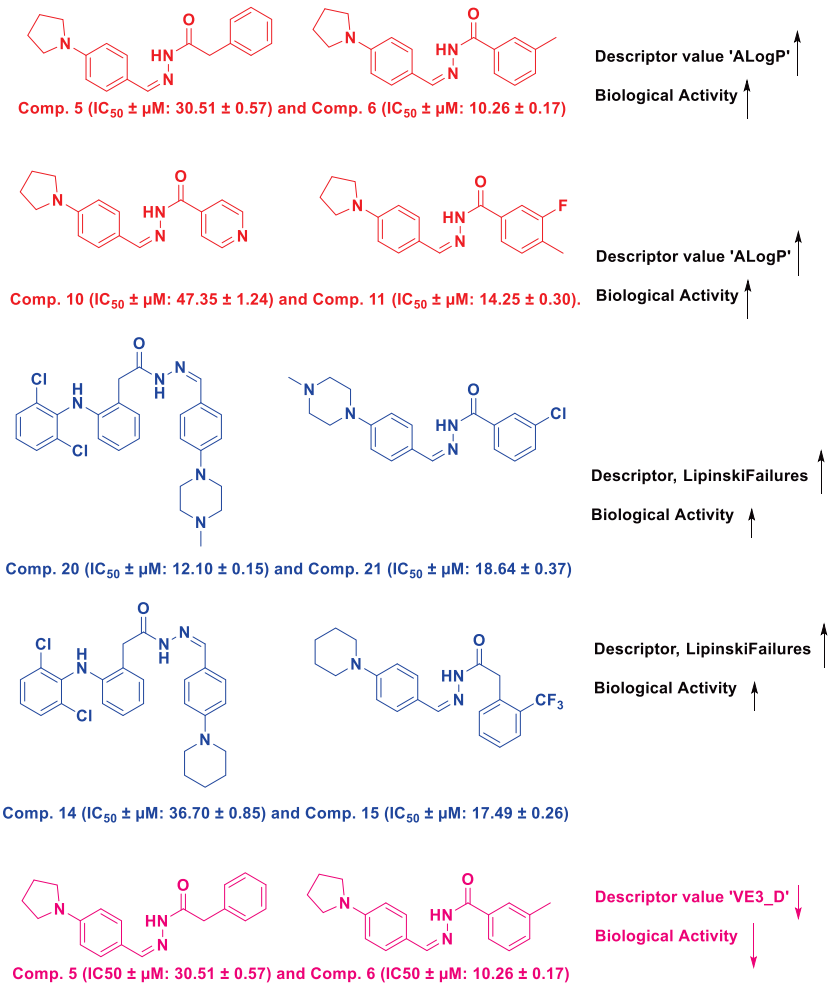

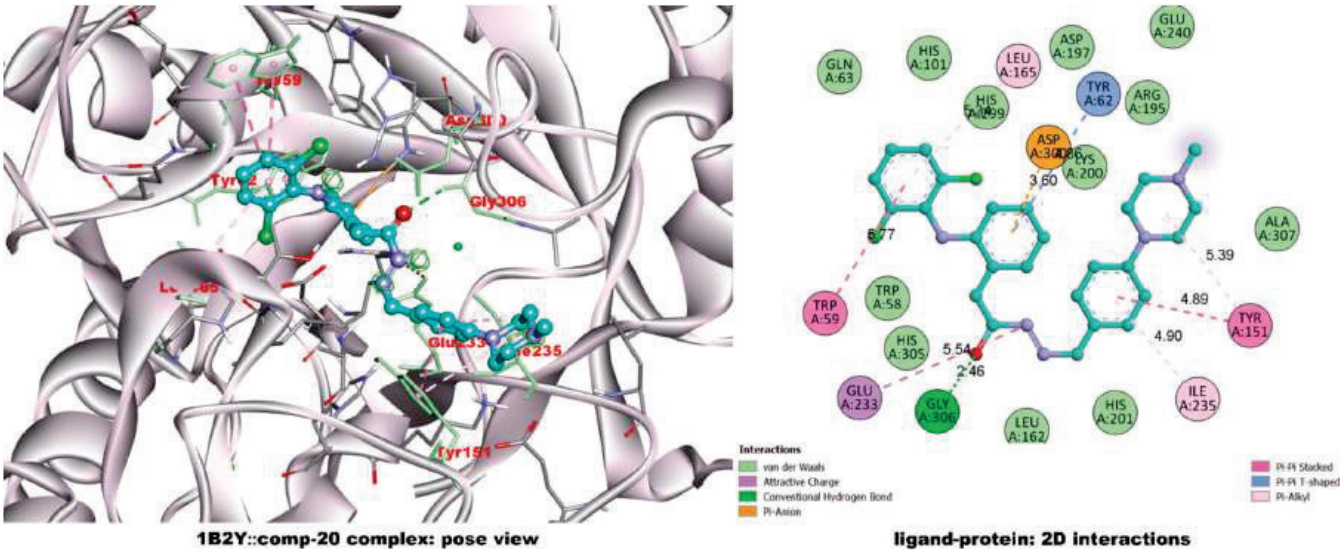

Fig. 6. *Two* and *three*-dimensional docking interactions of derivative **20** with target protein 1B2Y.

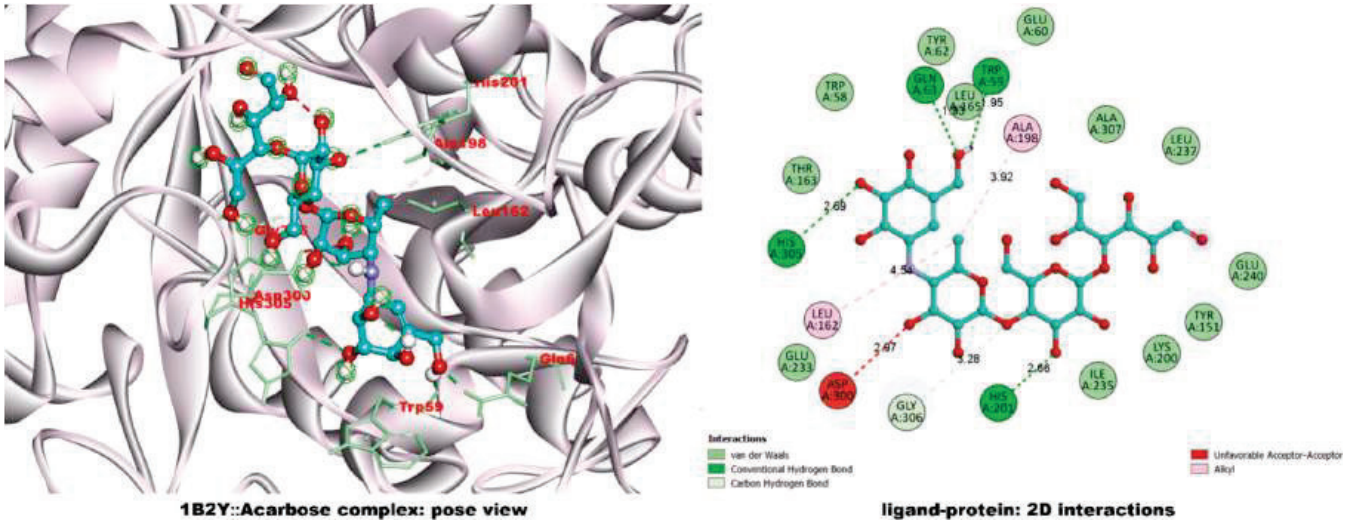

Fig. 7. *Two* and *three*-dimensional docking interactions of standard drug acarbose with target protein 1B2Y.

Table 6
In-silico pharmacokinetic and drug-likeness profile.

Comp id/ Std	GI[a] Absorption	BBB[b] permeant	P-gp[c] substrate	CYP1A2[d] inhibitor	CYP2C19 inhibitor	CYP2C9 inhibitor	CYP2D6 inhibitor	CYP3A4 inhibitor	Bioavailability Score	Lipinski #violations
5	Greater	✓	×	✓	✓	✓	✓	×	0.55	0
6	Greater	✓	×	✓	✓	✓	✓	×	0.55	0
7	Greater	✓	×	✓	✓	✓	✓	×	0.55	0
8	Greater	×	✓	×	✓	✓	✓	✓	0.55	1
9	Greater	✓	×	✓	✓	✓	✓	×	0.55	0
10	Greater	✓	×	✓	✓	×	✓	×	0.55	0
11	Greater	✓	×	✓	✓	✓	✓	×	0.55	0
12	Greater	✓	×	✓	✓	×	✓	×	0.55	0
13	Greater	✓	×	✓	✓	✓	✓	✓	0.55	0
14	Greater	×	✓	×	✓	✓	✓	×	0.55	1
15	Greater	✓	×	×	✓	✓	✓	✓	0.55	0
16	Greater	✓	×	×	✓	✓	✓	×	0.55	0
17	Greater	✓	×	✓	✓	✓	✓	✓	0.55	0
18	Greater	✓	×	✓	✓	✓	✓	×	0.55	0
19	Greater	✓	×	✓	×	✓	✓	×	0.55	0
20	Greater	✓	✓	×	✓	✓	✓	✓	0.55	0
21	Greater	✓	×	×	✓	✓	✓	✓	0.55	0
22	Greater	✓	✓	×	×	×	✓	×	0.55	0
23	Greater	✓	×	×	✓	×	✓	✓	0.55	0
Acarbose	Lower	×	✓	×	×	×	×	×3	0.17	3

[a]GI: gastrointestinal absorptions, [b]BBB: blood–brain barrier permeation, [c]P-gp: P-glycoprotein substrate, [d]CYP: cytochrome P450 inhibitors.

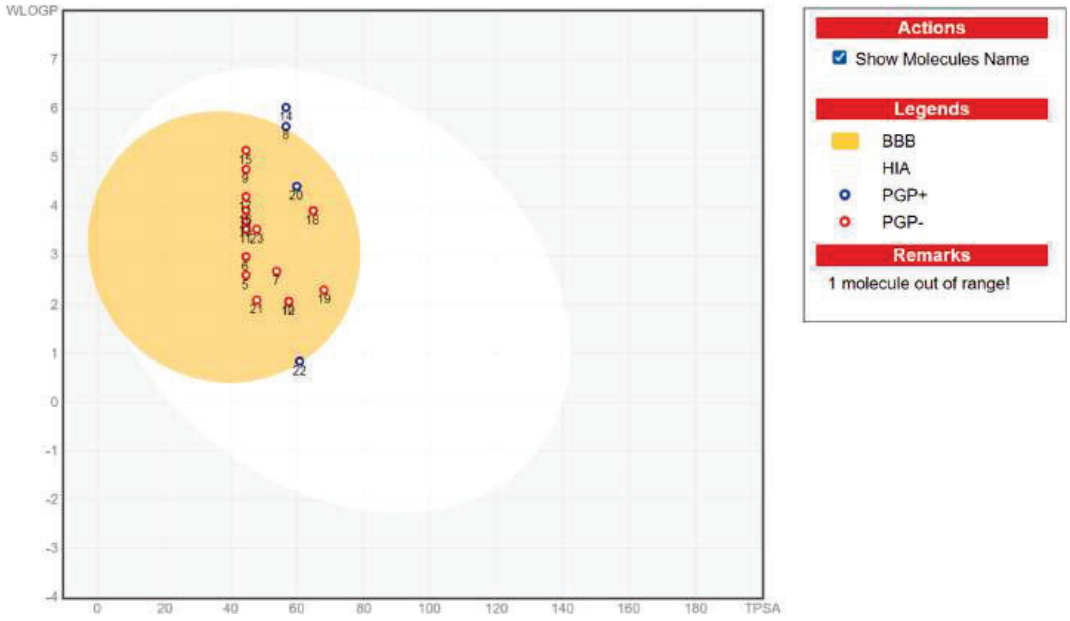

Fig. 8. The Brain or Intestinal EstimateD (BOILED-Egg) diagram: plot of WLOGP against TPSA.

(GI) absorption. Further, CYP (cytochrome P450) enzyme superfamily is crucial for drug elimination via metabolic biotransformation. Drug metabolism and interactions can be impacted by inhibiting CYP enzymes. A useful initial screening tool for assessing drug likeness is Lipinski's rule of five [57,58].

The ADME & pharmacokinetic profiles of the compounds **5**–**23** are encapsulated in Table 6. All analogues exhibited high GI absorption and excluding 8 and 14, all are capable of crossing BBB. Furthermore, apart from compounds 8, 14, 20, and 22, all analogues are non-substrates of P-gp (P-glycoprotein). Further, every compound acted as an inhibitor of CYP2D6. Also, all scaffolds except 19 and 22, inhibited CYP2C19; and except 10, 12, 22, and 23, inhibited CYP2C9. The Swiss ADME web tool was used to determine bioavailability score of 0.55. Drug-likeness studies indicated that the analogues are orally active, adhering to Lipinski's rule of 5 with no more than 1 violation [57].

2.6. The 'BOILED-egg model' analysis

The BOILED-Egg model offers an intuitive visual method to assess a molecule's likelihood of passive absorption in the gastrointestinal tract (HIA) and its ability to penetrate the blood–brain barrier (BBB). This diagram is achieved by plotting the molecule's WLOGP (a measure of lipophilicity) against its TPSA (which reflects polarity). The 'white' part of the egg signifies a high probability of gastrointestinal absorption, while the 'yellow' (yolk) area indicates a strong likelihood of brain penetration. These regions are not exclusive, meaning a molecule can fall into both categories simultaneously. In addition to the positioning within the egg, molecules are further classified based on their interaction with P-glycoprotein (P-gp), a transporter protein involved in drug efflux. Molecules predicted to be substrates of P-gp, those likely to be pumped out of cells and are marked with blue dots, while non-substrates are marked with red dots [56,58].

The BOILED-egg model is valuable as it provides a quick, visual evaluation of two critical pharmacokinetic properties, which are essential for drug design. This screening approach aids drug development by evaluating the potential for passive absorption in the GI tract (white region) and penetration of the BBB (yellow yolk region) [49,50]. BOILED-egg model analysis on the synthesized compounds was achieved via the SwissADME web tool [44]. All analogues exhibited passive GI absorption and except three molecules (8, 14, and 22) all showed BBB penetration (Fig. 8). Specifically, compounds 8, 14, and 22 were also found substrates of P-gp^{+}, showing their active efflux, and not crossing the BBB. Whereas, compound 20 laid in the BBB region exhibiting active efflux (P-gp +) by P-glycoprotein. Thus, with their high absorption profile, such analogues may have potential applications as an α-glucosidase inhibitor in advanced in-vivo studies.

2.7. QSAR model

In order to generate a statistically robust 2D-QSAR model, we used the 'QSAR-INSubria' V. 2.2.4 [developed at University of Insubria, Italy] [55,56]. In total, we have generated 1407 molecular descriptors (1D, and 2D), wherein 1077 descriptors were excluded by the 'QSARINS' descriptor selection criteria (descriptors with null values or '0' were automatically excluded). Finally, we used 330 descriptors, generated from 'PaDEL', for the development of multilinear regression based-QSAR models (MLR-QSAR) [55,56]. Total of 20 models were generated, however, only the top model with good internal and external validation parameters was selected for the visualization. This criterion is well-known from 'OECD (the Organisation for Economic Co-operation and Development)' (Fig. 9). The four parametric **model-1**, was found to be best out of 20 ranked QSAR models. The **model-1** is as follows:

$$\boldsymbol{pIC_{50}} = 2.9787 + 0.1679*\boldsymbol{ALogP}\ (\pm 0.528) + 0.3173*\boldsymbol{LipinskiFailures}\ (\pm 0.6918) + 1.0728*\boldsymbol{topoShape}\ (\pm 0.3118) - 0.0659*\boldsymbol{VE3\_D}\ (-0.6354) \qquad \textbf{model-1}$$

Internal and External Validations

R^2: 0.9167; R^2_{adj}: 0.8834; R^2- R^2_{adj}: 0.0333; LOF: 0.0157; K_{xx}: 0.3262; Delta K: 0.0689; $RMSE_{tr}$:0.0585; MAE_{tr}: 0.0492; RSS_{tr}: 0.0514; CCC_{tr}: 0.9566; s: 0.0717; F: 27.5299.

Internal validation criteria

Q^2_{loo}: 0.8127; R^2- Q^2_{loo}: 0.1041; $RMSE_{cv}$: 0.0878; MAE_{cv}: 0.0744; $PRESS_{cv}$: 0.1156; CCC cv: 0.9072; Q^2_{LMO}: 0.7487; R^2_{scr}: 0.2913.

External validation criteria

$RMSE_{ext}$:0.2434; MAE_{ext}: 0.2272; $PRESS_{ext}$: 0.2371; R^2_{ext}: 0.1538; Q^2-F_1: 3.6746; CCC_{ext}: 0.2732; r^2_m aver.: 0.0095; Calc. external data regr. angle from diagonal: 3.6386°.

The **model-1** followed the standard validation criteria for the model

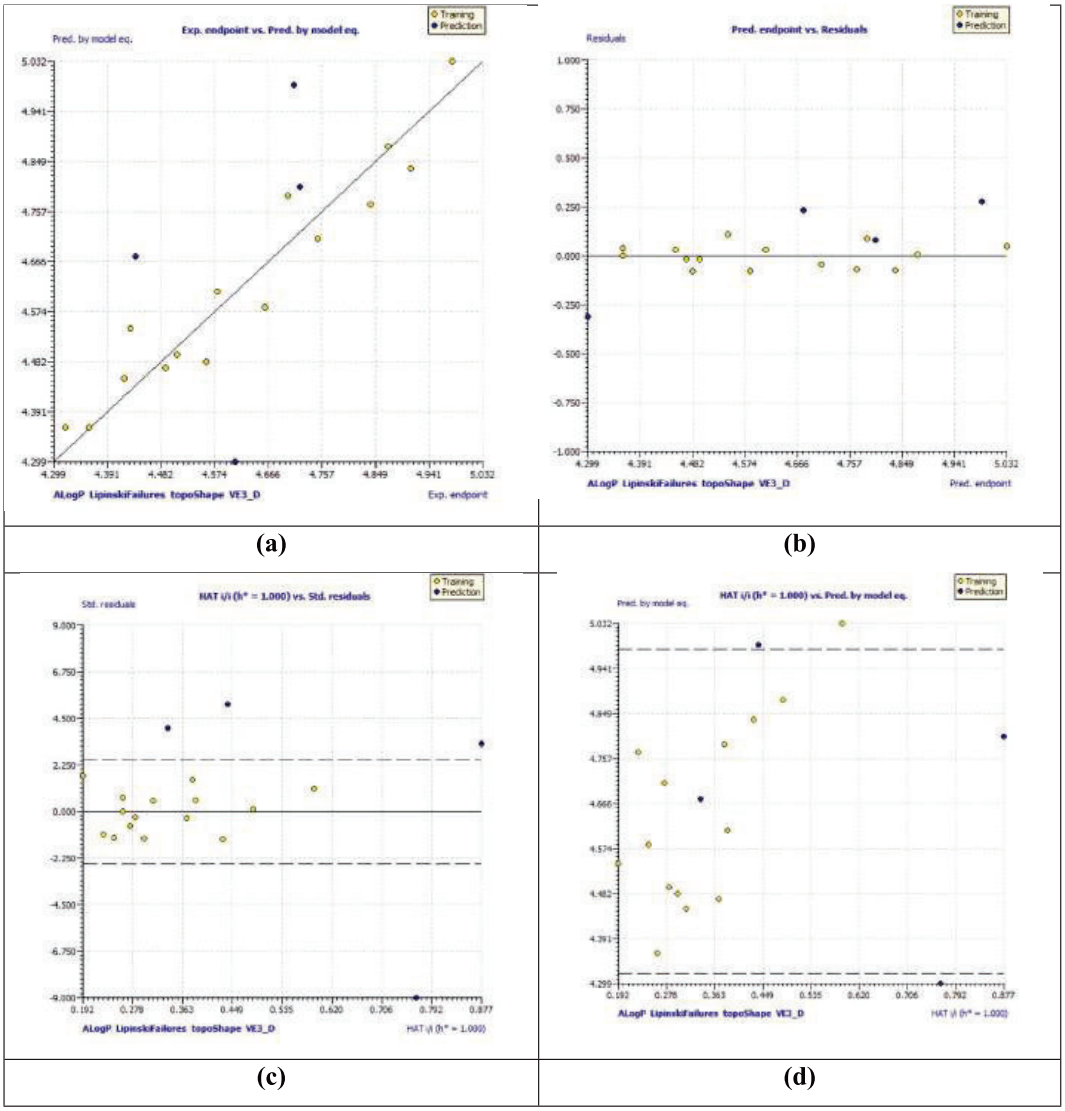

Fig. 9. (a) External endpoints Vs. Predicted endpoints by model-1; (b) Residual plot; (c)HAT(i/i)(h*= 1000) Vs. Std. residuals; and (d) Insubria Plot (Applicability Domain).

acceptability and was chosen further for the interpretation. From **model-1**, it was evident that the descriptor '***ALogP'*** [The Ghose-Crippen-Viswanadhan octanol–water partition coefficient] was positively correlated with the biological activity (BA). The ALogP is determined using the ALogP model, which employs a regression equation based on the hydrophobicity contributions of 115 different atom types. The said trend can be observed with **5** (IC_{50} = 30.51 ± 0.57 μM), **6** (IC_{50} = 10.26 ± 0.17 μM), **10** (IC_{50} = 47.35 ± 1.24 μM) and **11** (IC_{50} = 14.25 ± 0.30 μM).

Other descriptors, ***LipinskiFailures*** [failure to the Lipinski rule of 5] and ***topoShape*** [Petitjean topological shape index, a topological descriptor] were also found to be positively correlated with BA. For descriptor ***LipinskiFailures,*** the trend can be seen with **20** (IC_{50} = 12.10 ± 0.15 μM), **21** (IC_{50} = 18.64 ± 0.37 μM), **22** (IC_{50} = 37.22 ± 0.89 μM) and **23** (IC_{50} = 19.53 ± 0.34 μM). For '***topoShape'***, we found this trend in **14** (IC_{50} = 36.70 ± 0.85 μM) and **15** (IC_{50} = 17.49 ± 0.26 μM).

However, descriptor '***VE3_D'*** [Logarithmic coefficient sum of the last eigenvector from topological distance matrix, a Topological Distance Matrix descriptor] was negatively correlated with the BA. The decreased in descriptor value '***VE3_D'*** decreased the activity of compounds, e.g. **5** (IC_{50} = 30.51 ± 0.57 μM), **6** (IC_{50} = 10.26 ± 0.17 μM), **7** (IC_{50} = 27.44 ± 0.53 μM) and **8** (IC_{50} = 36.11 ± 0.67 μM).

3. Conclusion

In this work, a series of novel hydrazones **5**–**23** were synthesized to create non-carbohydrate based α-glucosidase inhibitors. *In-vitro* analysis demonstrated that all derivatives exhibited potent inhibition capabilities, with compounds **6,11,13,15** and **20** showing particularly strong potency with lower IC_{50} values. Some derivatives are also active as α-amylase inhibitors. Molecular docking studies indicated that nitrogen-saturated heterocycles, phenyl rings and methyl group are key moieties for binding to the enzyme's active site. QSAR models suggested that AlogP and Lipinski Failures are significant relative to descriptors such as hydrogen bond donors. *In silico* pharmacokinetics, ADME and drug-likeness studies, along with BOILED-egg model analysis, predicted that all analogues showed passive gastrointestinal absorption, while all except three molecules (**8, 14, and 22**) demonstrated blood–brain barrier penetration. Based on these results, we conclude that these derivatives have potential for future drug development aimed at treating diabetes mellitus.

4. Experimental

4.1. General Information

Melting points (m.p) of all prepared derivatives were taken on Gallen Kamp m.p apparatus. Shimadzu FTIR 8400 at range 4000–400 cm^{-1} was used to record IR spectra by use of KBr pellets. A Bruker Ultra-Shield 300 MHz spectrometer was utilized to acquire 13C and 1H spectra at 75 MHz for 13C and 300 MHz for 1H NMR in DMSO-d_6, using TMS as the internal standard. JEOL JMS-700 was used for taking mass spectra, ESI-MS. Merck silica gel GF_{254} TLC was used in monitoring reaction progress and purity as well.

4.2. Preparation of aromatic aldehydes with pyrrolidinyl, piperidinyl, and N-methyl piperazinyl nucleus **3a-c**

The precursors **3a-c** were prepared by already reported procedure [47,59]. To a solution of pyrrolidine/piperidine/*N*-methylpiperazine (1 mmol) in 5–10 mL DMF, 2 mmol of K_2CO_3 was added. After stirring at 80 °C for half an hour, 4-flurobenzaldehyde (1 mmol) was taken in reaction mixture stirring was continued for another 12–16 h. Soon after completion, reaction mixture was allowed to cool. It was then added slowly to cool water. Yellow precipitates were then collected, washed and filtered to afford **3a-c** and used in second step without further purification.

4.3. Synthesis of nitrogen containing heterocycle-based hydrazones **5–23**

Equimolar amounts (0.01 mol) of both nitrogen-skeleton containing *p*-substituted aromatic aldehydes **3a-c** and hydrazides **4a-k** were dissolved in 10–15 mL ethanol in reaction vessel. After addition of few drops of glacial acetic acid (catalyst), the reaction mixture was allowed to reflux for 8–10 h. TLC was used to monitor the reaction progress. After completion of reaction, the reaction was kept at cool temperature till the formation of solid precipitates. The product was then filtered, washed with ethanol & vacuum dried.

4.3.1. 2-Phenyl-N'-{4-(pyrrolidin-1-yl)benzylidene} acetohydrazide (**5**)

Light green solid; Yield 75 %; m.p. 201–202 °C; IR cm^{-1}: 3464, 3179, 3024, 2965, 2827, 1646, 1605, 1500, 1370, 1340, 1250, 1170,1050, 980, 950, 740; ^{1}H NMR (300 MHz, DMSO-d_6): δ 1.95 (4H, t), 3.27 (4H, t), 3.48 (1H, s), 3.93 (1H, s), 6.55 (2H, dd), 7.23 (1H, m), 7.30 (4H, m), 7.48 (2H, dd), 7.84 (0.6H, s), 8.03 (0.5H, s), 11.06 (0.6H, s), 11.28 (0.4H, s); ^{13}C NMR (75 MHz, DMSO- d_6): δ 25.42, 41.72, 47.67, 112, 121.21, 121.40, 126.75, 126.97, 128.59, 128.64, 128.75, 128.95, 129.46, 129.85, 136.47, 144.38, 148.02, 149.11, 149.29, 166.35, 172.12; HRMS calc. for $C_{19}H_{21}N_3O$ 307.1684, found 307.1682.

4.3.2. 3-Methyl-N'-{4-(pyrrolidin-1-yl)benzylidene}benzohydrazide (**6**)

Green solid; Yield 70 %; m.p. 204–206 °C; IR cm^{-1}: 3227, 3042, 2951, 2841, 1650, 1613, 1490, 1470, 1310, 1220, 1170, 1080, 850, 790, 680; ^{1}H NMR (300 MHz, DMSO- d_6): δ 1.95 (4H, t), 2.08 (3H, s) 3.29 (4H, t), 6.61 (2H, d), 7.54 (3H, m), 7.64 (1H, m), 7.93 (1H, t), 7.84 (1H, m), 8.28 (1H, s), 11.61 (1H, s); ^{13}C NMR (75 MHz, DMSO- d_6): δ 27.110, 32.844, 49.36, 113.715, 122.815, 128.453, 129.31, 130.83, 132.60, 133.39, 135.33, 137.94, 151.13, 151.52, 163.24; HRMS calc. for $C_{19}H_{21}N_3O$ 307.1684, found 307.1687.

4.3.3. 4-Methoxy-N'-{4-(pyrrolidin-1-yl)benzylidene}benzohydrazide (**7**)

Light green solid; Yield 75 %; m.p. 229–231 °C; IR cm^{-1}: 3420, 3225, 3052, 2966, 2844, 1647, 1490, 1470, 1310, 1240, 1170, 1070, 790, 730, 690, 670; ^{1}H NMR (300 MHz, DMSO- d_6): δ 1.96 (4H, t), 3.28 (4H, t), 3.82 (3H, s), 6.60 (2H, d), 7.04 (2H, d), 7.53 (2H, d), 7.89 (2H, d), 8.28 (1H, s), 11.40 (1H, s); ^{13}C NMR (75 MHz, DMSO- d_6): δ 25.43, 47.68, 55.85, 112.02, 114.08, 121.48, 126.30, 128.94, 129.77, 148.72, 149.27, 162.19, 162.49; HRMS calc. for $C_{19}H_{21}N_3O_2$ 324.1712 $[M + H]^+$, found 324.1711.

4.3.4. 2-[2-{(2,6-Dichlorophenyl)amino}phenyl]-N'-{4-(pyrrolidin-1-yl) benzylidene} acetohydrazide (**8**)

White solid; Yield 93 %; m.p. 245–247 °C; IR cm^{-1}: 3464, 3214, 3028, 2950, 2845, 1644, 1603, 1480, 1290, 1180, 1020, 760, 730; ^{1}H NMR (300 MHz, DMSO- d_6): δ 1.96 (4H, t), 3.27 (4H, t), 3.66 (1H, s), 4.08 (1H, s), 6.30 (1H, dd), 6.57 (2H, d), 6.87 (1H, m), 7.05 (1H, dd), 7.23 (2H, m), 7.52 (4H, m) 7.90 (1H, s) 8.06 (0.5H, s), 8.28 (0.5H, s) 11.34 (0.5H, s), 11.52 (0.5H, s); ^{13}C NMR (75 MHz, DMSO- d_6): δ 25.42, 36.18, 47.68, 112.02, 115.88, 116.54, 120.95, 121.10, 121.28, 124.65, 125.55, 126.03, 127.73, 128.78, 129.16, 129.66, 129.86, 130.52, 130.88, 131.59, 137.43, 143.40, 143.65, 149.00 149.26, 149.44, 167.65, 172.75; HRMS calc. for $C_{25}H_{24}Cl_2N_4O$ 489.1224 $[M + Na]^+$, found 489.1228.

4.3.5. N'-{4-(Pyrrolidin-1-yl)benzylidene}-2-{2-(trifluoromethyl)phenyl} acetohydrazide (**9**)

Dark green solid; Yield 62 %; m.p. 242–244 °C; IR cm^{-1}: 3468, 3173, 3087, 2974, 2846, 1668, 1600, 1510, 1360, 1270, 1230, 1109, 780, 740; ^{1}H NMR (300 MHz, DMSO- d_6): δ 1.95 (4H, t), 3.26 (4H, t), 3.75 (1H, s), 4.18 (1H, s) 6.55 (2H, d), 7.47 (4H, m), 7.62 (1H, m), 7.70 (1H, d), 7.87 (0.7H, s), 8.04 (0.3H, s), 11.19 (0.7H, s), 11.32 (0.3H, s); ^{13}C NMR (75 MHz, DMSO- d_6): δ 25.41, 36.50, 47.67, 112.02, 121.30, $J_{C\text{-}F}$ = 125.9 (m), 126.06, 127.54, 128.57, 128.97, 132.60, 132.71, 133.62, 133.80, 132.89, 144.56, 149.15, 149.29, 165.31, 171.12; HRMS calc. for $C_{20}H_{20}F_3N_3O$ 398.1456 $[M + Na]^+$, found 398.1457.

4.3.6. N'-{4-(Pyrrolidin-1-yl)benzylidene}isonicotinohydrazide (**10**)

Yellowish green solid; Yield 65 %; m.p. 224–226 °C; IR cm^{-1}: 3452, 3187, 2970, 2845, 1665, 1602, 1500, 1483, 1375, 1270, 1170, 770, 710; ^{1}H NMR (300 MHz, DMSO- d_6): δ 1.96 (4H, t), 3.29 (4H, t), 6.60 (2H, d), 7.55 (2H, d), 7.79 (2H, t), 8.75 (2H, d), 8.30 (1H, s), 11.75 (1H, s); ^{13}C NMR (75 MHz, DMSO- d_6): δ 25.43, 47.68, 112.04, 120.92, 121.93, 129.30, 141.30, 149.56, 149.91, 150.54, 150.71, 161.46; HRMS calc. for $C_{17}H_{18}N_4O$ 317.1378 $[M + Na]^+$, found 317.1374.

4.3.7. 3-Fluoro-4-methyl-N'-{4-(pyrrolidin-1-yl)benzylidene} benzohydrazide (**11**)

Green solid; Yield 69 %; m.p. 224–226 °C; IR cm^{-1}: 3438, 3201, 3040, 2970, 2851, 1650, 1609, 1490, 1370, 1260, 1180, 790; ^{1}H NMR (300 MHz, DMSO- d_6): δ 1.969 (4H, t), 2.306 (3H, s) 3.291 (4H, t), 6.59 (2H, d), 7.43 (1H, t), 7.52 (2H, d), 7.65 (1H, d), 7.68 (1H, s) 8.29 (1H, s), 11.525 (1H, s); ^{13}C NMR (75 MHz, DMSO- d_6): δ 14.68, 25.43, 47.68, 112.03, 114.17, 121.21, 123.85, 128.46, 128.72, 129.12, 132.18, 133.80, 149.41, 149.59, 159.16, 161.60; HRMS calc. for $C_{19}H_{20}FN_3O$ 325.1590, found 325.1585.

4.3.8. N'-{4-(Pyrrolidin-1-yl)benzylidene}nicotinohydrazide (**12**)

Yellowish green solid; Yield 65 %; m.p. 187–189 °C; IR cm^{-1}: 3435, 3198, 3020, 2960, 2850, 1650, 1600, 1497, 1480, 1375, 1180, 970, 790, 730; ^{1}H NMR (300 MHz, DMSO- d_6): δ 1.972 (4H, t), 3.297 (4H, t), 6.59 (2H, d), 7.55 (3H, m), 8.22 (1H, d), 8.74 (1H, d), 9.04 (1H, s), 8.28 (1H, s), 11.69 (1H, s); ^{13}C NMR (75 MHz, DMSO- d_6): δ 25.43, 47.69, 112.04, 121.04, 124.05, 129.21, 129.98, 136.78, 148.89, 149.49, 149.96, 152.46, 161.57; HRMS calc. for $C_{17}H_{18}N_4O$ 294.1480, found 294.1479.

4.3.9. 3-Chloro-N'-{4-(piperidin-1-yl)benzylidene}benzohydrazide (**13**)

Dark purple solid; Yield 60 %; m.p. 166–168 °C; IR cm^{-1}: 3431, 3235, 3068, 2935, 2795, 1657, 1601, 1470, 1440, 1260, 1230, 1050, 740, 780; ^{1}H NMR (300 MHz, DMSO- d_6): δ 1.582 (6H, m), 3.26 (4H, m), 6.98 (2H, d), 7.56 (3H, m), 7.64 (1H, m), 7.86 (1H, d), 7.94 (1H, s), 8.30 (1H, s), 11.70 (1H, s); ^{13}C NMR (75 MHz, DMSO- d_6): δ 24.38, 25.42, 48.81, 123.58, 126.80, 127.68, 128.97, 130.94, 131.81, 133.69, 136.13, 149.27, 152.90, 161.75; HRMS calc. for $C_{19}H_{20}ClN_3O$ 342.1373 $[M + H]^+$, found 342.1371.

*4.3.10. 2-[2-{(2,6-Dichlorophenyl)amino}phenyl]-N'-{4-(piperidin-1-yl) benzylidene} acetohydrazide **(14)***

Light purple solid; Yield 79 %; m.p. 214–216 °C; IR cm^{-1}: 3461, 3189, 3021, 2923, 2846, 1650, 1600, 1487, 1340, 1260, 1230, 1050, 760, 750; ^1H NMR (300 MHz, DMSO- d_6): δ 1.57 (6H, m), 3.26 (4H, m), 3.66 (1H, s), 4.09 (1H, s), 6.29 (1H, dd), 6.86 (1H m), 6.95 (2H, d), 7.05 (1H, q), 7.22 (2H, dt), 7.53 (4H, m), 7.85 (0.5H, s) 7.92 (0.5H, s), 8.07 (0.5H, s), 8.23 (0.5H, s), 11.41 (0.5H, s), 11.60 (0.5H, s); ^{13}C NMR (75 MHz, DMSO- d_6): δ 24.38, 25.40, 48.79, 48.89, 114.96, 115.0, 115.01, 115.14, 115.93, 116.55, 121.01, 121.30, 123.35, 123.57, 124.61, 125.41, 125.63, 126.03, 127.76, 127.90, 128.58, 12897, 129.65, 129.69, 129.88, 130.49, 130.91, 131.55, 137.42, 137.53, 143.39, 143.64, 144.98, 148.41, 152.76, 152.90, 167.84, 168.31, 172.95; HRMS calc. for $C_{26}H_{26}Cl_2N_4O$ 481.1561 $[M + H]^+$, found 481.1563.

*4.3.11. N'-{4-(Piperidin-1-yl)benzylidene}-2-{2-(trifluoromethyl)phenyl} acetohydrazide **(15)***

Purple solid; Yield 78 %; m.p. 208–210 °C; IR cm^{-1}: 3450, 3180, 3097, 2940, 2830, 1672, 1609, 1420, 1280, 1230, 1090, 760, 740; ^1H NMR (300 MHz, DMSO- d_6): δ 1.51 (6H, m), 3.20 (4H, m), 3.709 (1H, s), 4.13 (1H, s) 6.89 (2H, d), 7.45 (4H, m), 7.57 (1H, t), 7.64 (1H, d), 7.83 (0.7H, s), 8.00 (0.3H, s), 11.21 (0.7H, s), 11.34 (0.3H, s); ^{13}C NMR (75 MHz, DMSO- d_6): δ 24.37, 25.39, 36.48, 48.90, 115.04, 115.19, 123.66, 123.79, $J_{C\text{-}F}$ = 125.9(m), 127.58, 127.76, 128.37, 128.77, 132.61, 133.68, 133.83, 144.02, 147.28, 152.68, 171.31; HRMS calc. for $C_{21}H_{22}F_3N_3O$ 390.1793 $[M + H]^+$, found 390.1794.

*4.3.12. 3-Fluoro-4-methyl-N'-{4-(piperidin-1-yl)benzylidene} benzohydrazide **(16)***

Purple solid; Yield 84 %; m.p. 217–219 °C; IR cm^{-1}: 3408, 3261, 2932, 2827, 1654, 1605, 1515, 1480, 1280, 1235, 1090, 770, 745; ^1H NMR (300 MHz, DMSO- d_6): δ 1.56 (6H, m), 2.27 (3H, s) 3.23 (4H, m), 6.94 (2H, d), 7.41 (1H, t), 7.52 (2H, d), 7.64 (2H, m), 8.28 (1H, s), 11.57 (1H, s); ^{13}C NMR (75 MHz, DMSO- d_6): δ 14.67, 14.71, 24.37, 25.42, 48.84, 114.21, 114.52, 115.05, 123.68, 128.92, 132.20, 133.70, 148.99, 152.86, 159.16, 161.76, 162.39, 162.39–159.16($J^1_{C\text{-}F}$ = 242.27 Hz); HRMS calc. for $C_{20}H_{22}F_1N_3O$ 340.1825 $[M + H]^+$, found 340.1820.

*4.3.13. N'-{4-(Piperidin-1-yl)benzylidene}-2-naphthohydrazide **(17)***

Light pink solid; Yield 63 %; m.p. 228–230 °C; IR cm^{-1}: 3460, 3140, 3010, 2930, 2852, 1643, 1601, 1495, 1320, 1240, 760, 740; ^1H NMR (300 MHz, DMSO- d_6): δ 1.59 (6H, m), 3.28 (4H, m), 6.98 (2H, d), 7.57 (5H, m), 7.71 (1H, d), 8.03 (1H, m), 8.08 (1H, d), 8.19 (2H, m), 11.76 (1H, s); ^{13}C NMR (75 MHz, DMSO- d_6): δ 24.39, 25.45, 48.81, 114.99, 115.05, 123.67, 125.48, 125.64, 126.17, 126.87, 127.46, 128.80, 128.92, 130.45, 130.73, 133.61, 148.47, 152.85, 164.77; HRMS calc. for $C_{23}H_{23}N_3O$ 358.1919 $[M + H]^+$, found 358.1915.

*4.3.14. 3-Hydroxy-N'-{4-(piperidin-1-yl)benzylidene}-2-naphthohydrazide **(18)***

Light brown solid; Yield 77 %; m.p. 259–261 °C; IR cm^{-1}: 3463, 3210, 3120, 2930, 2840, 1640, 1600, 1495, 1475, 1240, 760, 740; ^1H NMR (300 MHz, DMSO- d_6): δ 1.58 (6H, m), 3.28 (4H, m), 6.98 (2H, d), 7.33 (1H, m), 7.36 (1H, d), 7.50 (1H, t), 7.57 (2H, d), 7.77(1H, d), 7.90 (1H, d), 8.32 (1H, s), 8.46 (1H, s), 11.46 (1H, s), 11.81 (1H, s); ^{13}C NMR (75 MHz, DMSO- d_6): δ 24.39, 25.42, 48.78, 111.03, 115.00, 120.42, 123.46, 124.24, 126.30, 127.2, 128.66, 129.10, 130.41, 136.26, 149.56, 152.95, 154.83, 164.0; HRMS calc. for $C_{23}H_{23}N_3O_2$ 374.1868 $[M + H]^+$, found 374.1866.

*4.3.15. 3-Hydroxy-N'-{4-(4-methylpiperazin-1-yl)benzylidene}-2-naphthohydrazide **(19)***

Yellow solid; Yield 80 %; m.p. 274–276 °C; IR cm^{-1}: 3460, 3120, 3065, 2940, 2848, 2828 1660, 1600, 1240, 780, 750; ^1H NMR (300 MHz, DMSO- d_6): δ 2.247 (3H, s), 2.47 (4H, t), 3.28 (4H, t), 7.02 (2H, d), 7.32 (1H, s), 7.37 (1H, m), 7.52 (1H, t), 7.62, (2H, d), 7.76 (1H, d), 7.91 (1H, d), 8.34 (1H, s), 8.47 (1H, s), 11.90 (1H, s); ^{13}C NMR (75 MHz, DMSO- d_6): δ 31.16, 46.12, 47.42, 54.82, 111.02, 114.96, 117.90, 120.56, 124.21, 126.27, 127.33, 129.00, 129.11, 136.27, 149.46, 152.67, 154.85, 164.01; HRMS calc. for $C_{23}H_{24}N_4O_2$ 389.1977 $[M + H]^+$, found 389.1977.

*4.3.16. 2-[2-{(2,6-Dichlorophenyl)amino}phenyl]-N'-{4-(4-methylpiperazin-1-yl)benzylidene} acetohydrazide **(20)***

Yellow solid; Yield 86 %; m.p. 202–204 °C; IR cm^{-1}: 3460, 3271, 3180, 3026, 2905, 2814, 1659, 1604, 1255, 780, 750; ^1H NMR (300 MHz, DMSO- d_6): δ 2.18 (3H, s), 2.40 (4H, t), 3.20 (4H, t), 3.63 (1H, s), 4.06 (1H, s), 6.26 (1H, dd), 6.88 (1H, m), 6.94, (2H, m), 7.04 (1H, m), 7.15 (1H, t), 7.22 (1H, t), 7.50 (4H, m), 7.80 (0.5H, s), 7.89 (0.5H, s), 8.05 (0.5H, s), 8.18 (0.5H, s), 11.40 (0.5H, s) 11.58 (0.5H, s); ^{13}C NMR (75 MHz, DMSO- d_6): δ 36.16, 46.20, 47.48, 54.85, 114.89, 115.96, 116.55, 121.01, 121.30, 124.0, 124.28, 124.61, 125.40, 125.65, 126.03, 127.76, 127.91, 128.51, 128.88, 129.66, 129.69, 129.90, 130.48, 130.92, 131.56, 137.43, 137.53, 143.39, 143.63, 144.86, 148.30, 152.48, 152.63, 167.88, 172.99; HRMS calc. for $C_{26}H_{27}Cl_2N_5O$ 496.1670 $[M + H]^+$, found 496.1671.

*4.3.17. 3-Chloro-N'-{4-(4-methylpiperazin-1-yl)benzylidene} benzohydrazide **(21)***

Yellow solid; Yield 67 %; m.p. 230–232 °C; IR cm^{-1}: 3417, 3172, 2962, 2952, 2822, 1664, 1608, 1520, 778, 747; ^1H NMR (300 MHz, DMSO- d_6): δ 2.217 (3H, s), 2.43 (4H, t), 3.24 (4H, t), 7.01 (2H, d), 7.55 (3H, m), 7.65 (1H, d), 7.87 (1H, d), 7.94 (1H, d), 8.31 (1H, s), 11.71 (1H, s); ^{13}C NMR (75 MHz, DMSO- d_6): δ 46.20, 47.49, 54.87, 114.94, 124.27, 126.82, 127.69, 128.88, 130.95, 131.84, 133.69, 136.12, 149.14, 152.64, 161.78; HRMS calc. for $C_{19}H_{21}Cl_1N_4O$ 357.1482 $[M + H]^+$, found 357.1489.

*4.3.18. N'-{4-(4-Methylpiperazin-1-yl)benzylidene}isonicotinohydrazide **(22)***

Yellow solid; Yield 66 %; m.p. 249–251 °C; IR cm^{-1}: 3404, 3145, 2952, 2823, 1665, 1609, 1557, 1270, 762; ^1H NMR (300 MHz, DMSO- d_6): δ 2.216 (3H, s), 2.43 (4H, t), 3.25 (4H, t), 6.99 (2H, d), 7.57 (2H, d), 7.79 (2H, d), 8.32 (1H, s), 8.77 (2H, d), 11.85 (1H, s); ^{13}C NMR (75 MHz, DMSO- d_6): δ 46.17, 47.42, 54.83, 114.91, 121.96, 124.04, 129.02, 141.17, 149.84, 150.73, 152.74, 161.69; HRMS calc. for $C_{18}H_{21}N_5O$ 324.1824 $[M + H]^+$, found 324.1821.

*4.3.19. N'-{4-(4-Methylpiperazin-1-yl)benzylidene}-2-{2-(trifluoromethyl)phenyl}acetohydrazide **(23)***

Yellow solid; Yield 67 %; m.p. 247–249 °C; IR cm^{-1}: 3459, 3180, 3088, 2941, 2822, 1670, 1607, 1370, 1080, 757; ^1H NMR (300 MHz, DMSO- d_6): δ 2.211 (3H, s), 2.42 (4H, t), 3.21 (4H, t), 3.76 (1H, s), 4.19 (1H, s) 6.96 (2H, d), 7.50 (4H, m), 7.65 (2H, m), 7.90 (0.7H, s), 8.07 (0.3H, s), 11.29 (0.7H, s), 11.41 (0.3H, s); ^{13}C NMR (75 MHz, DMSO- d_6): δ 36.49, 46.18, 47.52, 47.60 114.95, 115.08, 124.39, 124.49, $J_{C\text{-}F}$ = 125.9(m), 127.93, 128.29, 128.68, 132.62, 133.67, 133.83, 143.89, 152.36, 152.47; HRMS calc. for $C_{21}H_{23}F_3N_4O$ 405.1902 $[M + H]^+$, found 405.1890.

4.4. In vitro α-glucosidase inhibition assay

The assay of inhibition of EC 3.2.1.20 enzyme was done by using pH 6.8 phosphate buffer (0.05 M) while keeping temperature 37℃ [60]. With different concentrations of substances (dissolved in DMSO) being tested, enzyme (2 units/ 2 mL) was kept at incubation at said temperature for 15 min in phosphate buffer. p-Nitro phenyl- α-D-glucopyranoside (0.7 mM) was then added and by using spectrophotometer, the absorbance variation at 400 nm was measured for 30 min. The compounds that were being tested were then substituted with DMSO- d_6 (7.5 %) (control experiment). Acarbose was used as a standard inhibitor. The kinetic study was conducted under consistent conditions, varying only

the substrate concentration, for the mechanistic study at four levels: 0.1, 0.2, 0.4, and 0.8 mM.

4.5. Statistical analysis

Excel and the SoftMax Pro package were used as applications to examine the results obtained for biological activity. Percent inhibition was calculated using the formula below.

$$\%Inhibition = 100 - \left(\frac{O.D_{test\ compound}}{O.D_{control}}\right) \times 100 \quad (1)$$

For all the identified inhibitors, EZ-FIT (Perrella Scientific, Inc., USA) was utilized to calculate the IC50. All experiments were conducted in triplicate to account for predicted mistakes, and Standard Error of Mean Values (SEM) is used to report variances in the results.

$$SE = \frac{\sigma}{\sqrt{n}} \quad (2)$$

To avoid errors, triplicate tests were done.

4.6. Molecular docking study

Molecular docking is vital for identifying interactions & potential binding sites between target molecules & proteins. This computational technique seeks an optimal conformation that minimizes the system's free energy. By predicting how a molecule interacts with a target protein, it aids in the design and development of new therapeutic agents by highlighting the most promising structures for further investigation [61]. AutoDockTools 1.5.6 software was used to accomplish docking studies [62]. The docking study used α-glucosidase and α-amylase target proteins with PDB IDs: 3A4A and 1B2Y. Docking study was achieved with identical coordinates of co-crystalized ligand with proteins. Detailed docking methodology is provided in the supplementary information file.

4.7. In vitro α-amylase inhibition assay

The method documented by Xiao et al. [63] was used to investigate the inhibitory effects of new compounds on α-amylase. This paper describes making a starch solution by dissolving 6 g in 240 mL of 0.4 M NaOH and heating it to 70 °C for 25 min. Additionally, after cooling in cold water, the pH of the solution was adjusted to 6.9 using 2.0 M HCl, and 300 mL of H2O was added. Five milligrams were dissolved in five milliliters of EtOH: H2O to create the sample solutions. Some PB solutions were made in case the entire enzyme was inhibited. After mixing the substrate (50 μL), PB solution (pH 6.9), and sample (5–200 μL) solutions, they were pre-incubated for 30 min at 37 °C. After that, 10 μL of an enzyme solution containing 50 μg/mL was added. For thirty minutes, the solution was incubated. At 580 nm, the absorbances were determined using spectrophotometry. The amount of α-amylase enzyme required to liberate 1.0 mg of maltose from starch in 3 min at pH 6.9 and 20 °C equals one unit [64].

4.8. QSAR analysis

The QSAR analysis was performed using the 'QSARINS'. The methodology was followed as per our earlier reported work [55,56].

4.9. In-Silico ADMET analysis

The in-silico pharmacokinetics analysis was made using the 'SwissADME' website, accessed on: 01-06-2024, via [https://www.swissadme.ch/] [55,56].

CRediT authorship contribution statement

Rehmatullah Farooqi: Methodology, Data curation, Conceptualization. **Saeed Ullah:** Software, Methodology, Investigation. **Ajmal Khan:** Writing – original draft, Project administration, Formal analysis. **Shailesh S. Gurav:** Methodology, Investigation. **Suraj N. Mali:** Writing – original draft, Investigation. **Hina Aftab:** Investigation, Data curation. **Mohammad Khalid Al-Sadoon:** Investigation, Funding acquisition, Formal analysis. **Ming-Hua Hsu:** Investigation, Data curation. **Parham Taslimi:** Investigation, Validation. **Ahmed Al-Harrasi:** Writing – review & editing, Conceptualization. **Zahid Shafiq:** Writing – review & editing, Conceptualization. **Silvia Schenone:** Writing – review & editing, Writing – original draft, Supervision.

Declaration of competing interest

The authors declare that they have no known competing financial interests or personal relationships that could have appeared to influence the work reported in this paper.

Acknowledgements

The authors would like to extend their sincere appreciation to the Researchers Supporting Project Number (RSP2025R410), King Saud University, Riyadh, Saudi Arabia.

Appendix A. Supplementary data

Supplementary data to this article can be found online at https://doi.org/10.1016/j.bioorg.2025.108155.

Data availability

The data that has been used is confidential.

References

[1] N. Sakran, Y. Graham, T. Pintar, W. Yang, R. Kassir, E.M. Willigendael, R. Singhal, Z.E. Kooreman, D. Ramnarain, K. Mahawar, The many faces of diabetes. Is there a need for re-classification? A narrative review, BMC Endocr. Disord. 22 (2022) 1–12.

[2] S. Safiri, N. Karamzad, J.S. Kaufman, A.W. Bell, S.A. Nejadghaderi, M.J. Sullman, M. Moradi-Lakeh, G. Collins, A.-A. Kolahi, Prevalence, deaths and disability-adjusted-life-years (DALYs) due to type 2 diabetes and its attributable risk factors in 204 countries and territories, 1990-2019: results from the global burden of disease study 2019, Front. Endocrinol. 13 (2022) 838027.

[3] H.K. Thabet, Y.A. Ammar, M. Imran, M.H. Helal, S.I. Alaqel, A. Alshehri, A. A. Mohd, M.S. Abusaif, A. Ragab, Unveiling anti-diabetic potential of new thiazole-sulfonamide derivatives: Design, synthesis, in vitro bio-evaluation targeting DPP-4, α-glucosidase, and α-amylase with in-silico ADMET and docking simulation, Bioorg. Chem. 151 (2024) 107671.

[4] S. Imran, M. Taha, N.H. Ismail, S.M. Kashif, F. Rahim, W. Jamil, M. Hariono, M. Yusuf, H. Wahab, Synthesis of novel flavone hydrazones: In-vitro evaluation of α-glucosidase inhibition, QSAR analysis and docking studies, Eur. J. Med. Chem. 105 (2015) 156–170.

[5] A. Singh, K. Singh, A. Sharma, K. Kaur, K. Kaur, R. Chadha, P.M.S. Bedi, Recent developments in synthetic α-glucosidase inhibitors: A comprehensive review with structural and molecular insight, J. Mol. Struct. 1281 (2023) 135115.

[6] X. Qu, X. Pan, J. Weidner, W. Yu, D. Alonzi, X. Xu, T. Butters, T. Block, J.-T. Guo, J. Chang, Inhibitors of endoplasmic reticulum α-glucosidases potently suppress hepatitis C virus virion assembly and release, Antimicrob. Agents Chemother. 55 (3) (2011) 1036–1044.

[7] J. Chang, W. Schul, T.D. Butters, A. Yip, B. Liu, A. Goh, S.B. Lakshminarayana, D. Alonzi, G. Reinkensmeier, X. Pan, Combination of α-glucosidase inhibitor and ribavirin for the treatment of dengue virus infection in vitro and in vivo, Antiviral Res. 89 (1) (2011) 26–34.

[8] Y. Wei, S. Xu, Z. Wu, M. Zhang, M. Bao, B. He, Exploring the causal relationships between type 2 diabetes and neurological disorders using a Mendelian randomization strategy, Medicine 103 (46) (2024) e40412, https://doi.org/10.1097/MD.0000000000040412.

[9] N. Asano, Glycosidase inhibitors: update and perspectives on practical use, Glycobiology 13 (10) (2003) 93R–104R.

[10] N. Agrawal, M. Sharma, S. Singh, A. Goyal, Recent advances of α-glucosidase inhibitors: A comprehensive review, Curr. Top. Med. Chem. 22 (25) (2022) 2069–2086.

[11] Y.-J. Shim, H.-K. Doo, S.-Y. Ahn, Y.-S. Kim, J.-K. Seong, I.-S. Park, B.-H. Min, Inhibitory effect of aqueous extract from the gall of Rhus chinensis on alpha-glucosidase activity and postprandial blood glucose, J. Ethnopharmacol. 85 (2–3) (2003) 283–287.

[12] H. Park, K.Y. Hwang, K.H. Oh, Y.H. Kim, J.Y. Lee, K. Kim, Discovery of novel α-glucosidase inhibitors based on the virtual screening with the homology-modeled protein structure, Bioorg. Med. Chem. 16 (1) (2008) 284–292.

[13] S.J. Storr, L. Royle, C.J. Chapman, U.M.A. Hamid, J.F. Robertson, A. Murray, R. A. Dwek, P.M. Rudd, The O-linked glycosylation of secretory/shed MUC1 from an advanced breast cancer patient's serum, Glycobiology 18 (6) (2008) 456–462.

[14] U. Hossain, A.K. Das, S. Ghosh, P.C. Sil, An overview on the role of bioactive α-glucosidase inhibitors in ameliorating diabetic complications, Food Chem. Toxicol. 145 (2020) 111738.

[15] J. Leroux-Stewart, R. Rabasa-Lhoret, J.L. Chiasson, α-Glucosidase inhibitors, International Textbook of Diabetes Mellitus (2015) 673–685.

[16] Rosak, C.; Mertes, G. Critical evaluation of the role of acarbose in the treatment of diabetes: patient considerations. Diabetes, metabolic syndrome and obesity: targets and therapy **2012**, 357-367.

[17] H. Wang, Y. Shen, L. Zhao, Y. Ye, 1-Deoxynojirimycin and its derivatives: A mini review of the literature, Curr. Med. Chem. 28 (3) (2021) 628–643.

[18] A.S. Dabhi, N.R. Bhatt, M.J. Shah, Voglibose: an alpha glucosidase inhibitor, J. Clin. Diagn. Res. 7 (12) (2013) 3023.

[19] N. Tiwari, A.K. Thakur, V. Kumar, A. Dey, V. Kumar, Therapeutic targets for diabetes mellitus: an update, Clin Pharmacol Biopharm 3 (1) (2014) 1.

[20] M. Fisher, Acarbose and alpha glucosidase inhibitors, Diabetes Drug Notes (2022) 229–238.

[21] P. Patel, D. Shah, T. Bambharoliya, V. Patel, M. Patel, D. Patel, V. Bhavsar, S. Padhiyar, B. Patel, A. Mahavar, A Review on the Development of Novel Heterocycles as α-Glucosidase Inhibitors for the Treatment of Type-2 Diabetes Mellitus, Med. Chem. 20 (5) (2024) 503–536.

[22] S. Naseem, S. Fatima, S. Ullah, A. Khan, S.N. Mali, R.D. Jawarkar, A. Syed, A. M. Elgorban, A. Al-Harrasi, Z. Shafiq, Carbonylbis (hydrazine-1-carbothioamide) derivatives as a new class of α-glucosidase inhibitors and their mechanistic insights via molecular docking and dynamic simulations, Arch. Pharm. 357 (3) (2024) 2300604.

[23] D.-S. Lee, J.-K. Woo, D.-H. Kim, M.-Y. Kim, S.-M.-K. Cho, J.-H. Kim, S.-P. Park, H.-Y. Lee, K.Z. Riu, D.-S. Lee, Antiviral Activity of Methylelaiophylin, an ${\alpha} $-Glucosidase Inhibitor, J. Microbiol. Biotechnol. 21 (3) (2011) 263–266.

[24] H.K. Thabet, M.S. Abusaif, M. Imran, M.H. Helal, S.I. Alaqel, A. Alshehri, A. A. Mohd, Y.A. Ammar, A. Ragab, Discovery of novel 6-(piperidin-1-ylsulfonyl)-2H-chromenes targeting α-glucosidase, α-amylase, and PPAR-γ: Design, synthesis, virtual screening, and anti-diabetic activity for type 2 diabetes mellitus, Comput. Biol. Chem. 111 (2024) 108097.

[25] M. Saeedi, A. Hadjiakhondi, S. Mohammad Nabavi, A. Manayi, Heterocyclic compounds: effective α-amylase and α-glucosidase inhibitors, Curr. Top. Med. Chem. 17 (4) (2017) 428–440.

[26] L. Kang, X. Gao, H. Liu, X. Men, H. Wu, P. Cui, J. Yan, Structure–activity relationship investigation of coumarin–chalcone hybrids with diverse side-chains as acetylcholinesterase and butyrylcholinesterase inhibitors, Molecular Diversity 22 (4) (2018) 893–906, https://doi.org/10.1007/s11030-018-9839-y.

[27] M. Mahdavi, K. Pedrood, M. Safavi, M. Saeedi, M. Pordeli, S.K. Ardestani, S. Emami, M. Adib, A. Foroumadi, A. Shafiee, Synthesis and anticancer activity of N-substituted 2-arylquinazolinones bearing trans-stilbene scaffold, Eur. J. Med. Chem. 95 (2015) 492–499.

[28] a) Y. Tian, D. Du, D. Rai, L. Wang, H. Liu, P. Zhan, E. De Clercq, C. Pannecouque, X. Liu, Fused heterocyclic compounds bearing bridgehead nitrogen as potent HIV-1 NNRTIs. Part 1: design, synthesis and biological evaluation of novel 5, 7-disubstituted pyrazolo [1, 5-a] pyrimidine derivatives, Bioorg. Med. Chem. 22 (7) (2014) 2052–2059;
b) J. Duan, C. Wang, Y. Yuan, Z. Hui, H. Zhang, N. Mao, X. Ye, Design, Synthesis, and Structure-Activity Relationship of Novel Pyridazinone-Based PARP7/HDACs Dual Inhibitors for Elucidating the Relationship between Antitumor Immunity and HDACs Inhibition, Journal of Medicinal Chemistry 67 (6) (2024) 4950–4976, https://doi.org/10.1021/acs.jmedchem.4c00090.

[29] A. Gomtsyan, Heterocycles in drugs and drug discovery, Chem. Heterocycl. Compd. 48 (2012) 7–10.

[30] S.N. Meena, M.S. Majik, S.C. Ghadi, S.G. Tilve, Quick identification of piperidine alkaloid from roots of Grewia nervosa and their glucosidase inhibitory activity, Chem. Biodivers. 14 (12) (2017) e1700400.

[31] A. Hernández-Guadarrama, M.A. Díaz-Román, I. Linzaga-Elizalde, B.E. Domínguez-Mendoza, A.B. Aguilar-Guadarrama, In Silico Analysis: Anti-Inflammatory and α-Glucosidase Inhibitory Activity of New α-Methylene-γ-Lactams, Molecules 29 (9) (2024) 1973.

[32] A. Kato, E. Hayashi, S. Miyauchi, I. Adachi, T. Imahori, Y. Natori, Y. Yoshimura, R. J. Nash, H. Shimaoka, I. Nakagome, α-1-C-Butyl-1, 4-dideoxy-1, 4-imino-l-arabinitol as a second-generation iminosugar-based oral α-glucosidase inhibitor for improving postprandial hyperglycemia, J. Med. Chem. 55 (23) (2012) 10347–10362.

[33] M. Özil, C. Parlak, N. Baltaş, A simple and efficient synthesis of benzimidazoles containing piperazine or morpholine skeleton at C-6 position as glucosidase inhibitors with antioxidant activity, Bioorg. Chem. 76 (2018) 468–477.

[34] M. Albratty, Quantitative structure–activity relationship modeling and docking of some synthesized bioactive oxopyrolidines against Staphylococcus aureus, J. Saudi Chem. Soc. 26 (4) (2022) 101509.

[35] P. Vicini, M. Incerti, P. La Colla, R. Loddo, Anti-HIV evaluation of benzo [d] isothiazole hydrazones, Eur. J. Med. Chem. 44 (4) (2009) 1801–1807.

[36] P. Vicini, M. Incerti, I.A. Doytchinova, P. La Colla, B. Busonera, R. Loddo, Synthesis and antiproliferative activity of benzo [d] isothiazole hydrazones, Eur. J. Med. Chem. 41 (5) (2006) 624–632.

[37] H. Zhou, Q.X. Li, L. Zeng, C. Cao, T. Zhang, Y. Zhou, H. He, Uracil hydrazones: design, synthesis, antimicrobial activities, and putative mode of action, Pest Manag. Sci. 80 (2) (2024) 414–425.

[38] S.S. Shah, D. Shah, I. Khan, S. Ahmad, U. Ali, A. Rahman, Synthesis and antioxidant activities of Schiff bases and their complexes: An updated review, Biointerface Res. Appl. Chem 10 (6) (2020) 6936–6963.

[39] F. Rahim, H. Ullah, R. Hussain, M. Taha, S. Khan, M. Nawaz, F. Nawaz, S.J. Gilani, M.N.B. Jumah, Thiadiazole based triazole/hydrazone derivatives: Synthesis, in vitro α-glucosidase inhibitory activity and in silico molecular docking study, J. Mol. Struct. 1287 (2023) 135619.

[40] S.U. Khan, A. Ashraf, M. Ashraf, M. Rafiq, K. Mahmood, M.N. Tahir, Z. Shafiq, Xanthenone-based hydrazones as potent α-glucosidase inhibitors: Synthesis, solid state self-assembly and in silico studies, Bioorg. Chem. 84 (2019) 372–383.

[41] M. Tasleem, S. Ullah, S.A. Halim, I. Urooj, N. Ahmed, R. Munir, A. Khan, A.F. El-kott, P. Taslimi, S. Negm, Synthesis of 3-hydroxy-2-naphthohydrazide-based hydrazones and their implications in diabetic management via in vitro and in silico approaches, Arch. Pharm. 357 (2) (2024) 2300544.

[42] G. Wang, M. Chen, J. Wang, Y. Peng, L. Li, Z. Xie, B. Deng, S. Chen, W. Li, Synthesis, biological evaluation and molecular docking studies of chromone hydrazone derivatives as α-glucosidase inhibitors, Bioorg. Med. Chem. Lett. 27 (13) (2017) 2957–2961.

[43] S. Khan, M. Tariq, M. Ashraf, S. Abdullah, M. Al-Rashida, M. Khalid, P. Taslimi, M. Fatima, R. Zafar, Z. Shafiq, Probing 2-acetylbenzofuran hydrazones and their metal complexes as α-glucosidase inhibitors, Bioorg. Chem. 102 (2020) 104082.

[44] Ahmad, M. U.; Rafiq, M.; Zahra, B.; Islam, M.; Ashraf, M.; al-Rashida, M.; Khan, A.; Hussain, J.; Shafiq, Z.; Al-Harrasi, A. Synthesis of benzimidazole based hydrazones as non-sugar based α-glucosidase inhibitors: Structure activity relation and molecular docking. Drug Development Research **2021**, 82 (7), 1033-1043.

[45] A. Ragab, M.S. Abusaif, D.S. Aboul-Magd, M.M. Wassel, G.A. Elhagali, Y.A. Ammar, A new exploration toward adamantane derivatives as potential anti-MDR agents: Design, synthesis, antimicrobial, and radiosterilization activity as potential topoisomerase IV and DNA gyrase inhibitors, Drug Dev. Res. 83 (6) (2022) 1305–1330.

[46] D.M. Elsisi, A. Ragab, A.A. Elhenawy, A.A. Farag, A.M. Ali, Y.A. Ammar, Experimental and theoretical investigation for 6-Morpholinosulfonylquinoxalin-2 (1H)-one and its haydrazone derivate: Synthesis, characterization, tautomerization and antimicrobial evaluation, J. Mol. Struct. 1247 (2022) 131314.

[47] MARkANDEwAR, R. A.; Zia, H. M.; Baseer, M. Impact of reaction dynamics on synthesis of novel nitrogen containing aldehydes. Oriental Journal of Chemistry **2013**, 29 (4), 1531-1534.

[48] M. Tasleem, J. Pelletier, J. Sévigny, Z. Hussain, A. Khan, A. Al-Harrasi, A.F. El-Kott, P. Taslimi, S. Negm, Z. Shafiq, Synthesis, in vitro, and in silico studies of morpholine-based thiosemicarbazones as ectonucleotide pyrophosphatase/phosphodiesterase-1 and-3 inhibitors, Int. J. Biol. Macromol. 266 (2024) 131068.

[49] P. Tisovský, K. Csicsai, J. Donovalová, R. Šandrik, R. Sokolík, A. Gáplovský, Effect of a= X-NH-Fragment,(X= C, N), on Z/E Isomerization and ON/OFF Functionality of Isatin Arylhydrazones,((Arylamino) methylene) indolin-2-ones and Their Anions, Molecules 25 (13) (2020) 3082.

[50] I. Tumosienė, K. Kantminienė, A. Klevinskas, V. Petrikaitė, I. Jonuškienė, V. Mickevičius, Antioxidant and anticancer activity of novel derivatives of 3-[(4-methoxyphenyl) amino] propanehydrazide, Molecules 25 (13) (2020) 2980.

[51] Pinheiro, P. d. S. M.; Franco, L. S.; Fraga, C. A. M. The Magic Methyl and Its Tricks in Drug Discovery and Development. Pharmaceuticals **2023**, 16 (8), 1157.

[52] D. Aynetdinova, M.C. Callens, H.B. Hicks, C.Y. Poh, B.D. Shennan, A.M. Boyd, Z. H. Lim, J.A. Leitch, D.J. Dixon, Installing the "magic methyl"–C–H methylation in synthesis, Chem. Soc. Rev. 50 (9) (2021) 5517–5563.

[53] S. Fernández-Tomé, T.J. Ashaolu, B. Hernández-Ledesma, Exploration of the nutritional and functional properties of underutilized grains as an alternative source for the research of food-derived bioactive peptides, Nutrients 15 (2) (2023) 351.

[54] I.A. Khan, M. Ahmad, U.A. Ashfaq, S. Sultan, M.E. Zaki, Discovery of amide-functionalized benzimidazolium salts as potent α-glucosidase inhibitors, Molecules 26 (16) (2021) 4760.

[55] R.D. Alharthy, S. Khalid, S. Fatima, S. Ullah, A. Khan, S.N. Mali, R.D. Jawarkar, S. S. Dhabarde, H. Kashtoh, P. Taslimi, Synthesis of the chromone-thiosemicarbazone scaffold as promising α-glucosidase inhibitors: An in vitro and in silico approach toward antidiabetic drug design, Arch. Pharm. (2024) e2400140.

[56] R. Basri, S. Ullah, A. Khan, S.N. Mali, O. Abchir, S. Chtita, A. El-Gokha, P. Taslimi, A.Y. Binsaleh, A.F. El-Kott, Synthesis, biological evaluation and molecular modelling of 3-Formyl-6-isopropylchromone derived thiosemicarbazones as α-glucosidase inhibitors, Bioorg. Chem. 139 (2023) 106739.

[57] O.A. Lotlikar, S.S. Gurav, S.N. Dandekar, S.R. Jadhav, A.B. Shaik, R.R. Bhandare, S. N. Mali, Microwave and ultrasound assisted green protocols for 5-methylthiazole induced Betti bases: molecular docking, in-silico pharmacokinetics, and anticancer activity studies, Green Chem. Lett. Rev. 17 (1) (2024) 2403608.

[58] S.R. Jadhav, S.S. Gurav, H. Yasin, P. Nagpal, S.N. Mali, Imidazo [1, 2-a] pyridine-appended chalcone and Schiff base conjugates: synthetic, spectrophotometric, biological, and computational aspects, Chem. Phys. Impact 9 (2024) 100694.

[59] H. Aftab, S. Ullah, A. Khan, M. Al-Rashida, T. Islam, K.A. Dahlous, S. Mohammad, H. Kashtoh, A. Al-Harrasi, Z. Shafiq, Design, synthesis, in vitro and in silico studies of novel piperidine derived thiosemicarbazones as inhibitors of dihydrofolate reductase, Sci. Rep. 14 (1) (2024) 22645.

[60] A.R. Pasha, A. Khan, S. Ullah, S.A. Halim, J. Hussain, M. Khalid, M.M. Naseer, A. F. El-kott, S. Negm, A. Al-Harrasi, et al., Synthesis of new diphenyl urea-clubbed imine analogs and its Implications in diabetic management through in vitro and in silico approaches, Sci. Rep. 13 (1) (2023) 1877.
[61] S.S. Gurav, K.T. Waghmode, S.N. Dandekar, S.D. Jadhav, O.A. Lotlikar, S. R. Jadhav, S.N. Mali, J.G. Naphade, New 2-Chloroimidazo [1, 2-a] pyridine induced Schiff bases: Synthesis, characterization, antimicrobial and A-498 and A-549 anticancer activity, molecular modeling, in-silico pharmacokinetics, and DFT studies, Chem. Phys. Impact 8 (2024) 100494.
[62] O. Trott, A.J. Olson, AutoDock Vina: Improving the speed and accuracy of docking with a new scoring function, efficient optimization, and multithreading, J. Comput. Chem. 31 (2) (2010) 455–461.
[63] Z. Xiao, R. Storms, A. Tsang, A quantitative starch? Iodine method for measuring alpha-amylase and glucoamylase activities, Anal. Biochem. 351 (2006) 146–148.
[64] A. Sujayev, N. Sadeghian, P. Taslimi, N. Kılınç, M. Akkuş, B. Özçelik, İ. Gülçin, Functionally substituted derivatives of novel thiourea and phenylthiourea as potent aldose reductase, α-amylase, and α-glycosidase inhibitors: in vitro and in silico studies, Macromol. Res. (2024) 1–15.

Spectral Data: H^1, ^{13}CNMR & HRMS of Compound 5

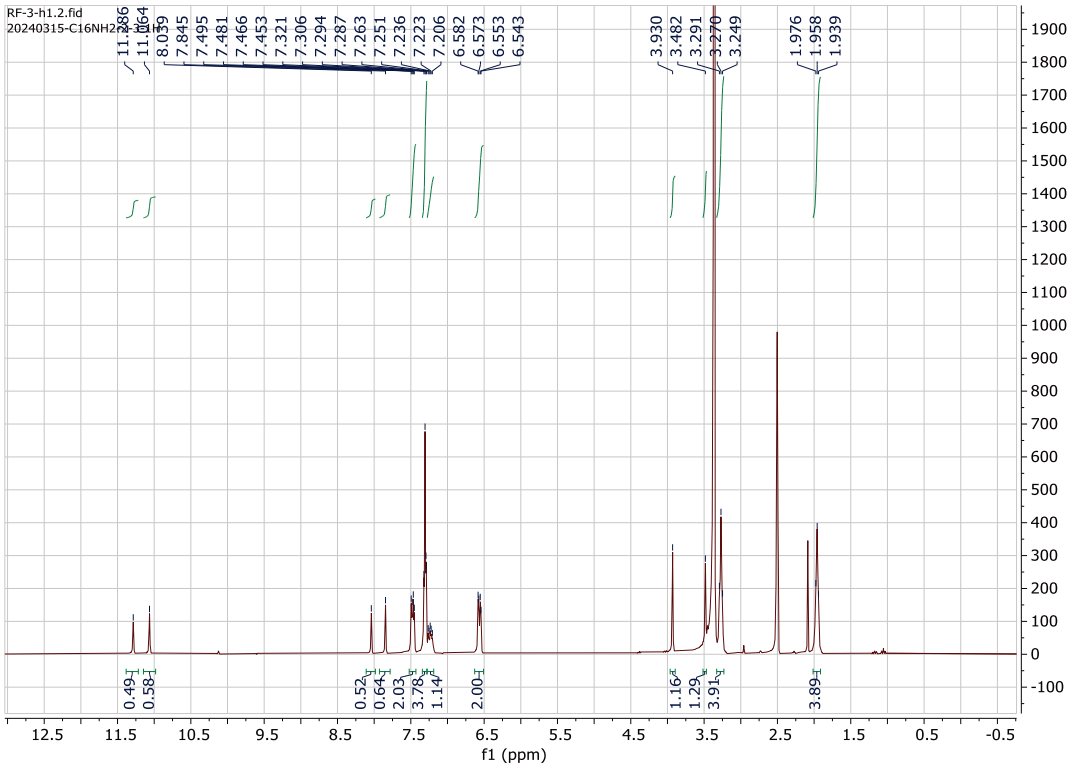

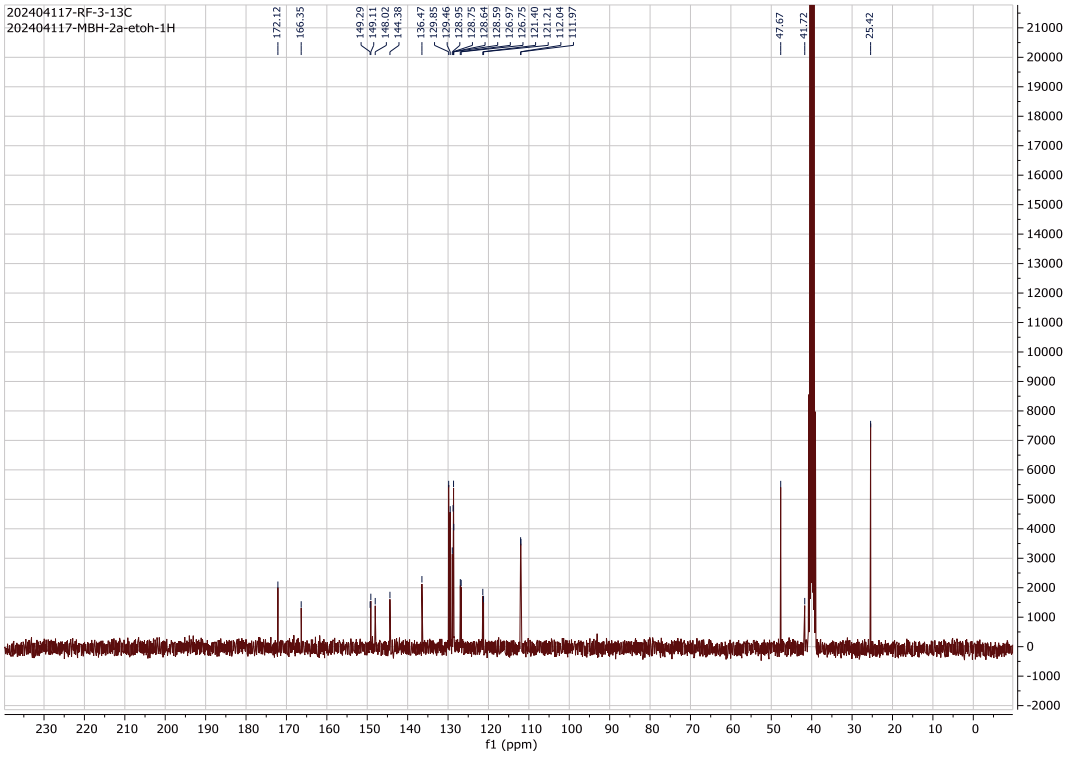

Data:RF-4
Comment:
Description:
Ionization Mode:ESI+
History:Average(MS[1] 0.12..0.23)

Acquired:5/15/2024 5:01:27 PM
Operator:AccuTOF
m/z Calibration File:20240515-TFANa_...
Created:12:00:00 AM
Created by:

Charge number:1 Tolerance:400.00[ppm], 400.00 .. 400.... Unsaturation Number:-300.5 .. 300.0 (...
Element:^{12}C:19 .. 19, ^{1}H:10 .. 22, ^{14}N:3 .. 3, ^{23}Na:0 .. 2, ^{16}O:1 .. 1

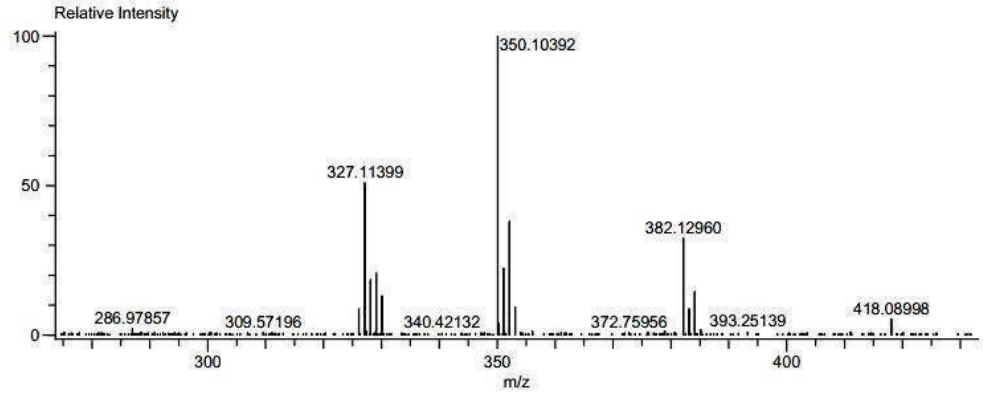

H[1], [13]CNMR & HRMS of Compound 6

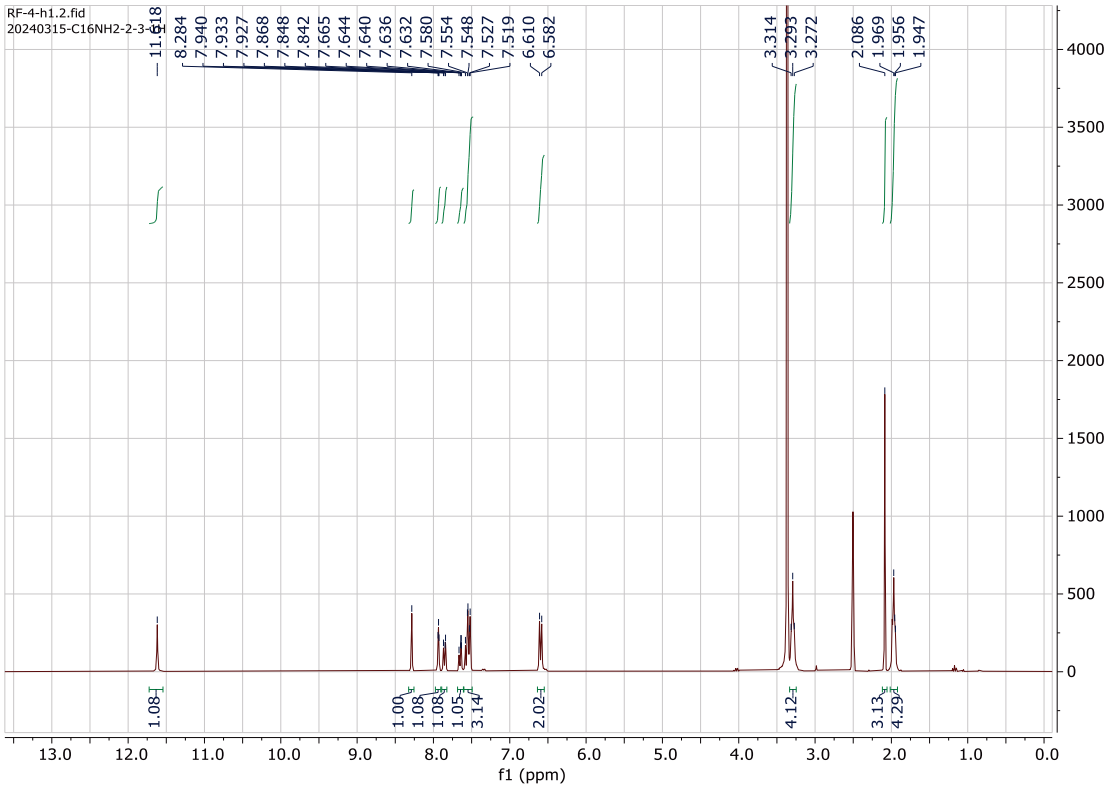

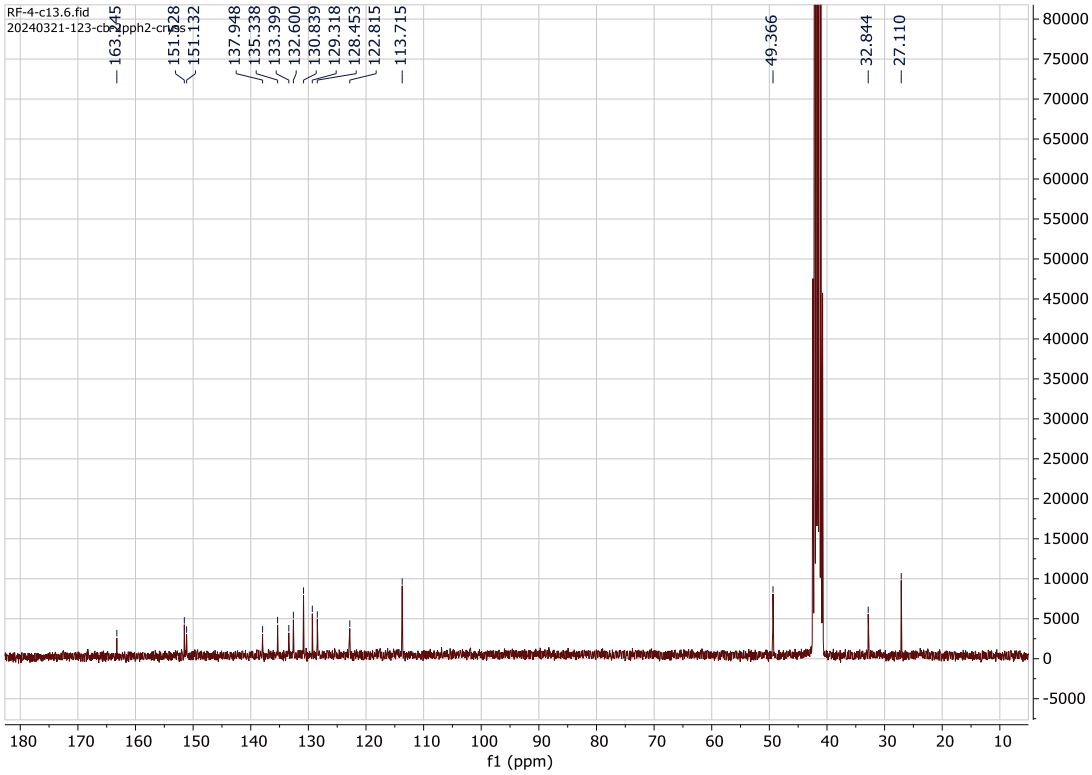

Data:RF-3
Comment:
Description:
Ionization Mode:ESI+
History:Average(MS[1] 0.18..0.20)

Acquired:5/15/2024 4:33:34 PM
Operator:AccuTOF
m/z Calibration File:20240515-TFANa_...
Created:5/16/2024 11:11:53 AM
Created by:AccuTOF

Charge number:1
Tolerance:400.00[ppm], 400.00 .. 400....
Unsaturation Number:-300.5 .. 300.0 (...
Element:^{12}C:19 .. 19, ^{1}H:10 .. 22, ^{14}N:3 .. 3, ^{23}Na:0 .. 2, ^{16}O:1 .. 1

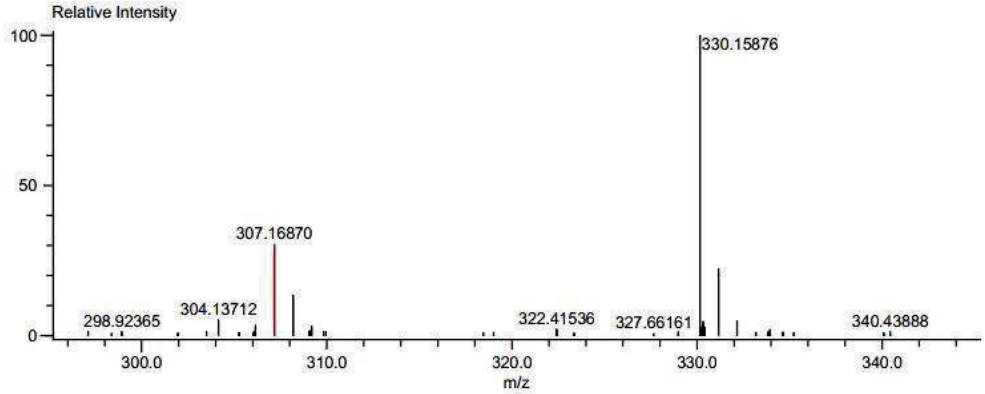

Mass	Intensity	Calc. Mass	Mass Difference [mDa]	Mass Difference [ppm]	Possible Formula
307.16870	5957.10	307.16846	0.24	0.77	$^{12}C_{19}{}^{1}H_{21}{}^{14}N_{3}{}^{16}O_{1}$

H[1], [13]CNMR & HRMS of Compound 7

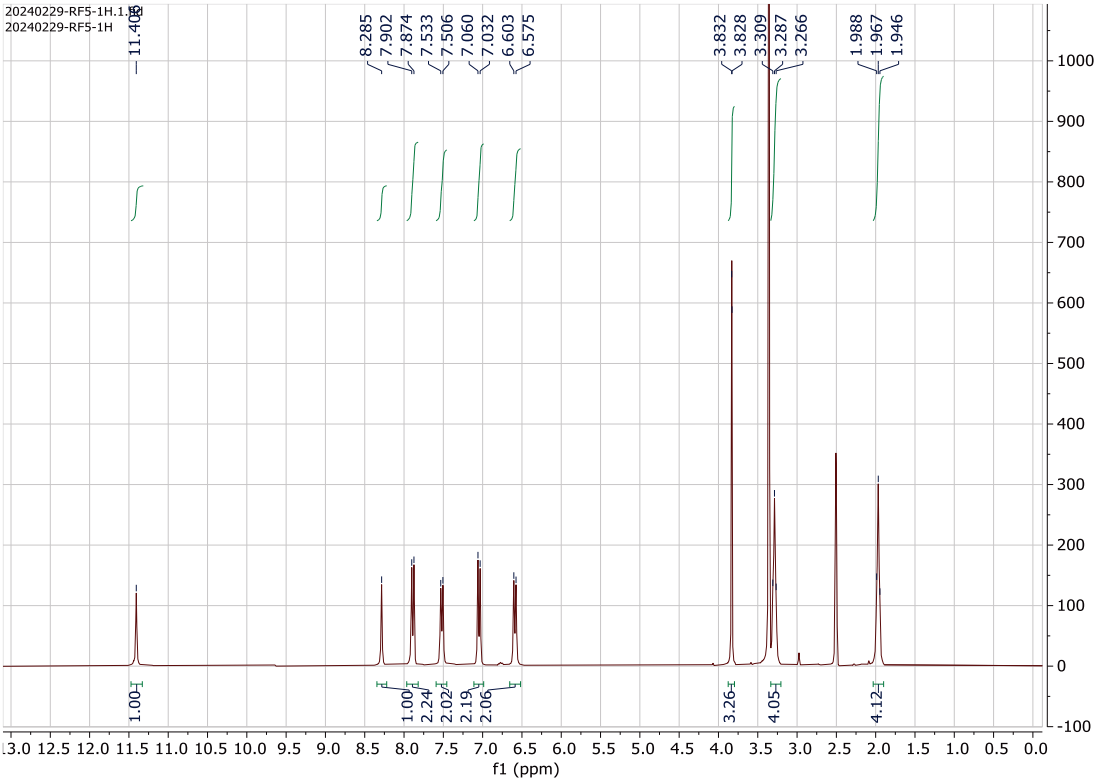

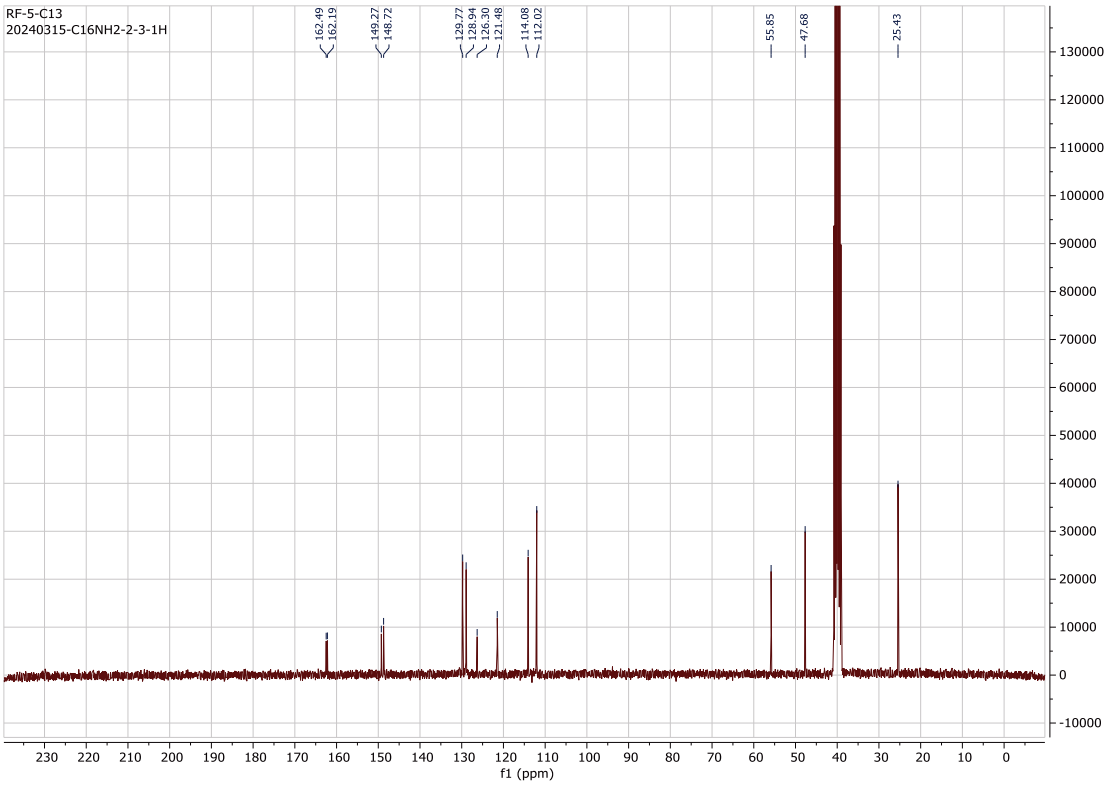

Data:RF-5
Comment:
Description:
Ionization Mode:ESI+
History:Average(MS[1] 0.11..0.30)

Acquired:5/15/2024 5:04:24 PM
Operator:AccuTOF
m/z Calibration File:20240515-TFANa_...
Created:5/16/2024 11:16:37 AM
Created by:AccuTOF

Charge number:1
Tolerance:400.00[ppm], 400.00 .. 400....
Unsaturation Number:-300.5 .. 300.0 (...
Element:^{12}C:19 .. 19, ^{1}H:10 .. 22, ^{14}N:3 .. 3, ^{23}Na:0 .. 2, ^{16}O:2 .. 2

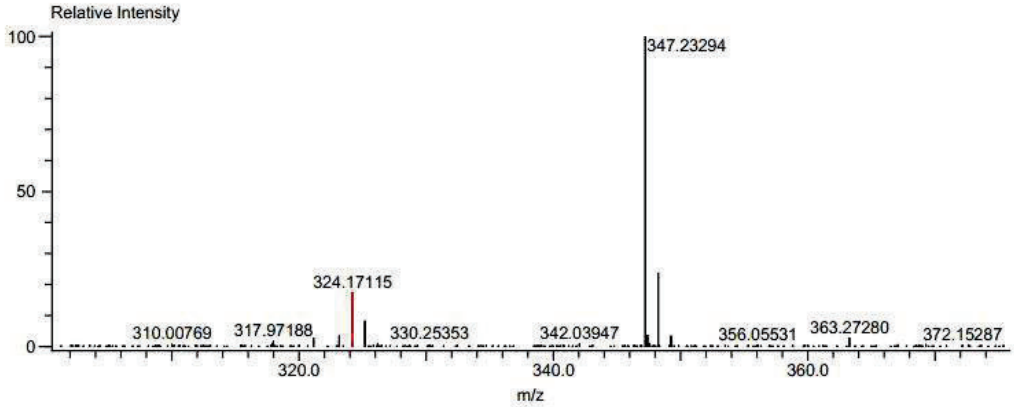

Mass	Intensity	Calc. Mass	Mass Difference [mDa]	Mass Difference [ppm]	Possible Formula
324.17115	2797.42	324.17120	-0.06	-0.17	$^{12}C_{19}{}^{1}H_{22}{}^{14}N_{3}{}^{16}O_{2}$

H[1], [13]CNMR & HRMS of Compound 8

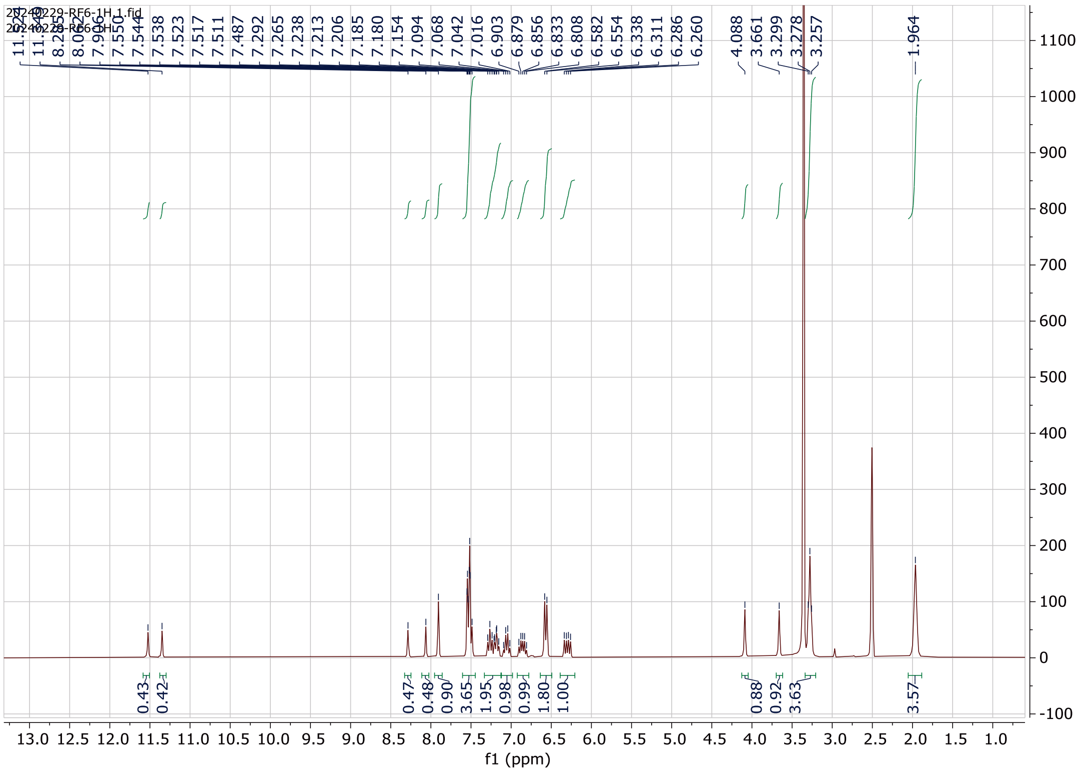

20240229-RF6-1H.1.fid
f1 (ppm)

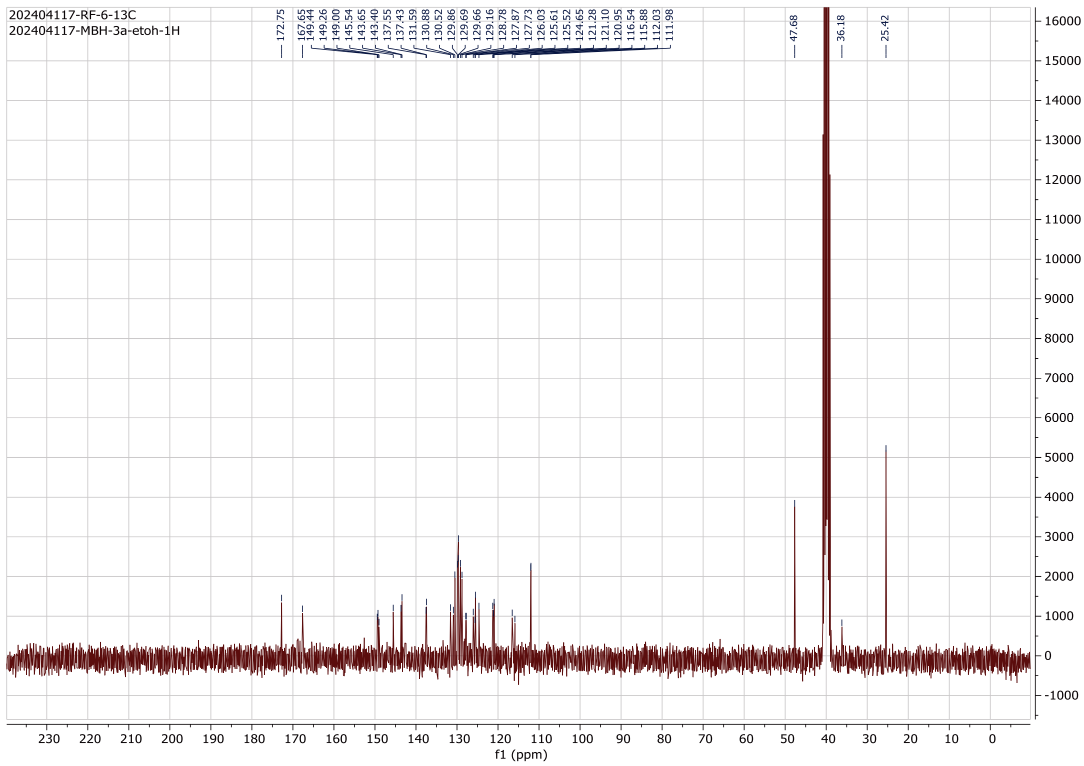

202404117-RF-6-13C
202404117-MBH-3a-etoh-1H
f1 (ppm)

Data:RF-6
Comment:
Description:
Ionization Mode:ESI+
History:Average(MS[1] 0.15..0.17)

Acquired:5/15/2024 5:07:30 PM
Operator:AccuTOF
m/z Calibration File:20240515-TFANa_...
Created:5/16/2024 11:19:02 AM
Created by:AccuTOF

Charge number:1 Tolerance:400.00[ppm], 400.00 .. 400.... Unsaturation Number:-300.5 .. 300.0 (...
Element:^{12}C:25 .. 25, ^{1}H:10 .. 25, ^{35}Cl:2 .. 2, ^{14}N:4 .. 4, ^{23}Na:0 .. 2, ^{16}O:1 .. 1

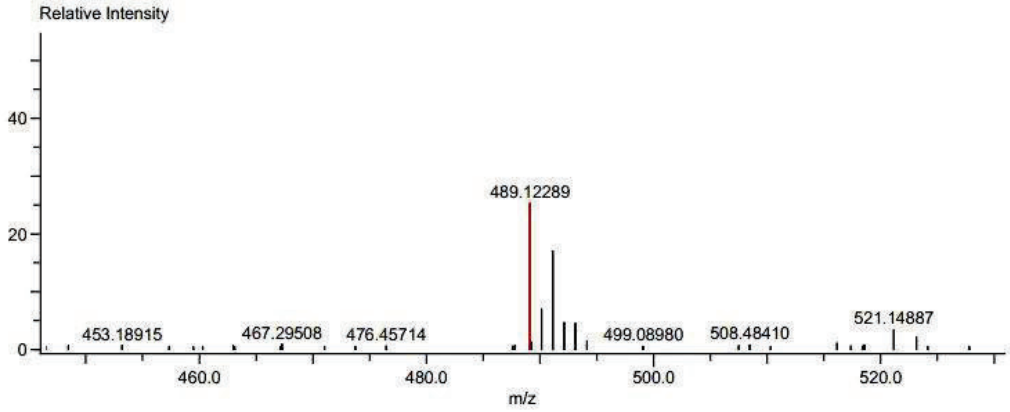

Mass	Intensity	Calc. Mass	Mass Difference [mDa]	Mass Difference [ppm]	Possible Formula
489.12289	9557.54	489.12249	0.40	0.82	$^{12}C_{25}{}^{1}H_{24}{}^{35}Cl_{2}{}^{14}N_{4}{}^{23}Na_{1}{}^{16}O_{1}$

H^{1}, ^{13}CNMR & HRMS of Compound 9

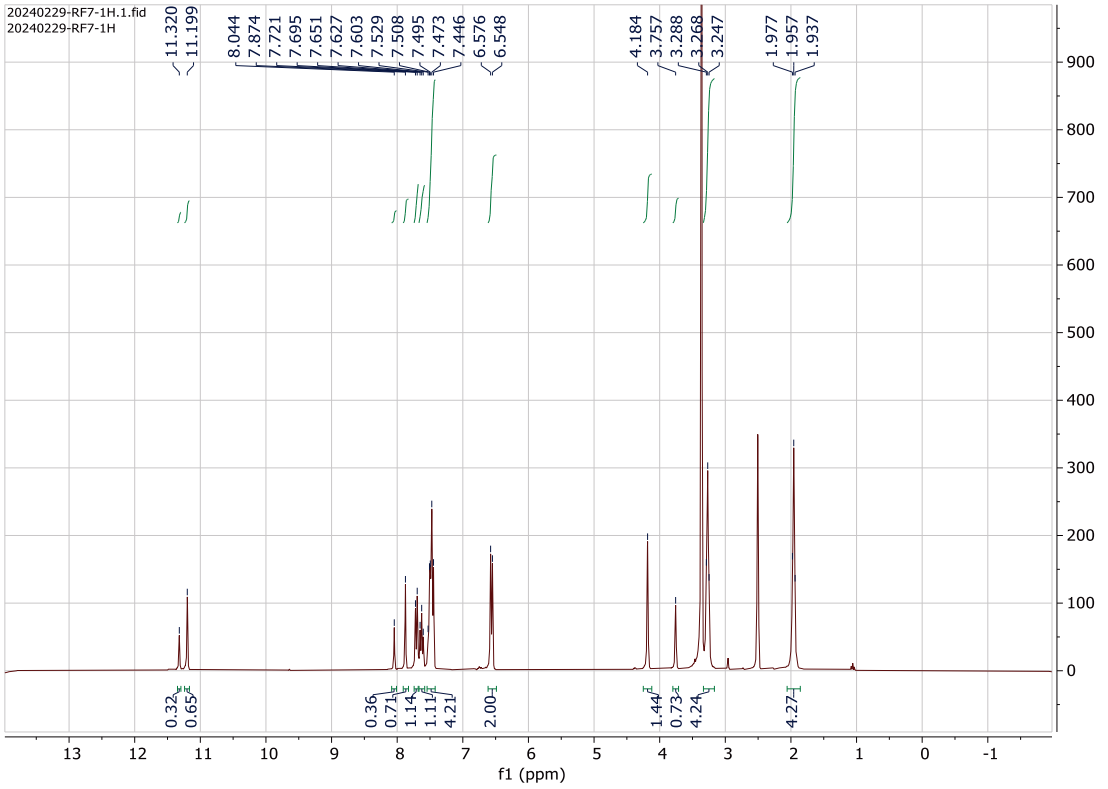
20240229-RF7-1H.1.fid
20240229-RF7-1H
11.320
11.199
8.044
7.874
7.721
7.695
7.651
7.627
7.603
7.529
7.508
7.495
7.473
7.446
6.576
6.548
4.184
3.757
3.288
3.268
3.247
1.977
1.957
1.937
0.32
0.65
0.36
0.71
1.14
1.11
4.21
2.00
1.44
0.73
4.24
4.27
f1 (ppm)

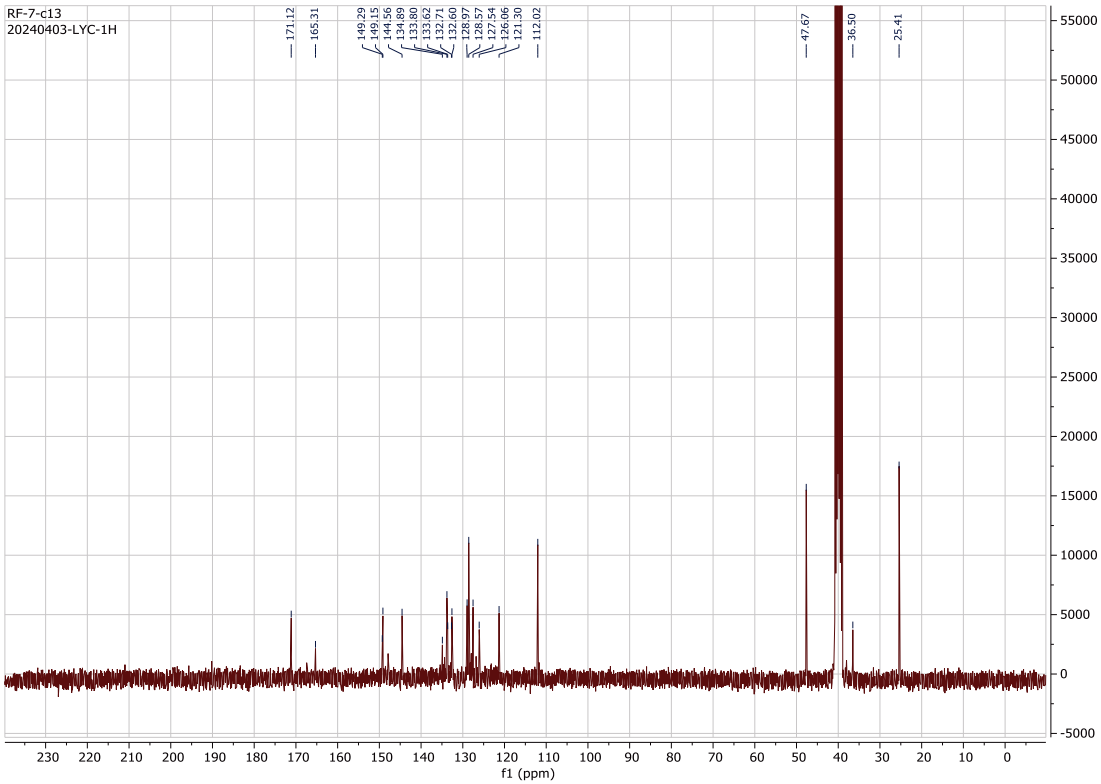
RF-7-c13
20240403-LYC-1H
171.12
165.31
149.29
149.15
144.56
134.89
133.80
133.62
132.71
132.60
128.97
128.57
127.54
126.06
121.30
112.02
47.67
36.50
25.41
f1 (ppm)

Data:RF-7
Comment:
Description:
Ionization Mode:ESI+
History:Average(MS[1] 0.19..0.23)

Acquired:5/15/2024 5:10:28 PM
Operator:AccuTOF
m/z Calibration File:20240515-TFANa_...
Created:5/16/2024 11:21:18 AM
Created by:AccuTOF

Charge number:1 Tolerance:400.00[ppm], 400.00 .. 400.... Unsaturation Number:-300.5 .. 300.0 (...
Element:^{12}C:20 .. 20, ^{1}H:10 .. 21, ^{19}F:3 .. 3, ^{14}N:3 .. 3, ^{23}Na:0 .. 2, ^{16}O:1 .. 1

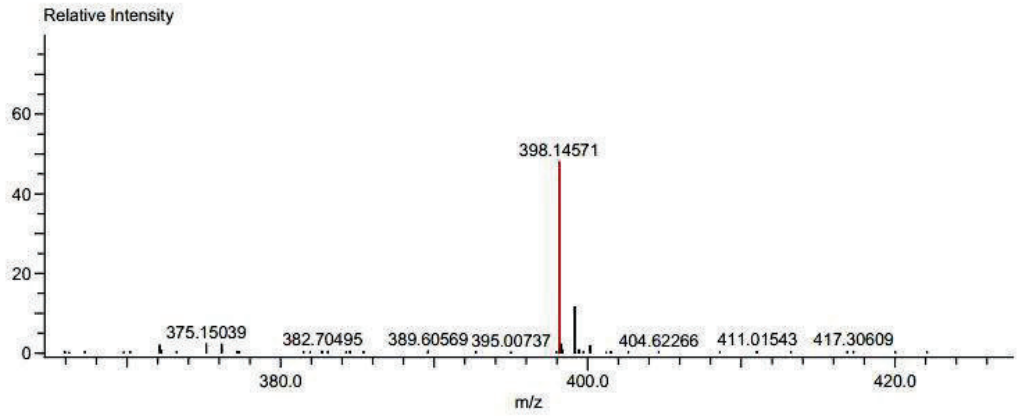

Mass	Intensity	Calc. Mass	Mass Difference [mDa]	Mass Difference [ppm]	Possible Formula
398.14571	20684.05	398.14562	0.10	0.25	$^{12}C_{20}{}^{1}H_{20}{}^{19}F_{3}{}^{14}N_{3}{}^{23}Na_{1}{}^{16}O_{1}$

H^{1}, ^{13}CNMR & HRMS of Compound 10

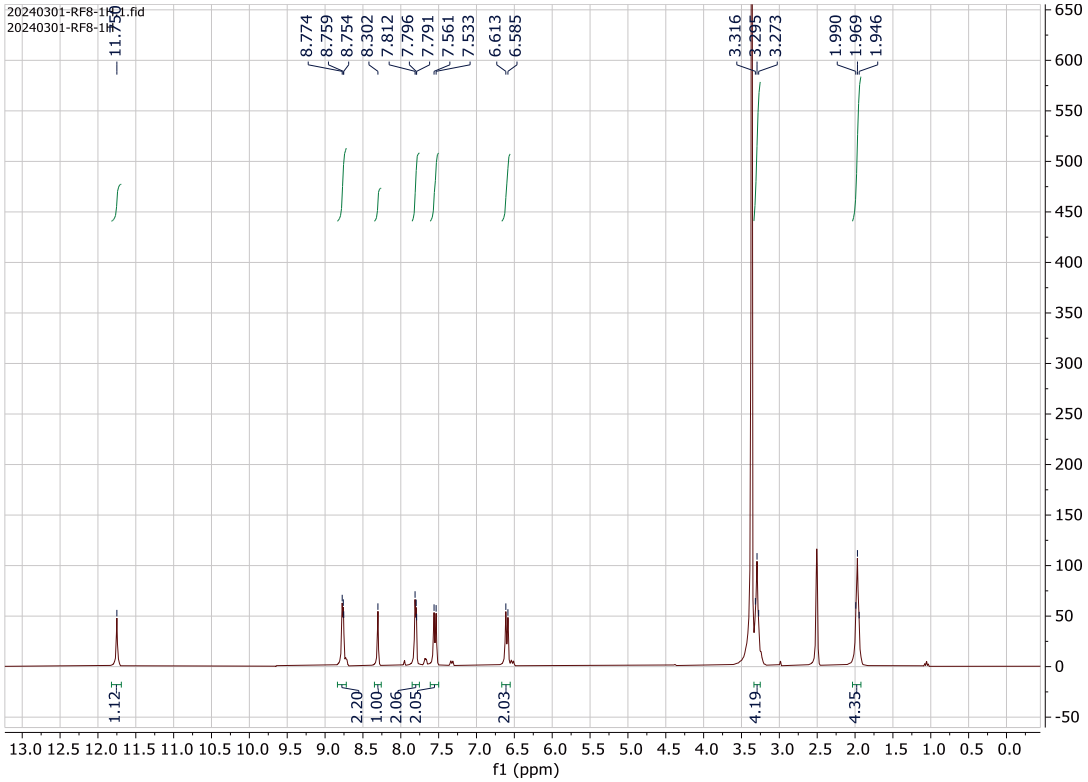

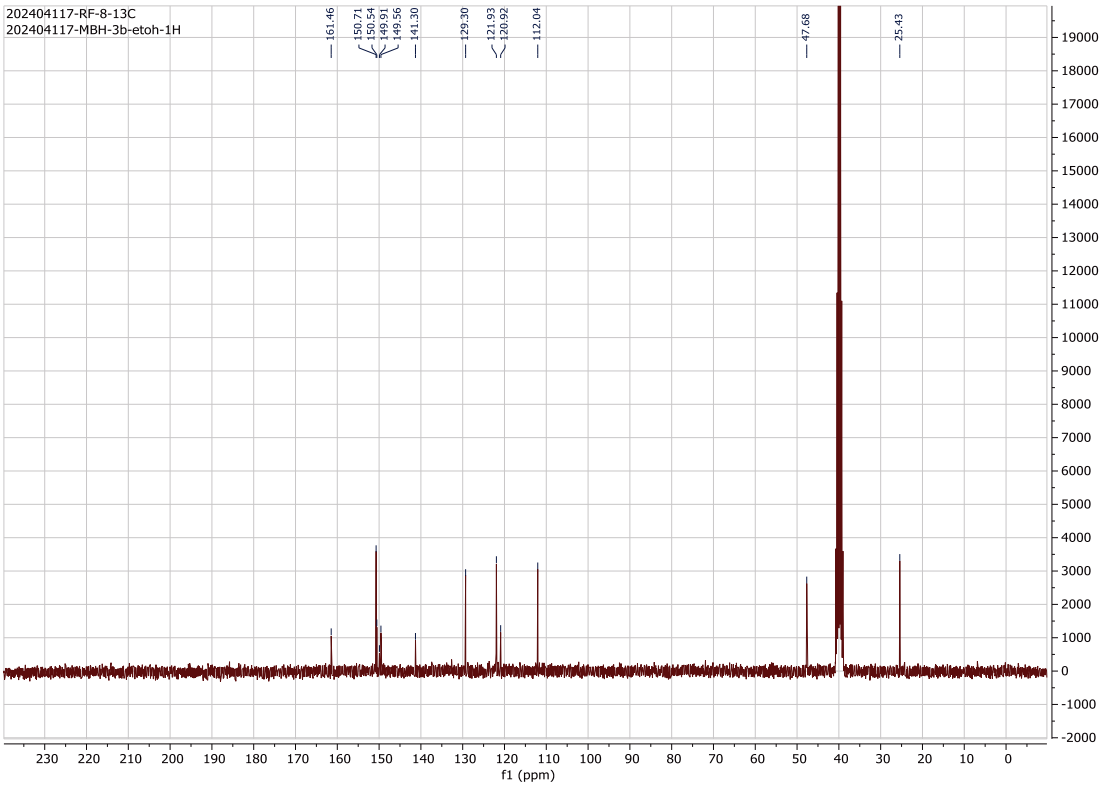

Data:RF-8
Comment:
Description:
Ionization Mode:ESI+
History:Average(MS[1] 0.17..0.20)

Acquired:5/15/2024 5:13:25 PM
Operator:AccuTOF
m/z Calibration File:20240515-TFANa_...
Created:5/16/2024 11:23:43 AM
Created by:AccuTOF

Charge number:1
Tolerance:400.00[ppm], 400.00 .. 400....
Unsaturation Number:-300.5 .. 300.0 (...
Element:^{12}C:17 .. 17, ^{1}H:10 .. 19, ^{14}N:4 .. 4, ^{23}Na:0 .. 2, ^{16}O:1 .. 1

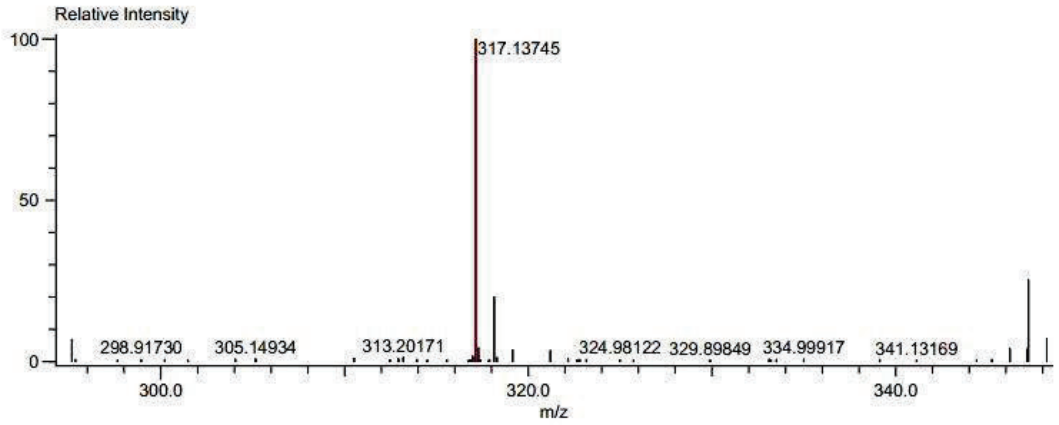

Mass	Intensity	Calc. Mass	Mass Difference [mDa]	Mass Difference [ppm]	Possible Formula
317.13745	27004.75	317.13783	-0.38	-1.21	$^{12}C_{17}{}^{1}H_{18}{}^{14}N_{4}{}^{23}Na_{1}{}^{16}O_{1}$

H^1, ^{13}CNMR & HRMS of Compound 11

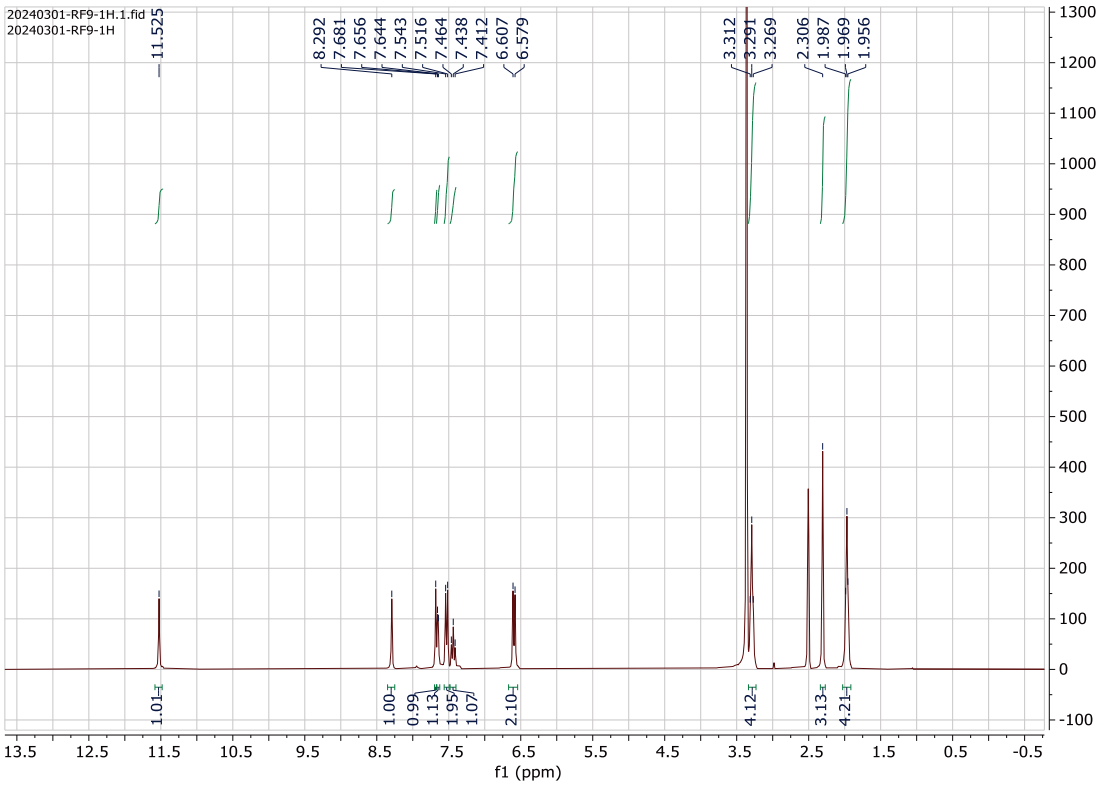

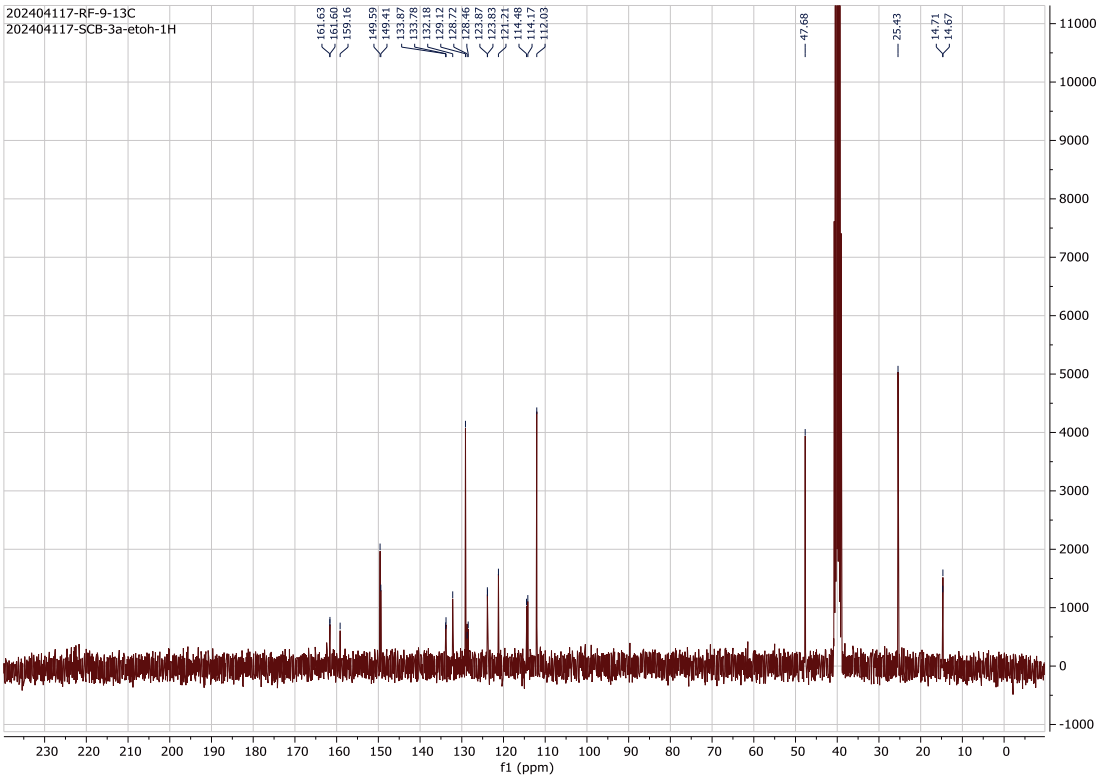

Data:RF-9
Comment:
Description:
Ionization Mode:ESI+
History:Average(MS[1] 0.16..0.20)

Acquired:5/15/2024 5:16:32 PM
Operator:AccuTOF
m/z Calibration File:20240515-TFANa_...
Created:5/16/2024 11:27:10 AM
Created by:AccuTOF

Charge number:1 Tolerance:400.00[ppm], 400.00 .. 400.... Unsaturation Number:-300.5 .. 300.0 (...
Element:^{12}C:19 .. 19, ^{1}H:10 .. 21, ^{19}F:1 .. 1, ^{14}N:3 .. 3, ^{23}Na:0 .. 2, ^{16}O:1 .. 1

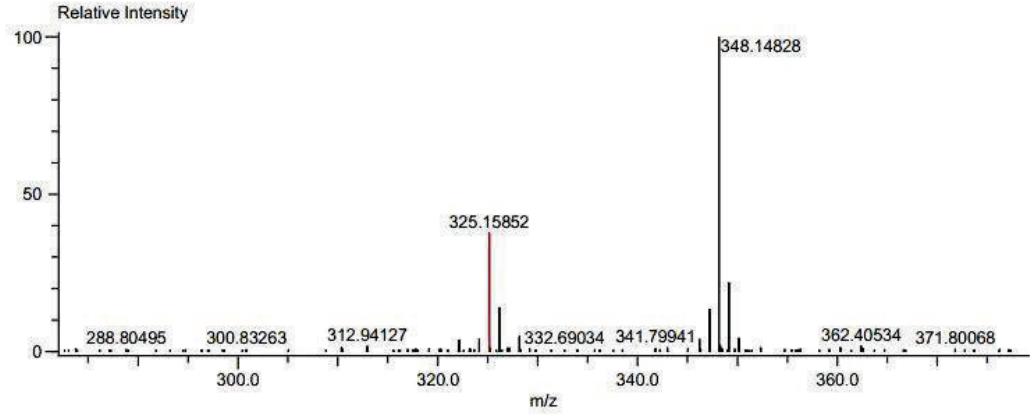

Mass	Intensity	Calc. Mass	Mass Difference [mDa]	Mass Difference [ppm]	Possible Formula
325.15852	7339.71	325.15904	-0.52	-1.61	$^{12}C_{19}{}^{1}H_{20}{}^{19}F_{1}{}^{14}N_{3}{}^{16}O_{1}$

H^{1}, ^{13}CNMR & HRMS of Compound 12

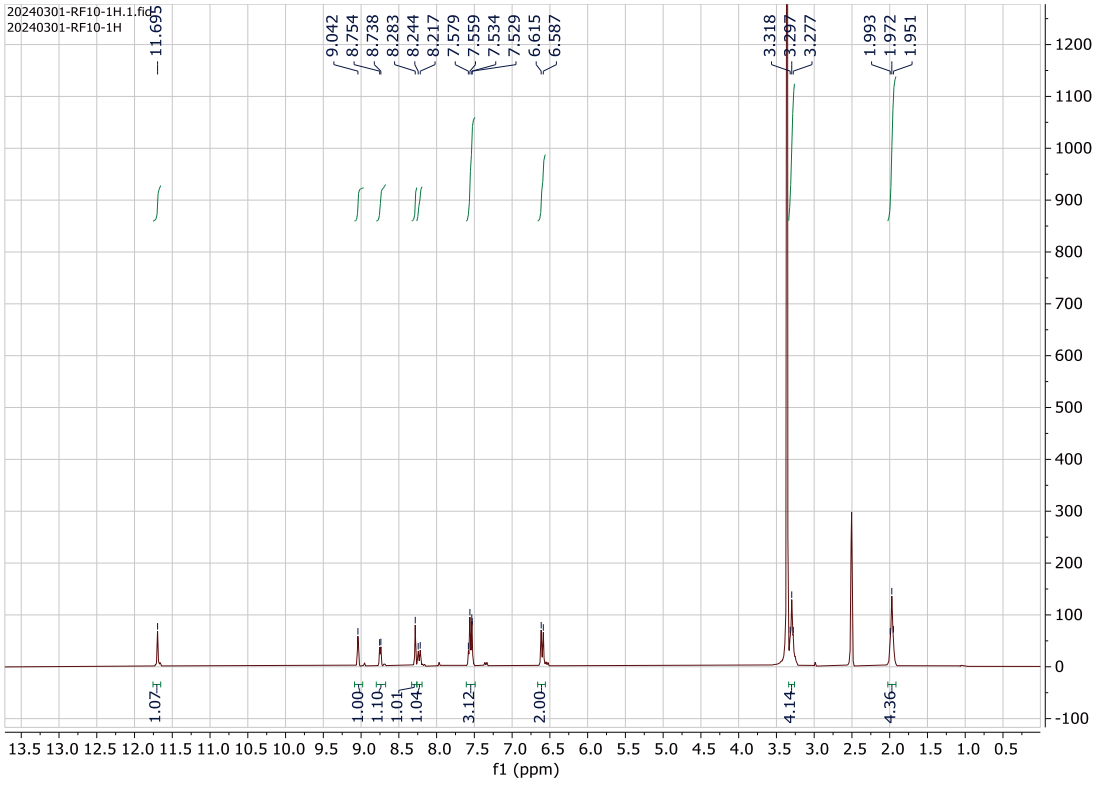

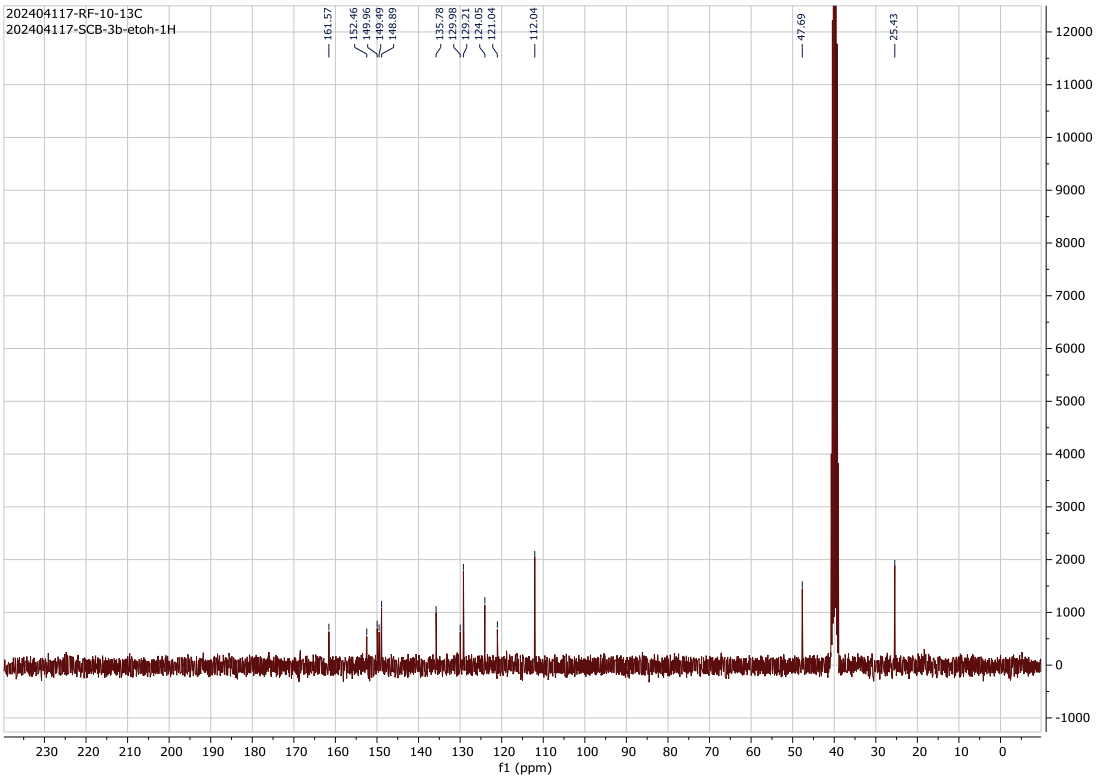

Data:RF-10
Comment:
Description:
Ionization Mode:ESI+
History:Average(MS[1] 0.17..0.19)

Acquired:5/15/2024 5:19:41 PM
Operator:AccuTOF
m/z Calibration File:20240515-TFANa_...
Created:5/16/2024 11:28:27 AM
Created by:AccuTOF

Charge number:1
Tolerance:400.00[ppm], 400.00 .. 400....
Unsaturation Number:-300.5 .. 300.0 (...
Element:^{12}C:17 .. 17, ^{1}H:10 .. 19, ^{14}N:4 .. 4, ^{23}Na:0 .. 2, ^{16}O:1 .. 1

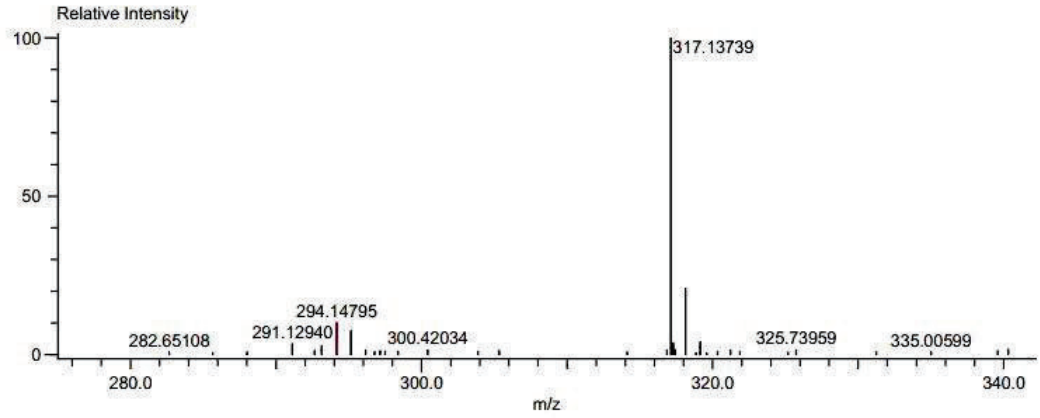

Mass	Intensity	Calc. Mass	Mass Difference [mDa]	Mass Difference [ppm]	Possible Formula
294.14795	2337.38	294.14806	-0.11	-0.37	$^{12}C_{17}{}^{1}H_{18}{}^{14}N_{4}{}^{16}O_{1}$

H[1], [13]CNMR & HRMS of Compound 13

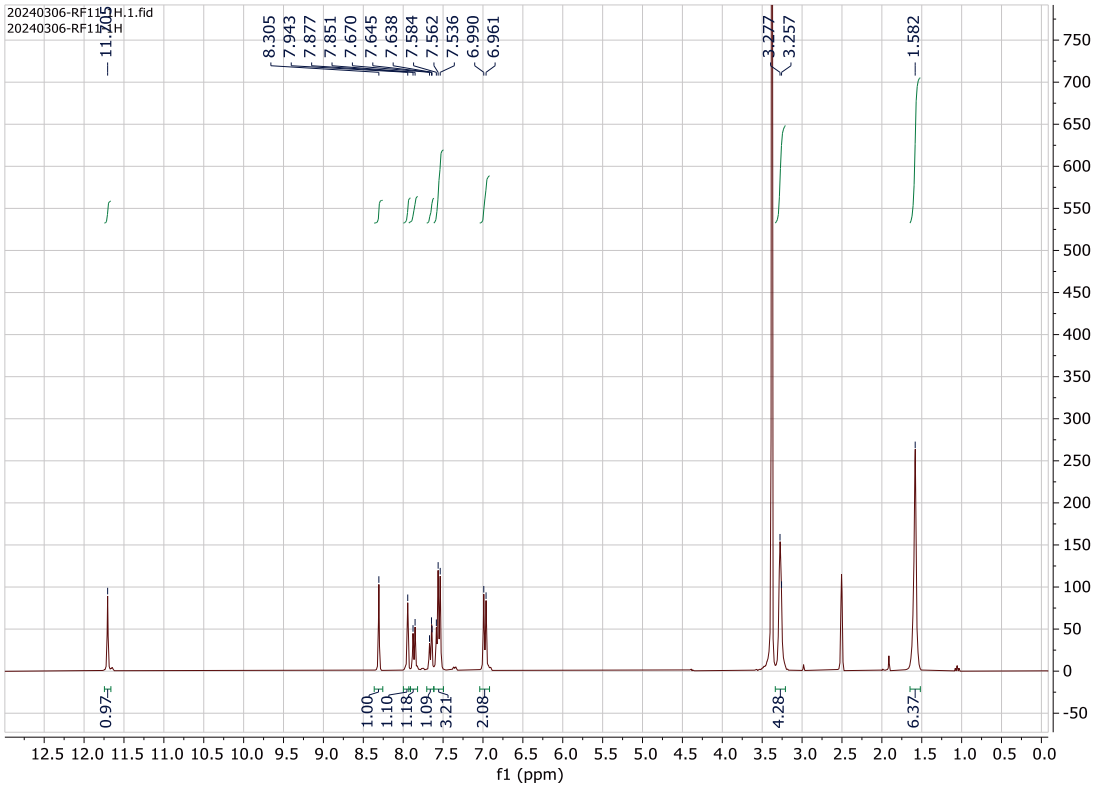

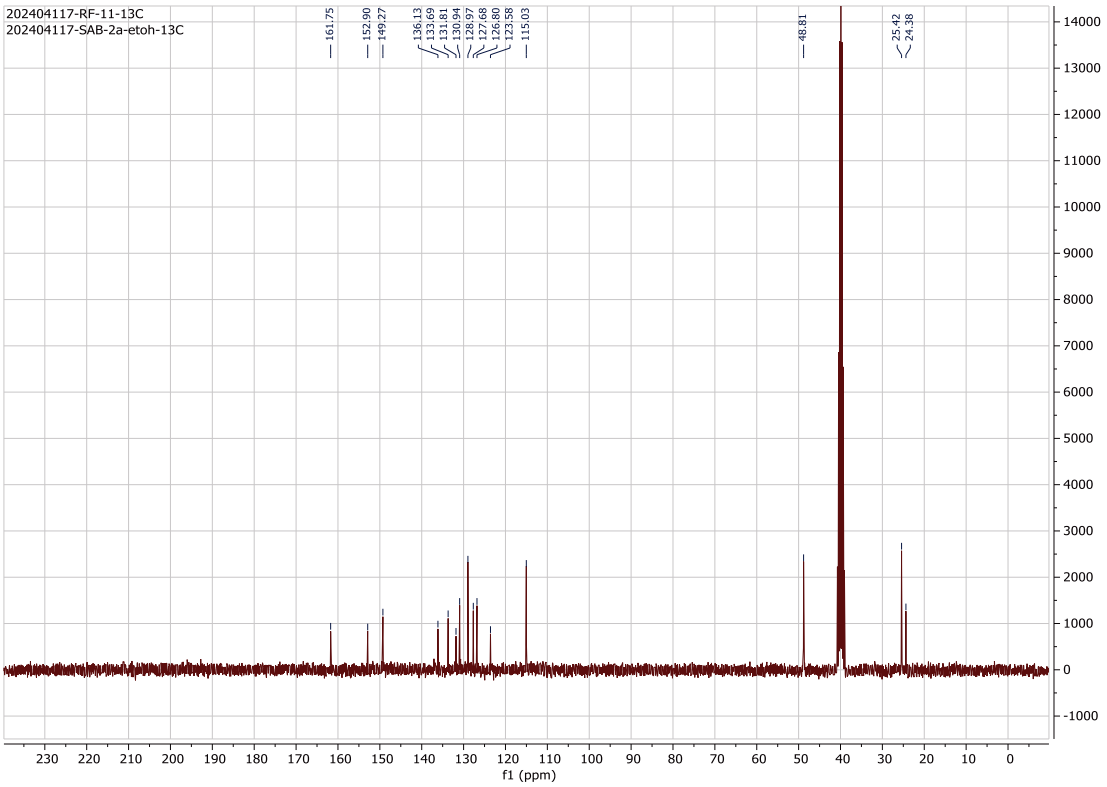

Data:RF-11
Comment:
Description:
Ionization Mode:ESI+
History:Average(MS[1] 0.15..0.19)

Acquired:5/15/2024 5:22:37 PM
Operator:AccuTOF
m/z Calibration File:20240515-TFANa_...
Created:5/16/2024 11:30:13 AM
Created by:AccuTOF

Charge number:1 Tolerance:400.00[ppm], 400.00 .. 400.... Unsaturation Number:-300.5 .. 300.0 (...
Element:^{12}C:19 .. 19, ^{1}H:10 .. 21, ^{35}Cl:1 .. 1, ^{14}N:3 .. 3, ^{23}Na:0 .. 2, ^{16}O:1 .. 1

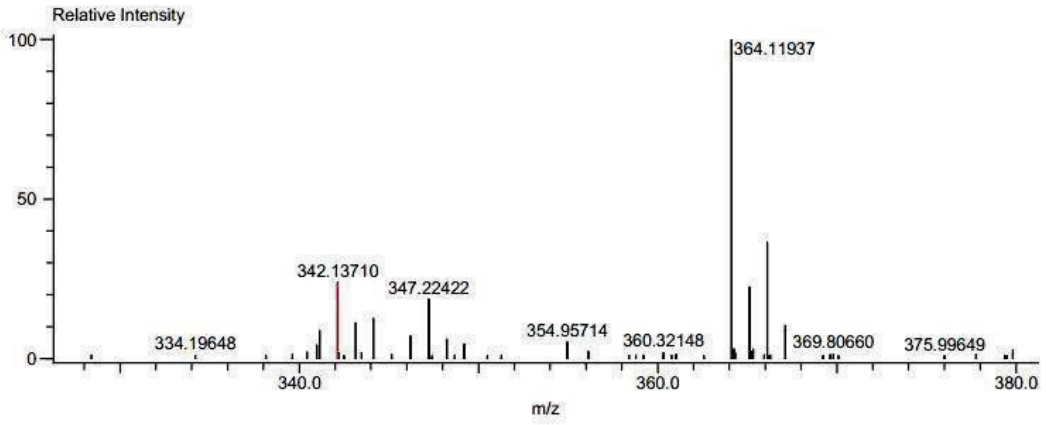

Mass	Intensity	Calc. Mass	Mass Difference [mDa]	Mass Difference [ppm]	Possible Formula
342.13710	3380.67	342.13731	-0.21	-0.62	$^{12}C_{19}{}^{1}H_{21}{}^{35}Cl_{1}{}^{14}N_{3}{}^{16}O_{1}$

H^{1}, ^{13}CNMR & HRMS of Compound 14

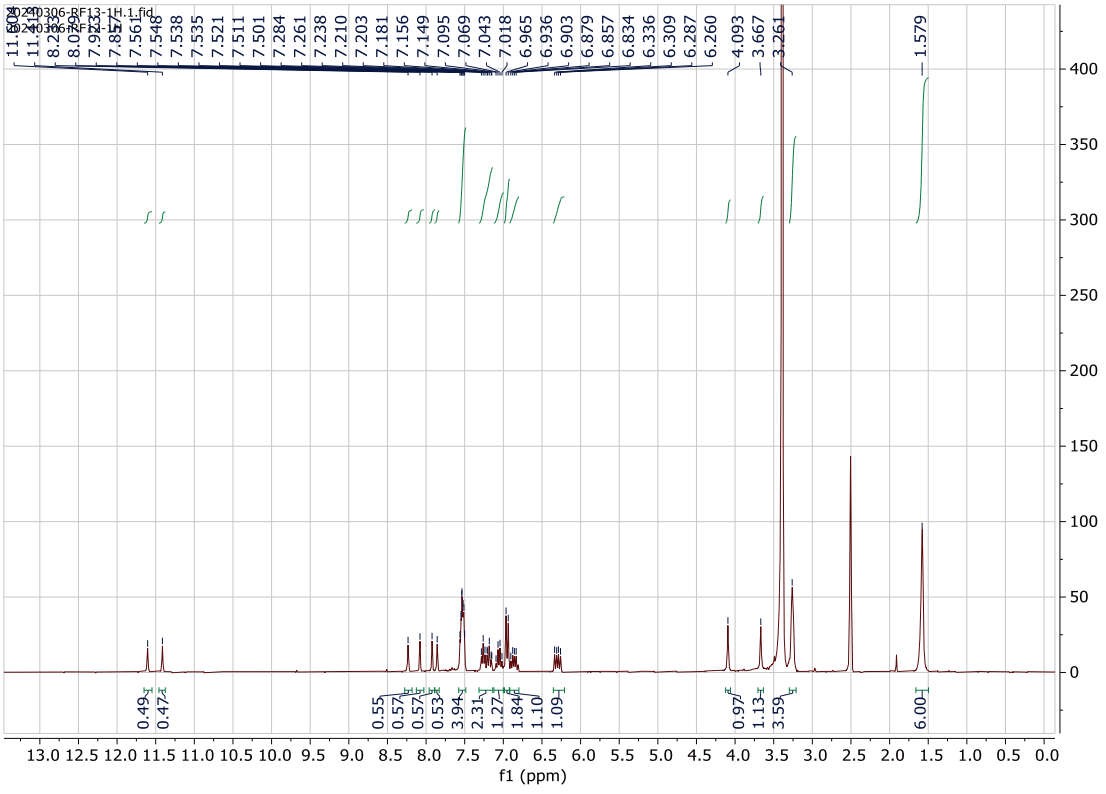

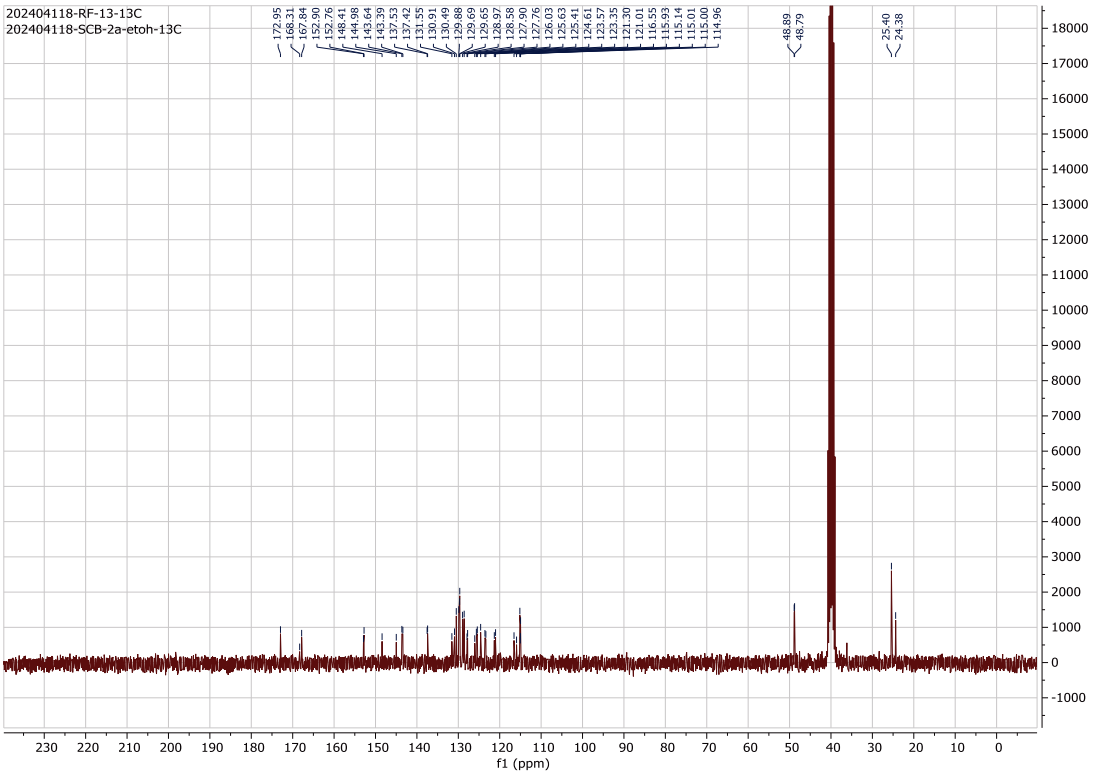

Data:RF-13
Comment:
Description:
Ionization Mode:ESI+
History:Average(MS[1] 0.17..0.22)

Acquired:5/15/2024 5:25:35 PM
Operator:AccuTOF
m/z Calibration File:20240515-TFANa_...
Created:5/16/2024 11:32:31 AM
Created by:AccuTOF

Charge number:1 Tolerance:400.00[ppm], 400.00 .. 400.... Unsaturation Number:-300.5 .. 300.0 (...
Element:^{12}C:26 .. 26, ^{1}H:10 .. 27, ^{35}Cl:2 .. 2, ^{14}N:4 .. 4, ^{23}Na:0 .. 2, ^{16}O:1 .. 1

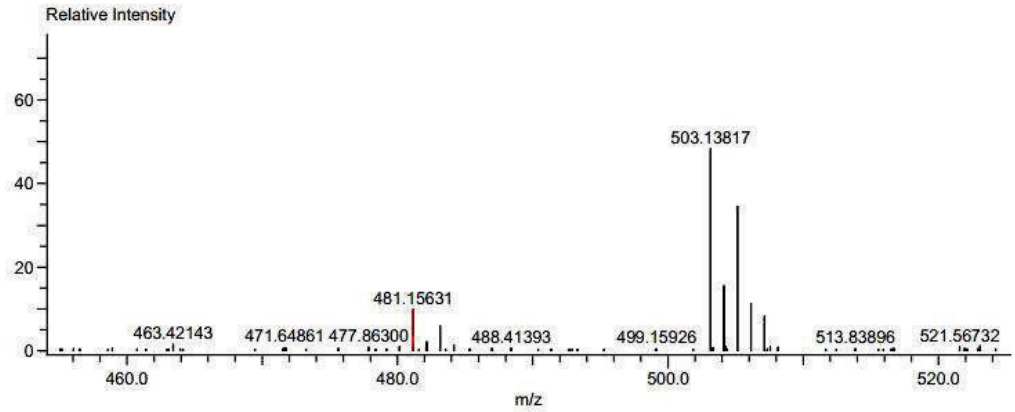

Mass	Intensity	Calc. Mass	Mass Difference [mDa]	Mass Difference [ppm]	Possible Formula
481.15631	2094.79	481.15619	0.12	0.24	$^{12}C_{26}{}^{1}H_{27}{}^{35}Cl_{2}{}^{14}N_{4}{}^{16}O_{1}$

H^1, ^{13}CNMR & HRMS of Compound 15

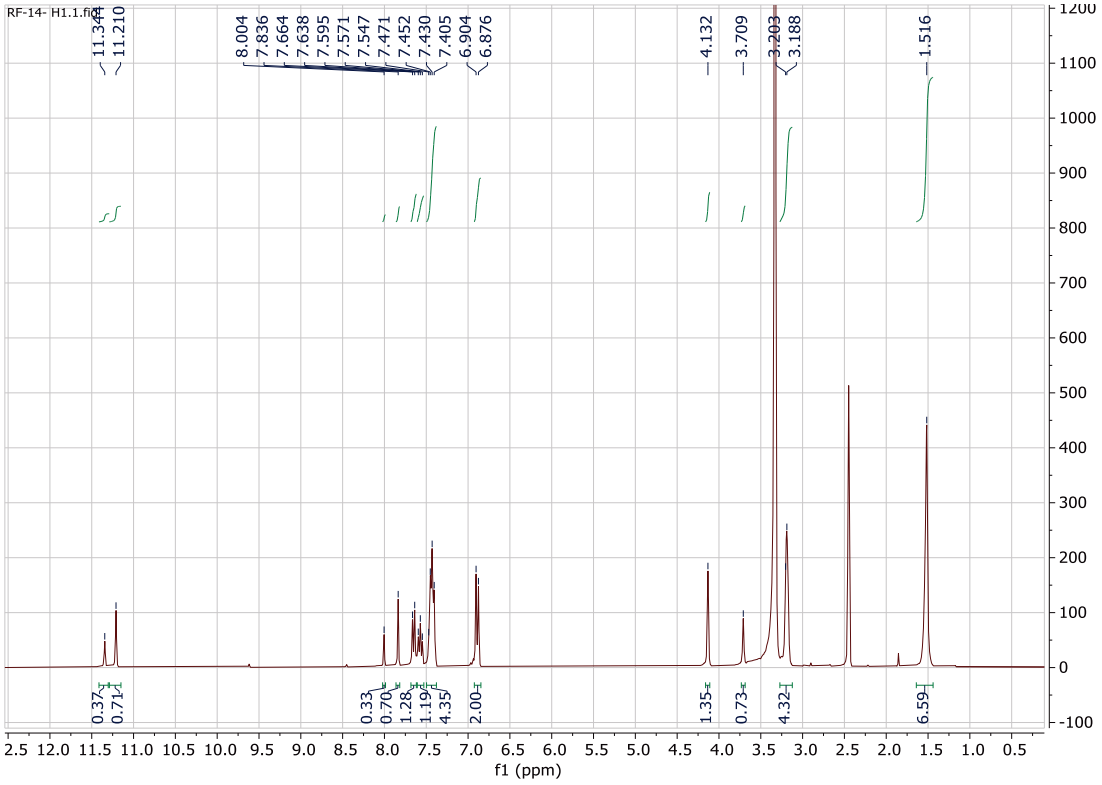

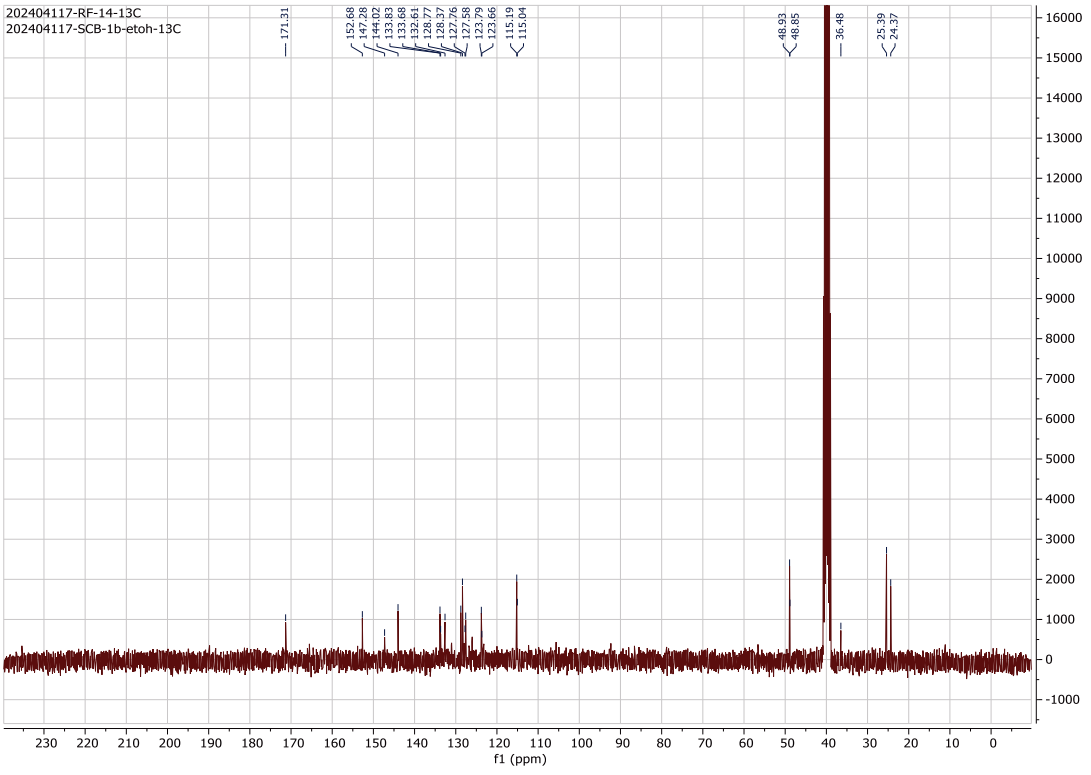

Data:RF-14
Comment:
Description:
Ionization Mode:ESI+
History:Average(MS[1] 0.17..0.20)

Acquired:5/15/2024 5:28:42 PM
Operator:AccuTOF
m/z Calibration File:20240515-TFANa_...
Created:5/16/2024 11:34:40 AM
Created by:AccuTOF

Charge number:1 Tolerance:400.00[ppm], 400.00 .. 400.... Unsaturation Number:-300.5 .. 300.0 (...
Element:^{12}C:21 .. 21, ^{1}H:10 .. 23, ^{19}F:3 .. 3, ^{14}N:3 .. 3, ^{23}Na:0 .. 2, ^{16}O:1 .. 1

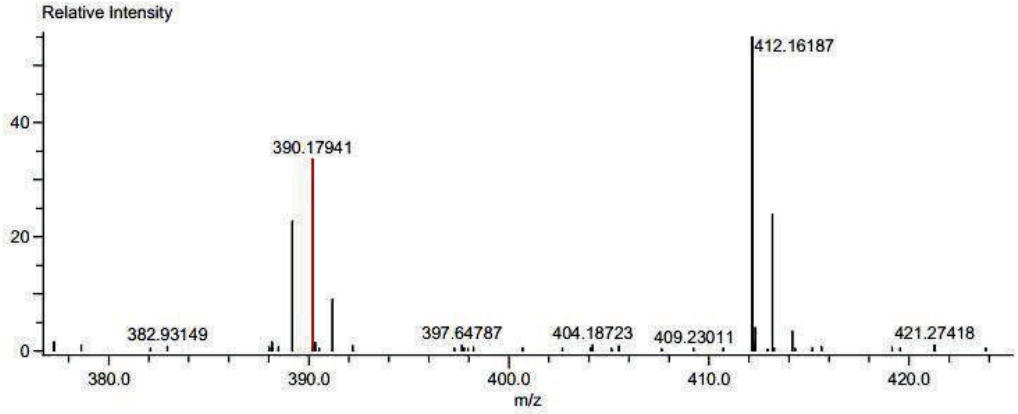

Mass	Intensity	Calc. Mass	Mass Difference [mDa]	Mass Difference [ppm]	Possible Formula
390.17941	9033.36	390.17932	0.09	0.24	$^{12}C_{21}{}^{1}H_{23}{}^{19}F_{3}{}^{14}N_{3}{}^{16}O_{1}$

H[1], [13]CNMR & HRMS of Compound 16

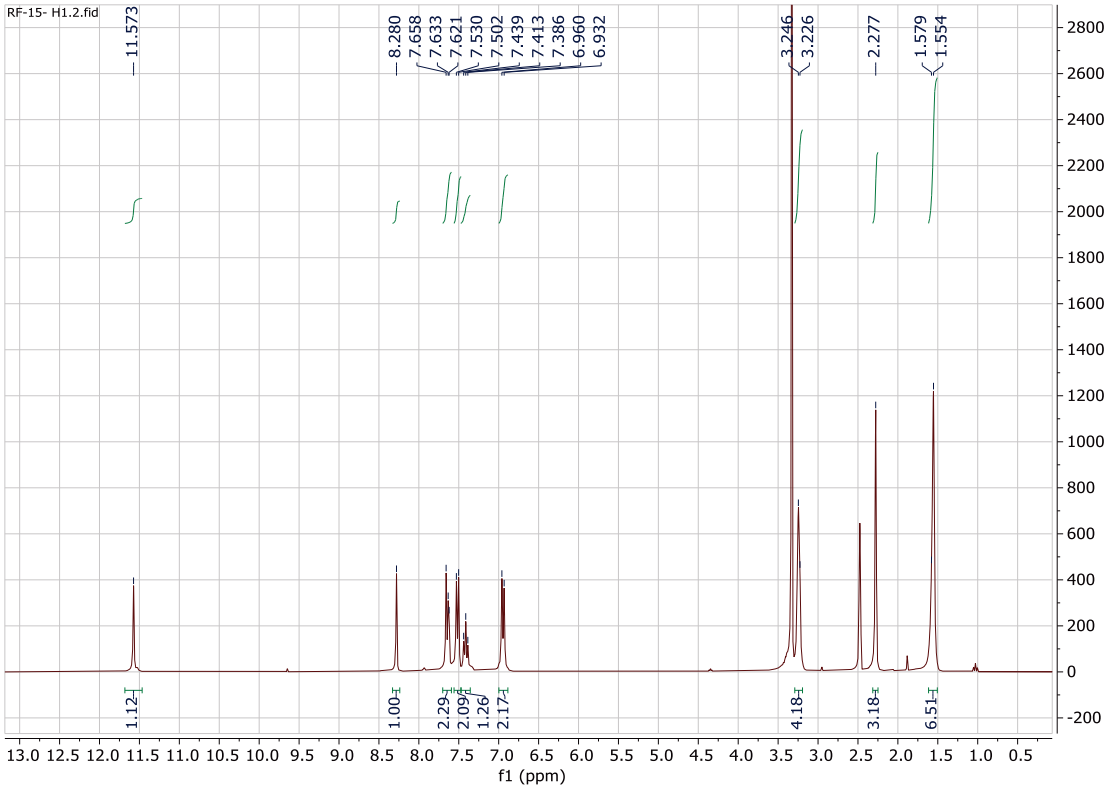

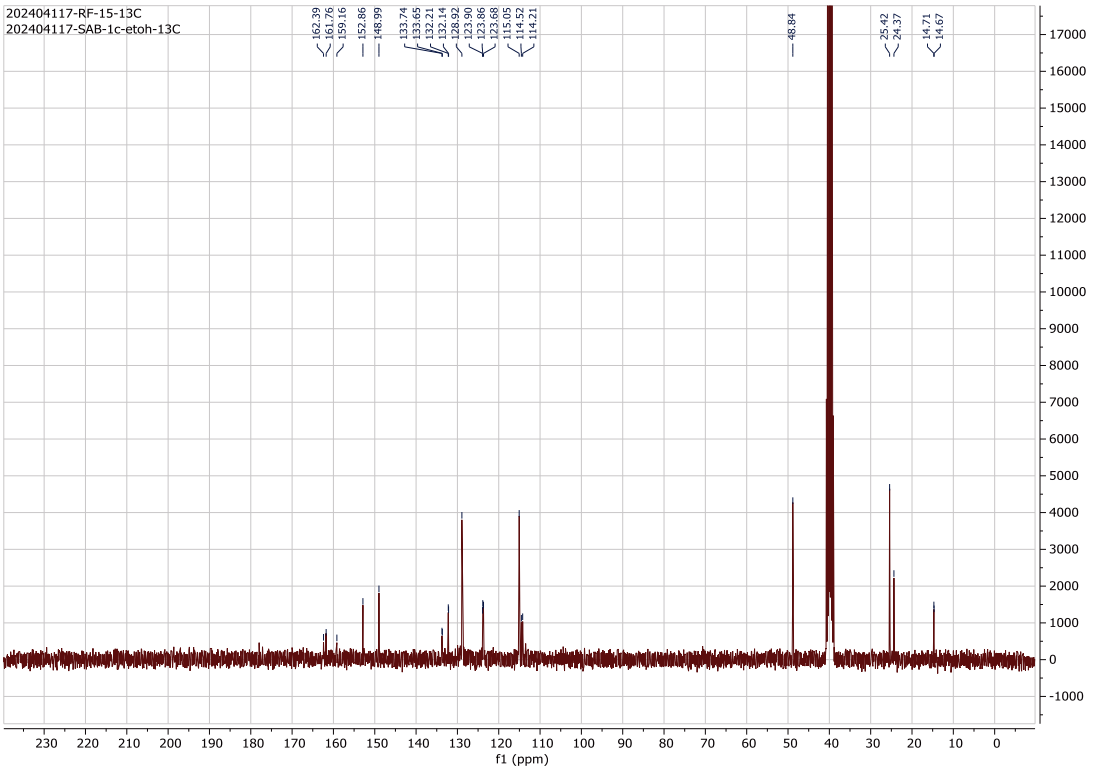

Data:RF-15
Comment:
Description:
Ionization Mode:ESI+
History:Average(MS[1] 0.20..0.23)

Acquired:5/15/2024 5:31:42 PM
Operator:AccuTOF
m/z Calibration File:20240515-TFANa_...
Created:5/16/2024 11:36:16 AM
Created by:AccuTOF

Charge number:1
Tolerance:400.00[ppm], 400.00 .. 400....
Unsaturation Number:-300.5 .. 300.0 (...
Element:^{12}C:20 .. 20, ^{1}H:10 .. 23, ^{19}F:1 .. 1, ^{14}N:3 .. 3, ^{23}Na:0 .. 2, ^{16}O:1 .. 1

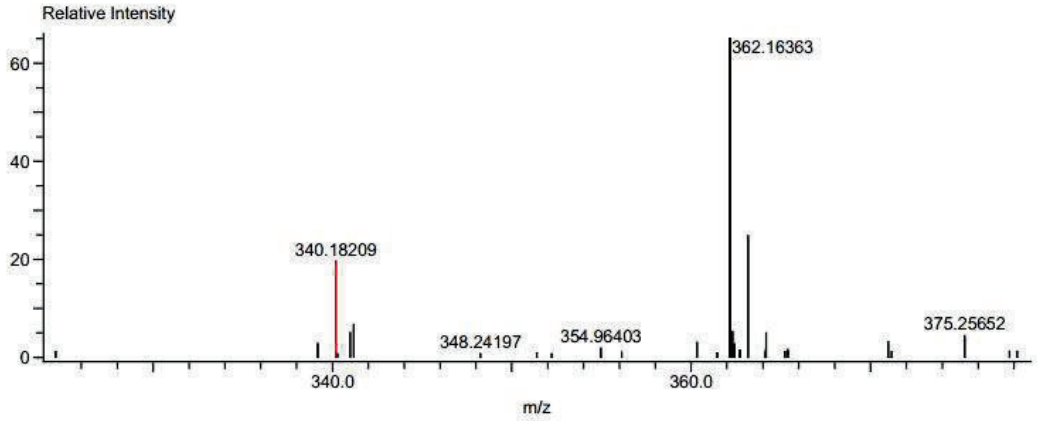

Mass	Intensity	Calc. Mass	Mass Difference [mDa]	Mass Difference [ppm]	Possible Formula
340.18209	3516.55	340.18251	-0.42	-1.23	$^{12}C_{20}{}^{1}H_{23}{}^{19}F_{1}{}^{14}N_{3}{}^{16}O_{1}$

H^1, ^{13}CNMR & HRMS of Compound 17

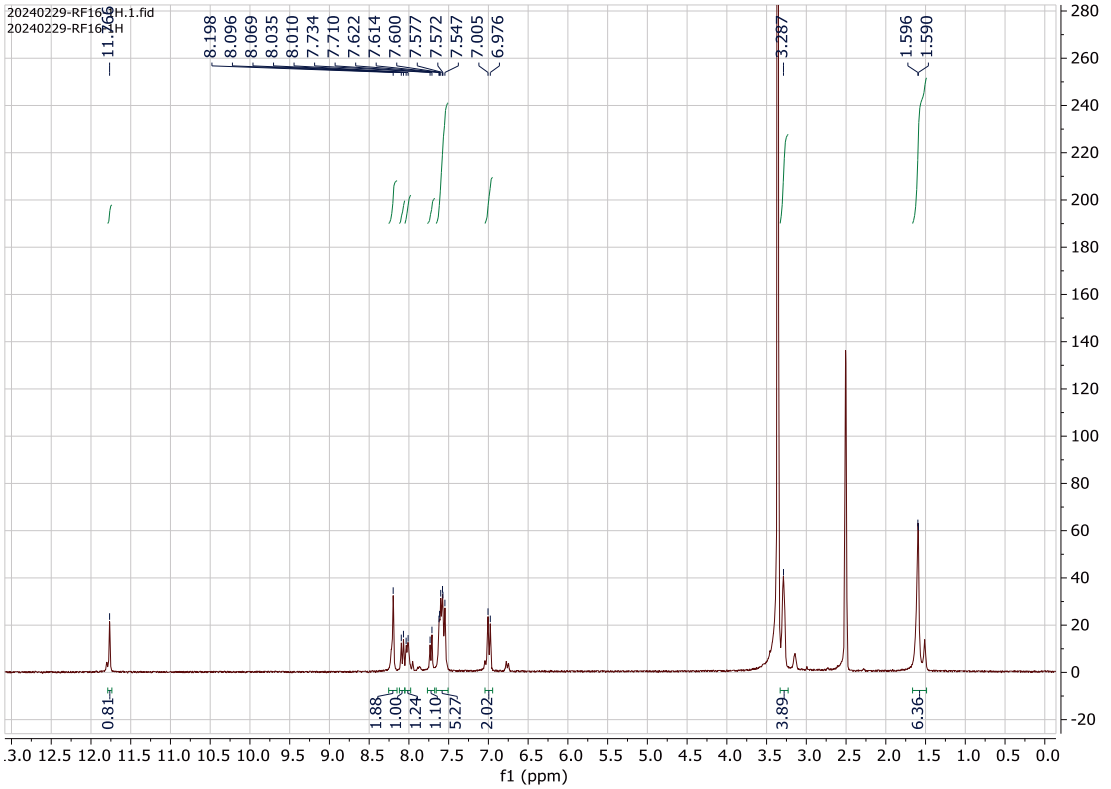

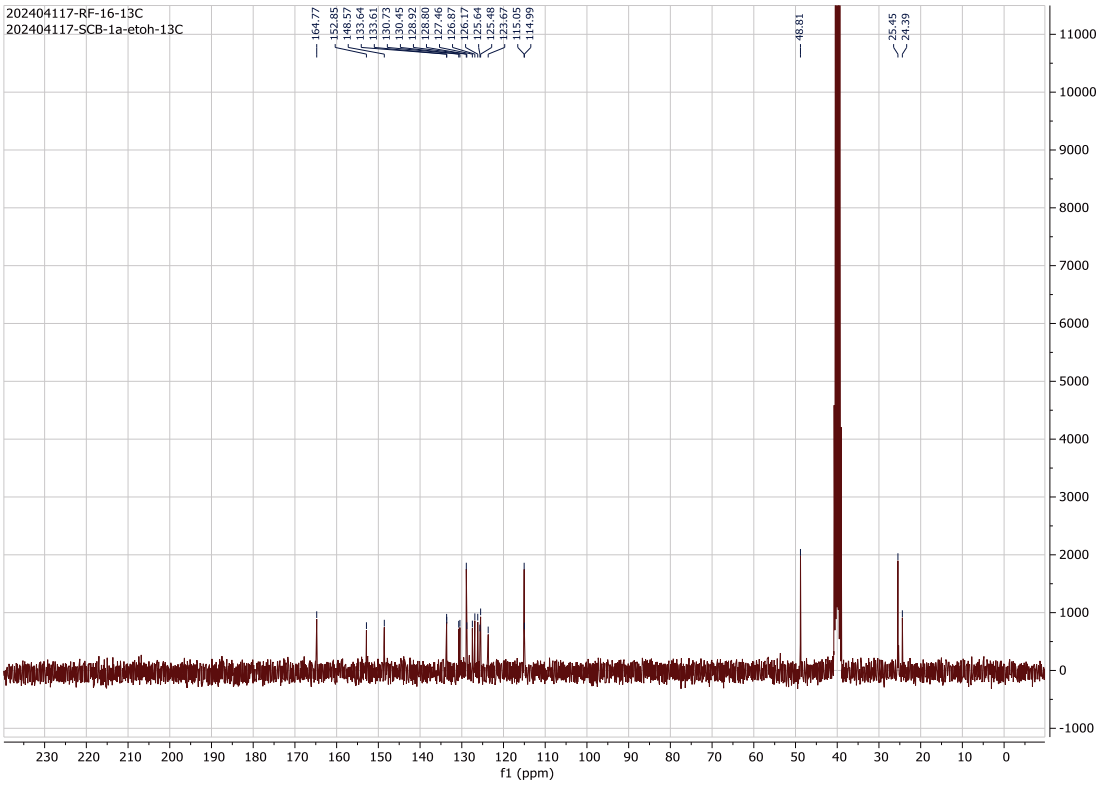

Data:RF-16
Comment:
Description:
Ionization Mode:ESI+
History:Average(MS[1] 0.12..0.14)

Acquired:5/15/2024 5:34:49 PM
Operator:AccuTOF
m/z Calibration File:20240515-TFANa_...
Created:5/16/2024 11:38:07 AM
Created by:AccuTOF

Charge number:1 Tolerance:400.00[ppm], 400.00 .. 400.... Unsaturation Number:-300.5 .. 300.0 (...
Element:^{12}C:23 .. 23, ^{1}H:10 .. 24, ^{14}N:3 .. 3, ^{23}Na:0 .. 2, ^{16}O:1 .. 1

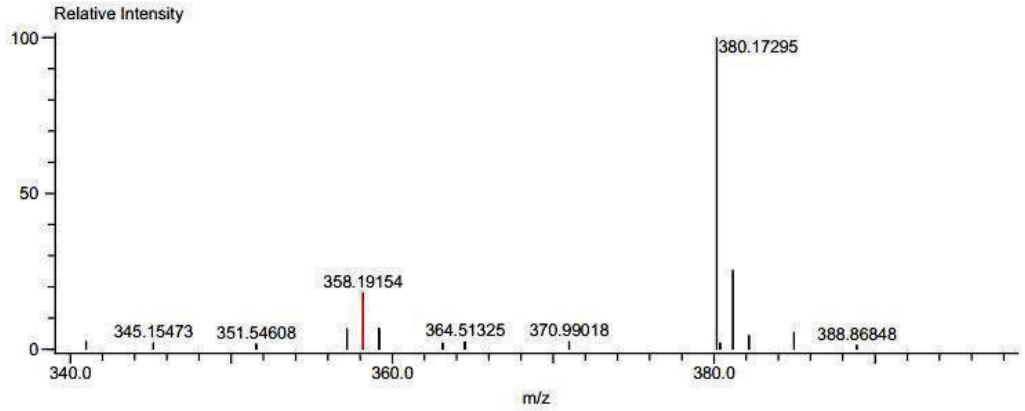

Mass	Intensity	Calc. Mass	Mass Difference [mDa]	Mass Difference [ppm]	Possible Formula
358.19154	3693.20	358.19194	-0.40	-1.11	$^{12}C_{23}{}^{1}H_{24}{}^{14}N_{3}{}^{16}O_{1}$

H^{1}, ^{13}CNMR & HRMS of Compound 18

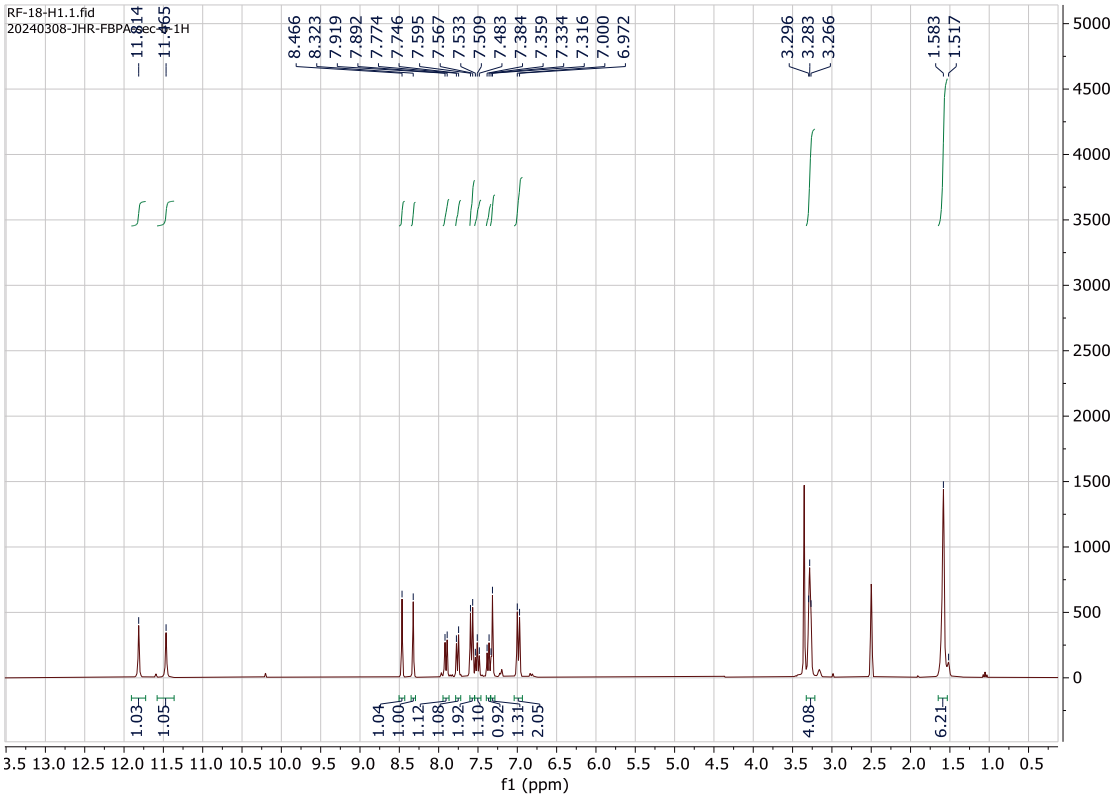

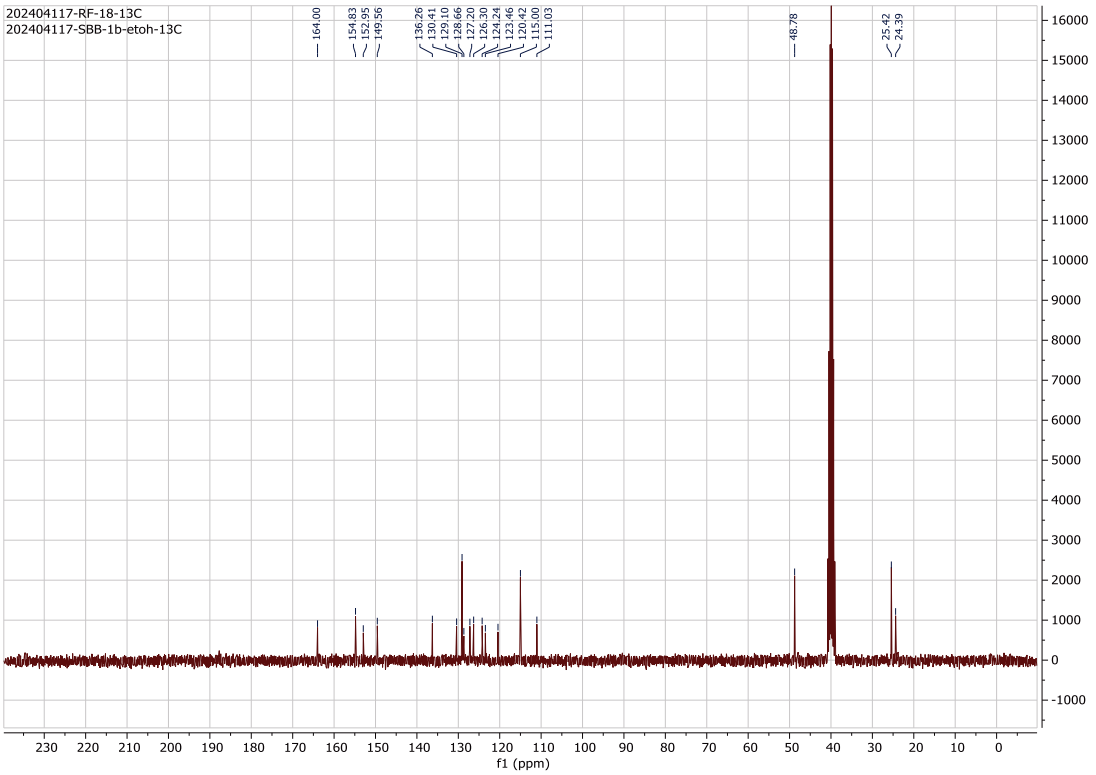

Data:RF-18
Comment:
Description:
Ionization Mode:ESI+
History:Average(MS[1] 0.16..0.19)

Acquired:5/15/2024 5:37:47 PM
Operator:AccuTOF
m/z Calibration File:20240515-TFANa_...
Created:5/16/2024 11:40:33 AM
Created by:AccuTOF

Charge number:1
Tolerance:400.00[ppm], 400.00 .. 400....
Unsaturation Number:-300.5 .. 300.0 (...
Element:^{12}C:23 .. 23, ^{1}H:10 .. 24, ^{14}N:3 .. 3, ^{23}Na:0 .. 2, ^{16}O:2 .. 2

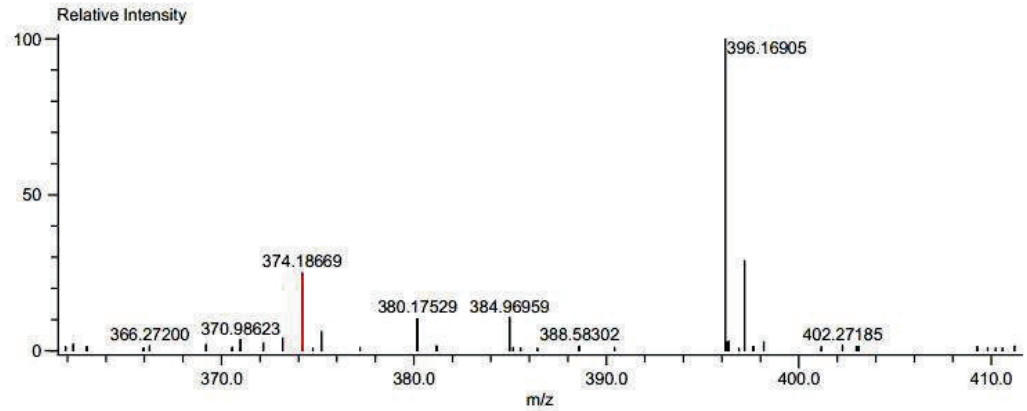

Mass	Intensity	Calc. Mass	Mass Difference [mDa]	Mass Difference [ppm]	Possible Formula
374.18669	3148.35	374.18685	-0.16	-0.43	$^{12}C_{23}{}^{1}H_{24}{}^{14}N_{3}{}^{16}O_{2}$

H[1], [13]CNMR & HRMS of Compound 19

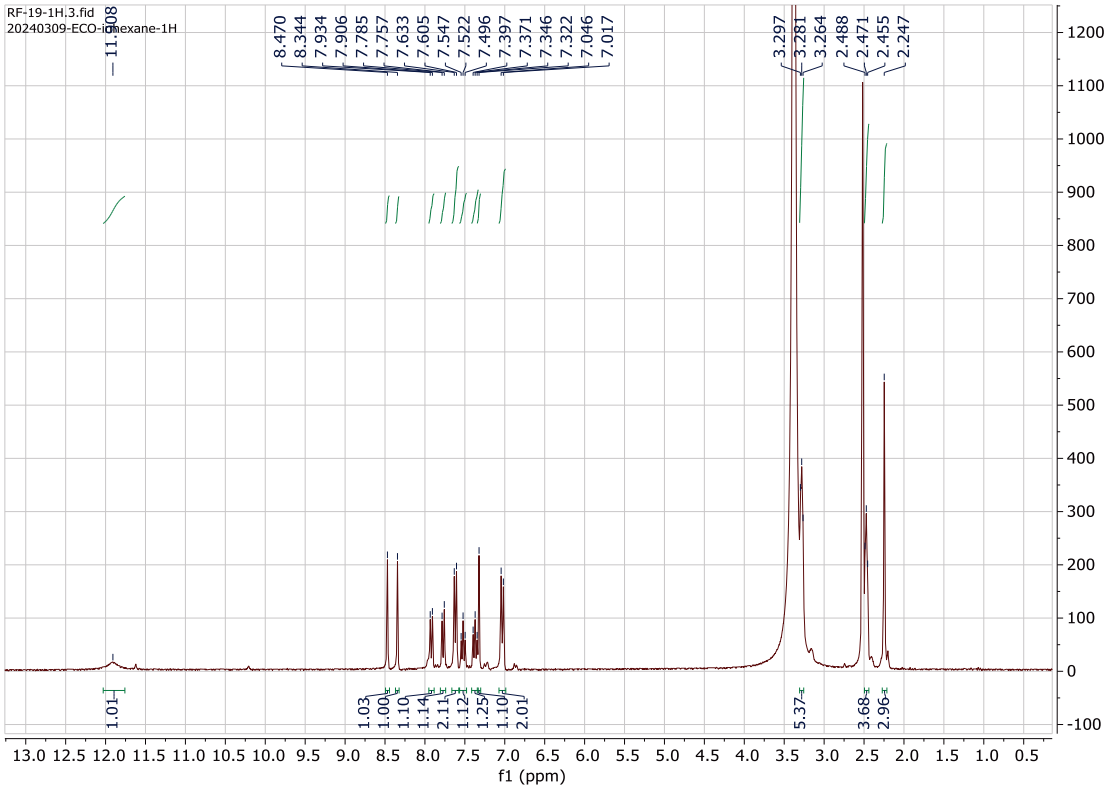

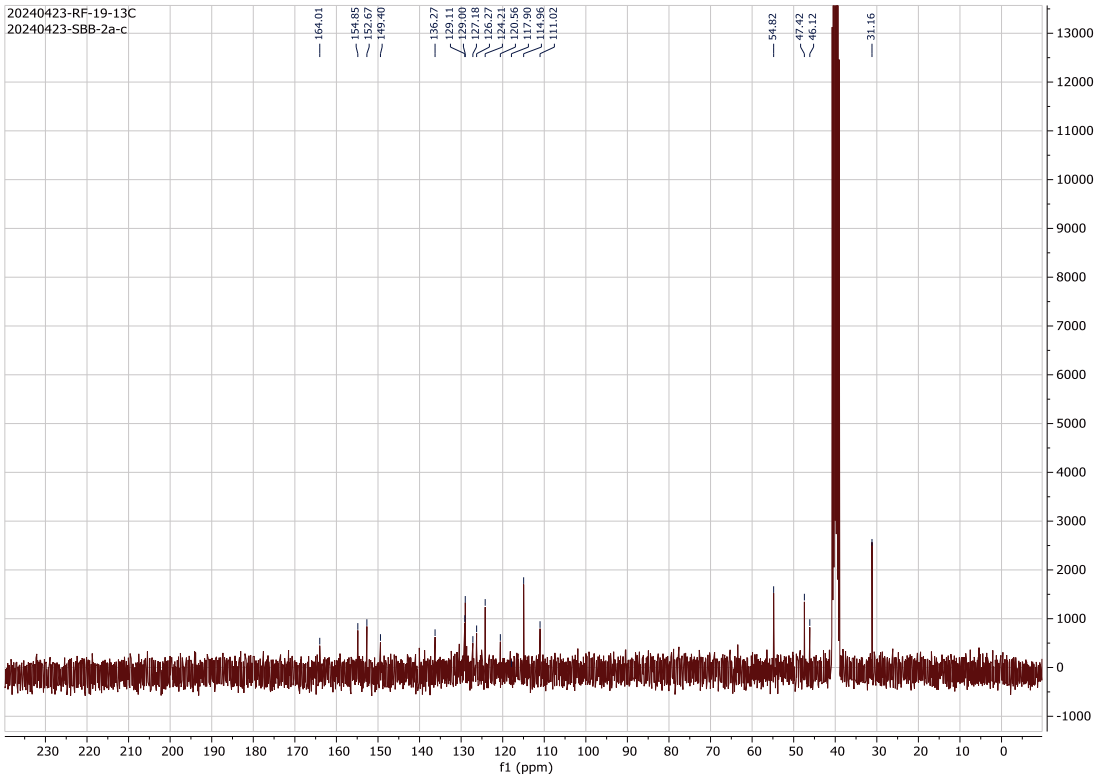

Data:RF-19
Comment:
Description:
Ionization Mode:ESI+
History:Average(MS[1] 0.14..0.21)

Acquired:5/15/2024 5:40:54 PM
Operator:AccuTOF
m/z Calibration File:20240515-TFANa_...
Created:5/16/2024 11:41:58 AM
Created by:AccuTOF

Charge number:1 Tolerance:400.00[ppm], 400.00 .. 400.... Unsaturation Number:-300.5 .. 300.0 (...
Element:^{12}C:23 .. 23, ^{1}H:10 .. 25, ^{14}N:4 .. 4, ^{23}Na:0 .. 2, ^{16}O:2 .. 2

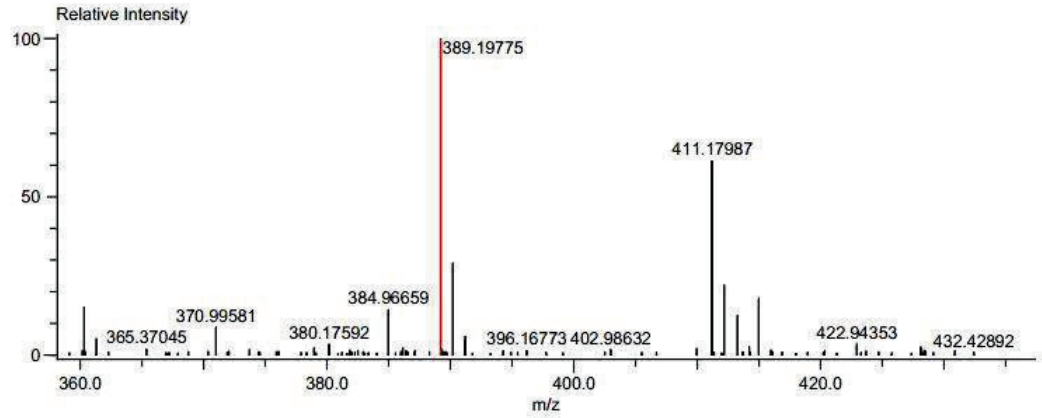

Mass	Intensity	Calc. Mass	Mass Difference [mDa]	Mass Difference [ppm]	Possible Formula
389.19775	8518.94	389.19775	0.00	0.00	$^{12}C_{23}{}^{1}H_{25}{}^{14}N_{4}{}^{16}O_{2}$

H^{1}, ^{13}CNMR & HRMS of Compound 20

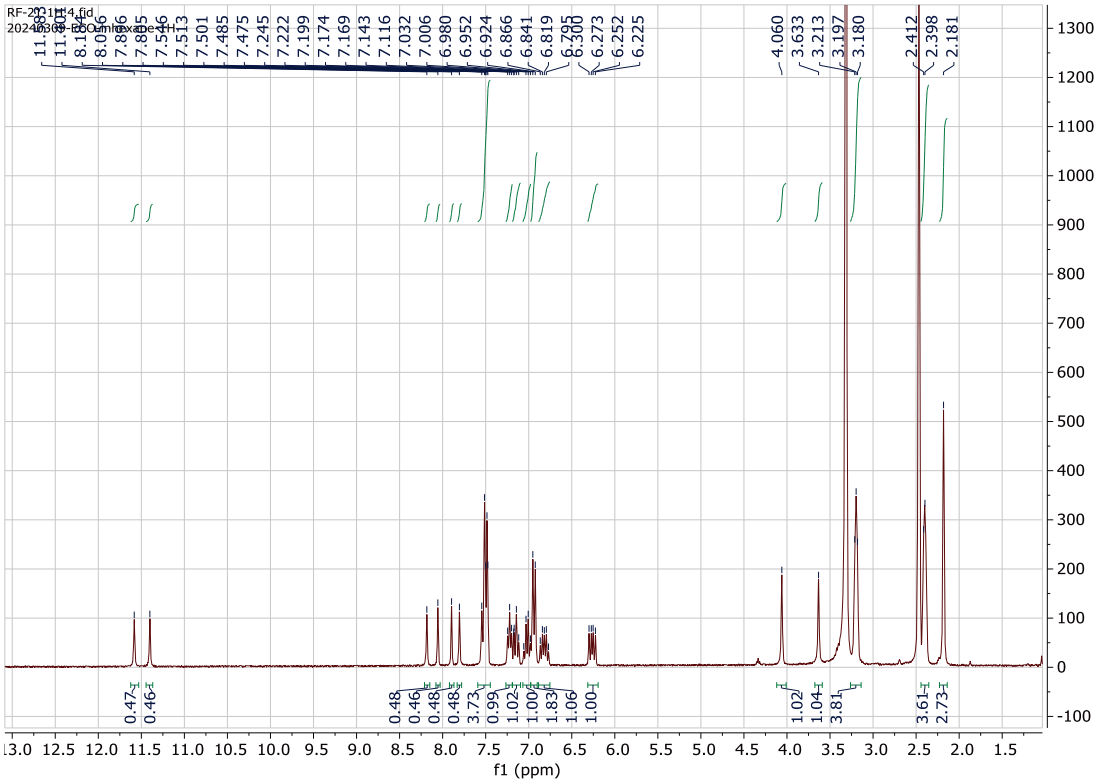

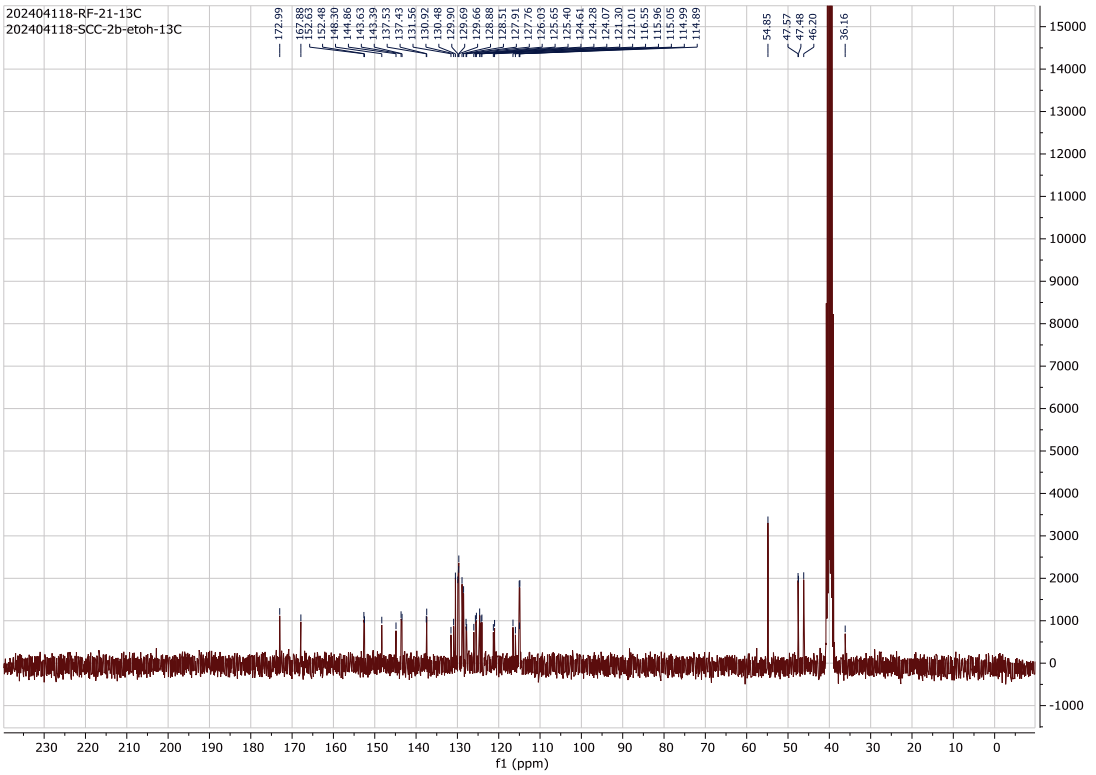

Data:RF-21
Comment:
Description:
Ionization Mode:ESI+
History:Average(MS[1] 0.14..0.18)

Acquired:5/15/2024 5:44:03 PM
Operator:AccuTOF
m/z Calibration File:20240515-TFANa_...
Created:5/16/2024 11:45:03 AM
Created by:AccuTOF

Charge number:1
Tolerance:400.00[ppm], 400.00 .. 400....
Unsaturation Number:-300.5 .. 300.0 (...
Element:^{12}C:26 .. 26, ^{1}H:10 .. 28, ^{35}Cl:2 .. 2, ^{14}N:5 .. 5, ^{23}Na:0 .. 2, ^{16}O:1 .. 1

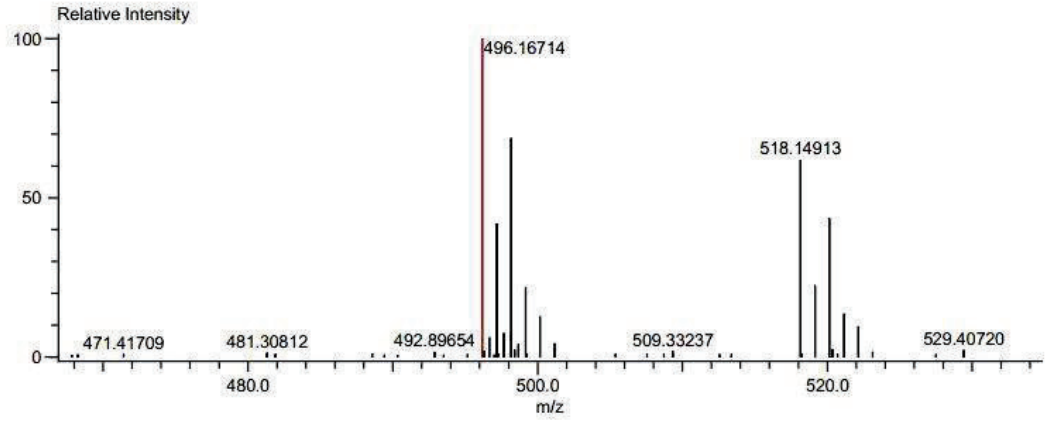

Mass	Intensity	Calc. Mass	Mass Difference [mDa]	Mass Difference [ppm]	Possible Formula
496.16714	16647.66	496.16709	0.05	0.11	$^{12}C_{26}{}^{1}H_{28}{}^{35}Cl_{2}{}^{14}N_{5}{}^{16}O_{1}$

H[1], [13]CNMR & HRMS of Compound 21

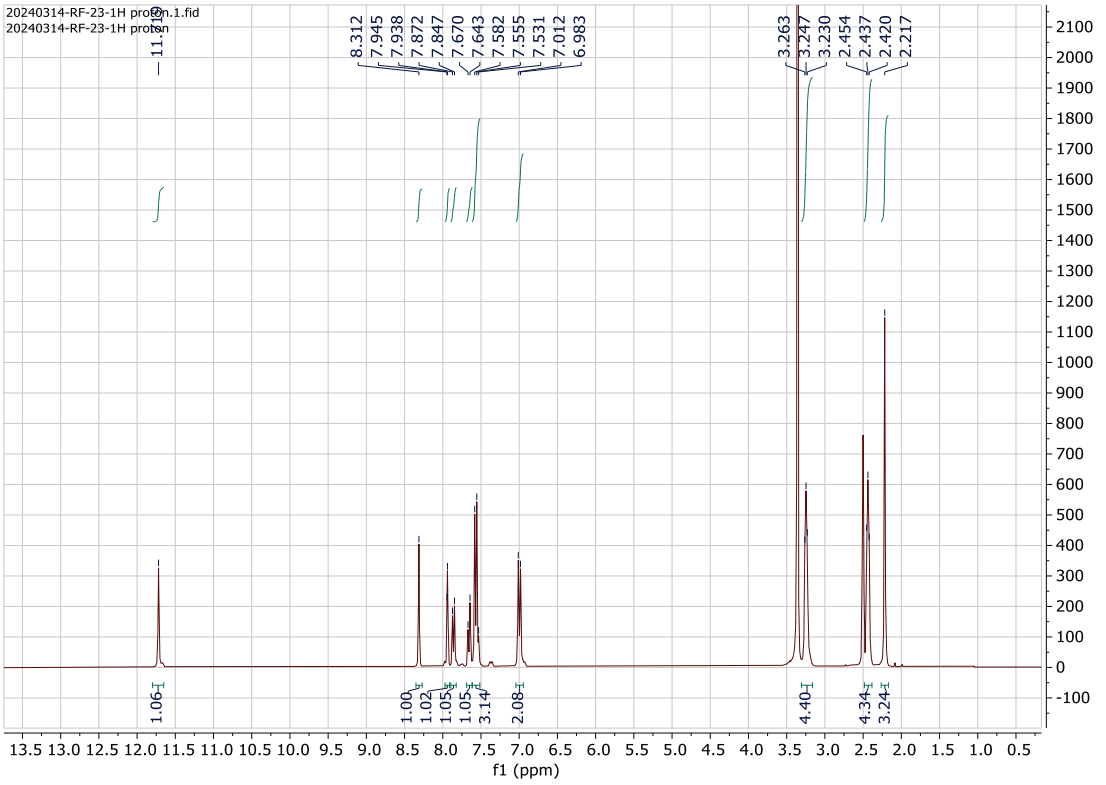

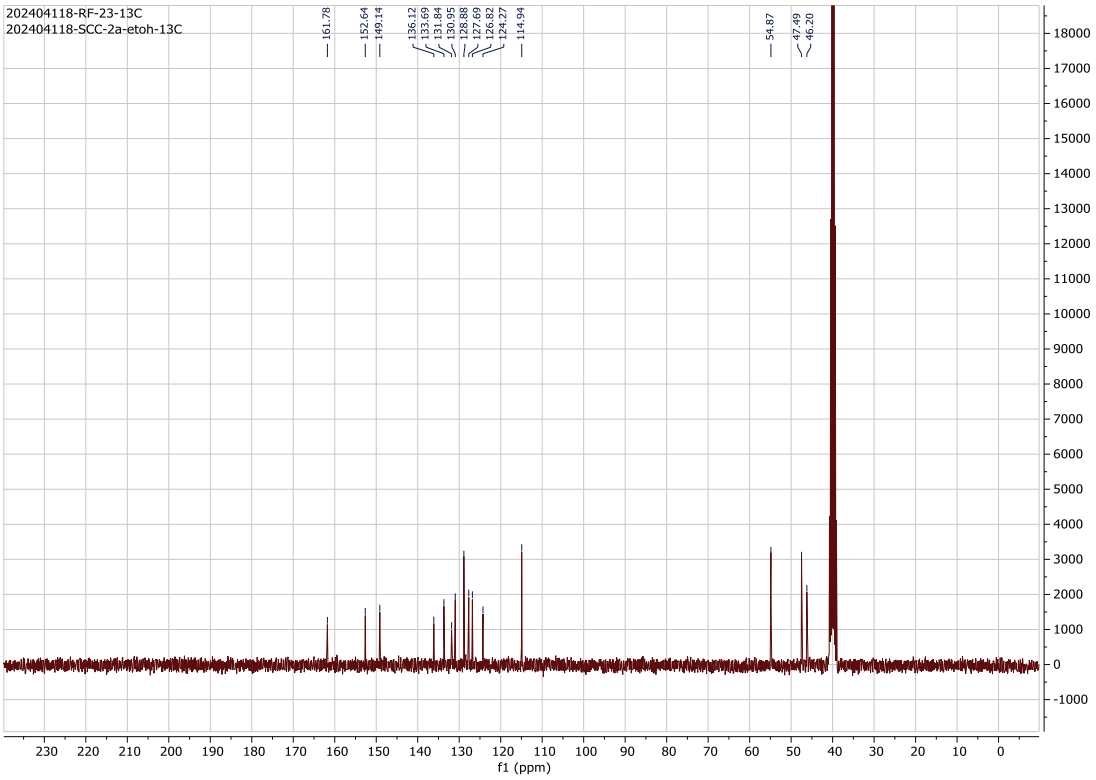

Data:RF-23
Comment:
Description:
Ionization Mode:ESI+
History:Average(MS[1] 0.34..0.39)

Acquired:5/15/2024 5:47:13 PM
Operator:AccuTOF
m/z Calibration File:20240515-TFANa_...
Created:5/16/2024 11:46:29 AM
Created by:AccuTOF

Charge number:1
Tolerance:400.00[ppm], 400.00 .. 400....
Unsaturation Number:-300.5 .. 300.0 (...
Element:^{12}C:19 .. 19, ^{1}H:10 .. 22, ^{35}Cl:1 .. 1, ^{14}N:4 .. 4, ^{23}Na:0 .. 2, ^{16}O:1 .. 1

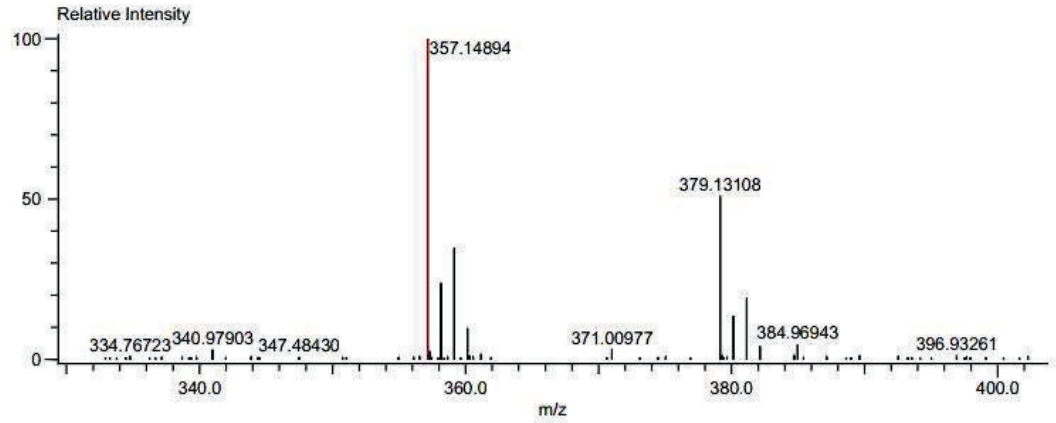

Mass	Intensity	Calc. Mass	Mass Difference [mDa]	Mass Difference [ppm]	Possible Formula
357.14894	20914.89	357.14821	0.72	2.02	$^{12}C_{19}{}^{1}H_{22}{}^{35}Cl_{1}{}^{14}N_{4}{}^{16}O_{1}$

H[1], [13]CNMR & HRMS of Compound 22

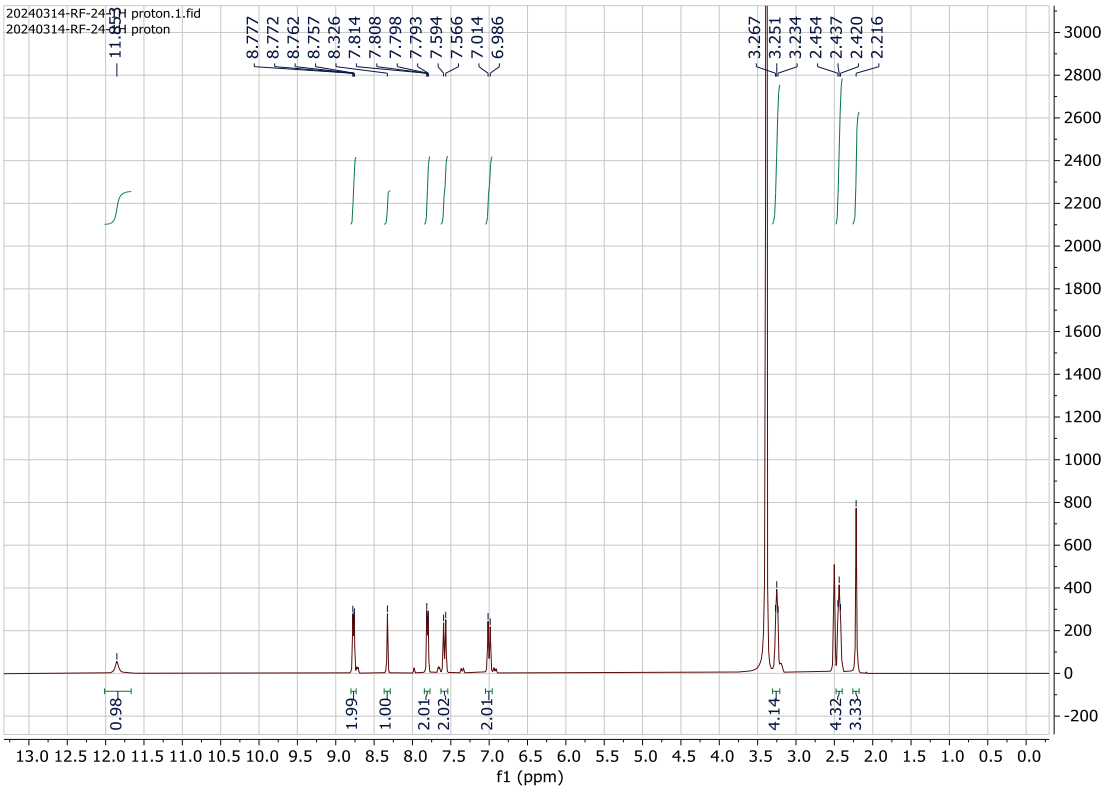

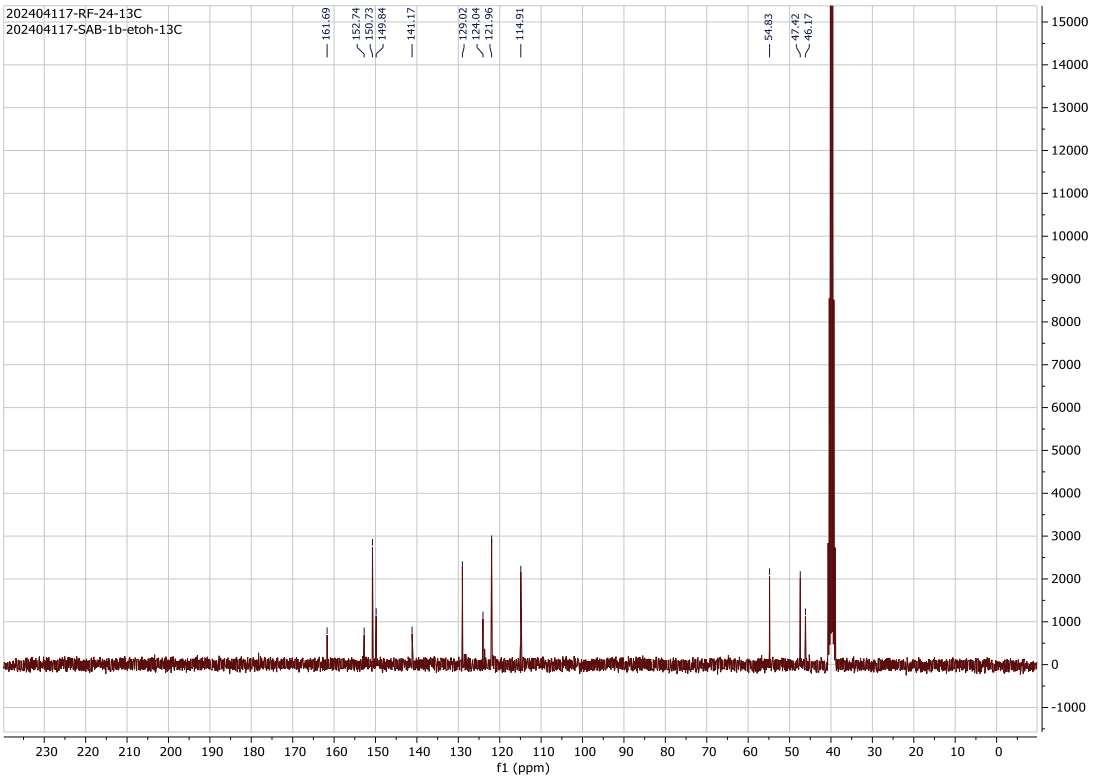

Data:RF-24
Comment:
Description:
Ionization Mode:ESI+
History:Average(MS[1] 0.12..0.17)

Acquired:5/15/2024 5:50:25 PM
Operator:AccuTOF
m/z Calibration File:20240515-TFANa_...
Created:5/16/2024 11:48:22 AM
Created by:AccuTOF

Charge number:1
Tolerance:400.00[ppm], 400.00 .. 400....
Unsaturation Number:-300.5 .. 300.0 (...
Element:^{12}C:18 .. 18, ^{1}H:10 .. 22, ^{14}N:5 .. 5, ^{23}Na:0 .. 2, ^{16}O:1 .. 1

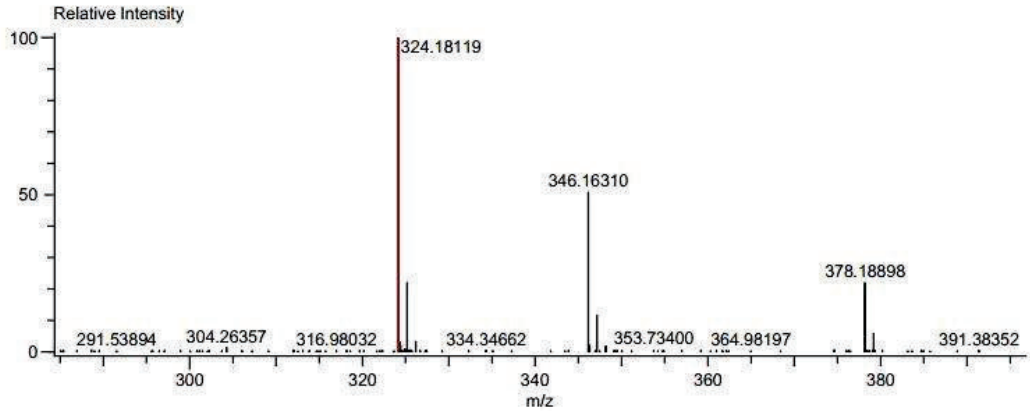

Mass	Intensity	Calc. Mass	Mass Difference [mDa]	Mass Difference [ppm]	Possible Formula
324.18119	41019.83	324.18243	-1.25	-3.85	$^{12}C_{18}{}^{1}H_{22}{}^{14}N_{5}{}^{16}O_{1}$

H[1], [13]CNMR & HRMS of Compound 23

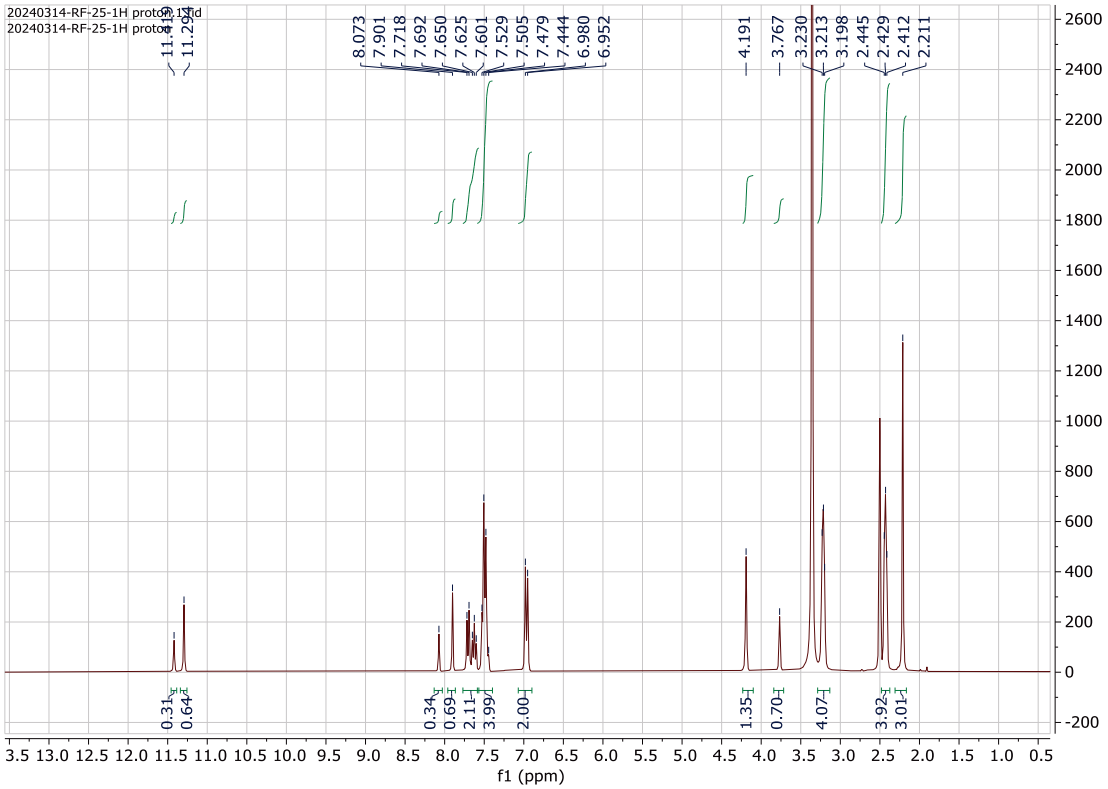

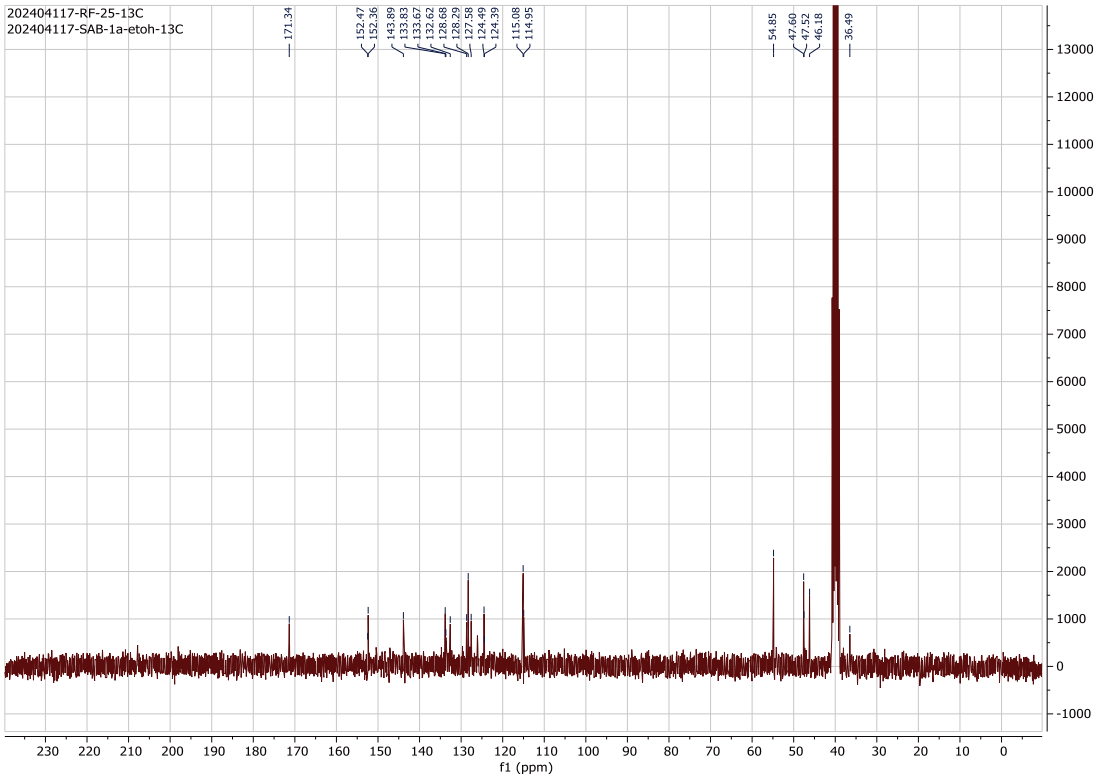

Data:RF-25
Comment:
Description:
Ionization Mode:ESI+
History:Average(MS[1] 0.16..0.19)

Acquired:5/15/2024 5:53:31 PM
Operator:AccuTOF
m/z Calibration File:20240515-TFANa_...
Created:5/16/2024 11:49:46 AM
Created by:AccuTOF

Charge number:1 Tolerance:400.00[ppm], 400.00 .. 400.... Unsaturation Number:-300.5 .. 300.0 (...
Element:^{12}C:21 .. 21, ^{1}H:10 .. 24, ^{19}F:3 .. 3, ^{14}N:4 .. 4, ^{23}Na:0 .. 2, ^{16}O:1 .. 1

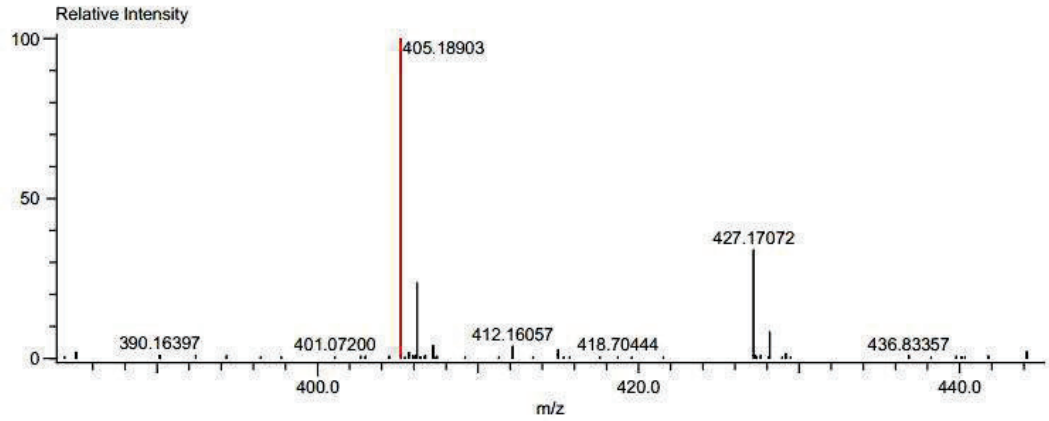

Mass	Intensity	Calc. Mass	Mass Difference [mDa]	Mass Difference [ppm]	Possible Formula
405.18903	44544.06	405.19022	-1.19	-2.93	$^{12}C_{21}{}^{1}H_{24}{}^{19}F_{3}{}^{14}N_{4}{}^{16}O_{1}$

Molecular docking studies

The structure of compounds was built using ChemDraw Ultra 12.0 software package. The stable configuration of ligands was obtained by minimizing energy via the MM2 level, utilizing the Chem3D Pro 12.0. A known protein database bank (https://www.rcsb.org/) was used to retrieve 3D-crystal structures of proteins with PDB IDs: 3A4A and 1B2Y. The binding interactions were analyzed using the Discovery Studio visualizer software (http://accelrys.com).

The protein and ligand preparation, grid generation, and docking were executed using a molecular modelling tool, AutoDockTools 1.5.6 software [1]. Target proteins were pre-processed to remove all water molecules, ions, and co-crystallized ligands as they may interfere with docking. Further optimization was achieved by adding all hydrogen atoms, and assigning partial charges- Kollman charges followed by merging non-polar hydrogen atoms. And saved the prepared protein structure in PDBQT format. The ligand preparation was achieved by adding the Gasteiger charges followed by merging all non-polar hydrogen atoms and then saving the ligand in PDBQT format, which is required by AutoDock Vina. The ligand was set up for docking with the help of AutoDockTools (ADT; Version 1.5.6) to define the torsional degrees of freedom to be considered during the docking process and all acyclic dihedral angles in the ligand were allowed to rotate freely. The docking was executed by means of the AutoDock Vina program using a configuration file. After docking, the pose with the least binding energy was selected as the best-docked ligand with the corresponding receptor using the PyMOL software and; the ligand-protein complex was saved in PDB format. Further, 2D and 3D ligand-receptor interactions were analyzed using Discovery Studio visualizer software.

The docking study used α-glucosidase and α-amylase target proteins with PDB Id: 3A4A and 1B2Y. Target 3A4A is a crystal structure of isomaltase derived from Saccharomyces cerevisiae (resolution: 1.60Å), with ≈84% similarity to α-glucosidase from S. cerevisiae. The receptor 1B2Y is a crystal structure of human pancreatic alpha-amylase complexed with the carbohydrate inhibitor acarbose. The targeted/site-specific docking was executed. Docking study was achieved with identical coordinates of co-crystalized ligand with proteins. For 3A4A, the grid box coordinates (x, y, z) 21.51, -7.70, and 23.55 were used along with grid size (x, y, z) of 40, 40, 40. And, for protein 1B2Y, the grid box was positioned with coordinates (x, y, z) 18.90, 5.79, 47.0 along with grid size (x, y, z) of 50, 50, 50.

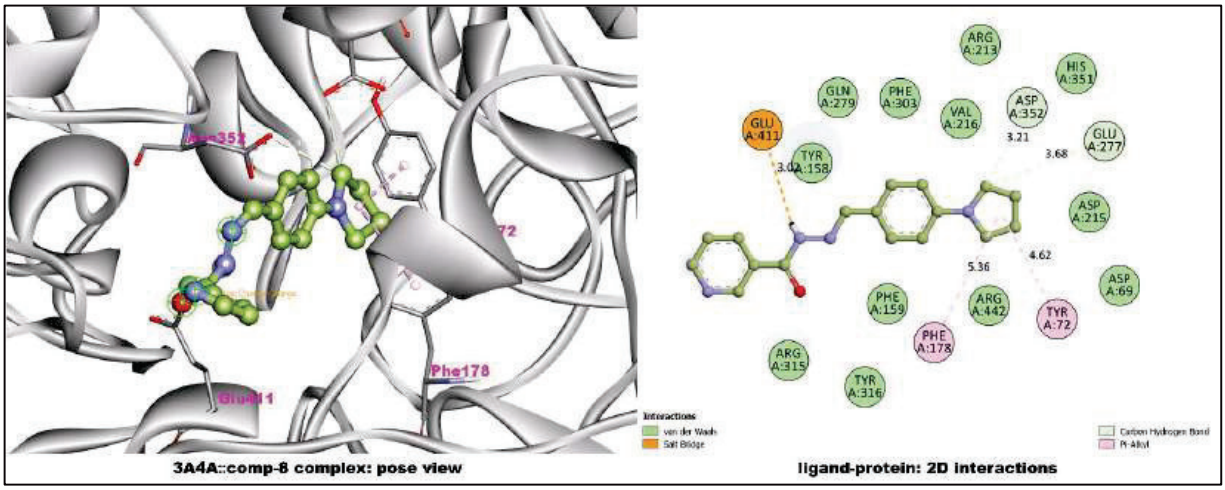

Fig-1: Two & three-dimensional docking interactions of compound 8 with protein 3A4A.

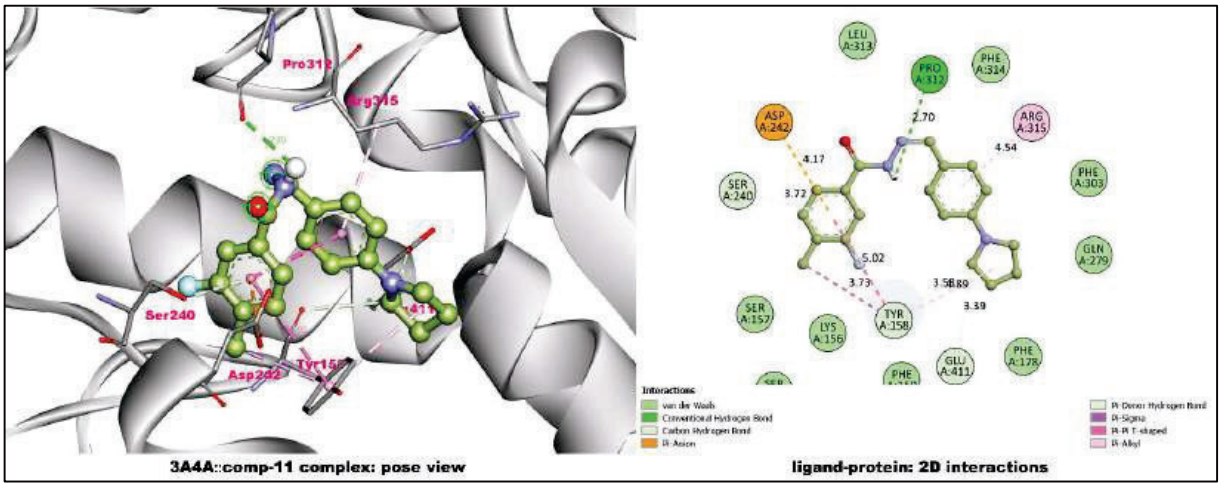

Fig-2: Two & three-dimensional docking interactions of compound 11 with protein 3A4A.

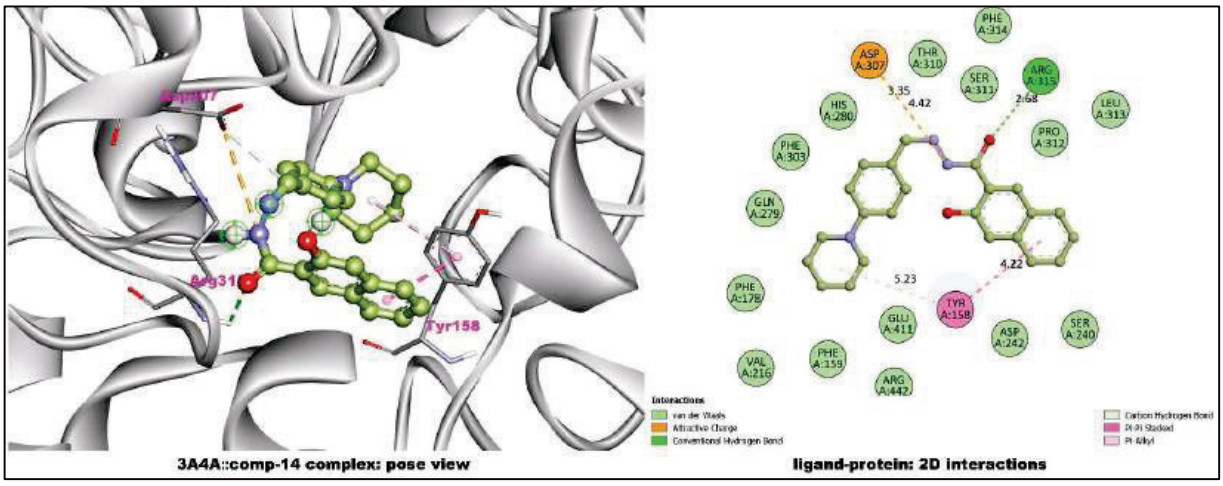

Fig-3: Two & three-dimensional docking interactions of compound 14 with protein 3A4A.

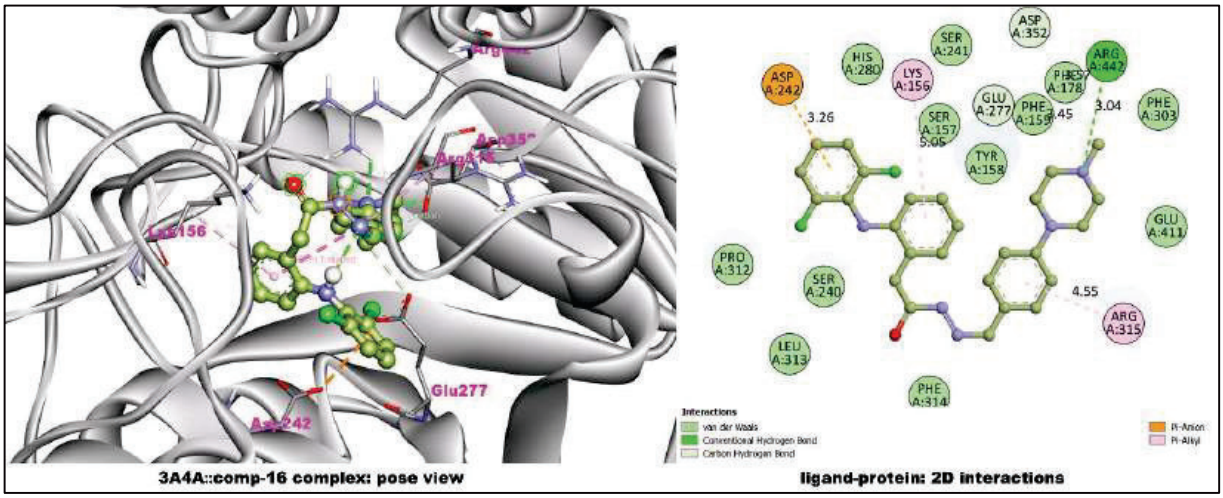

Fig-4: Two & three-dimensional docking interactions of compound 16 with protein 3A4A.

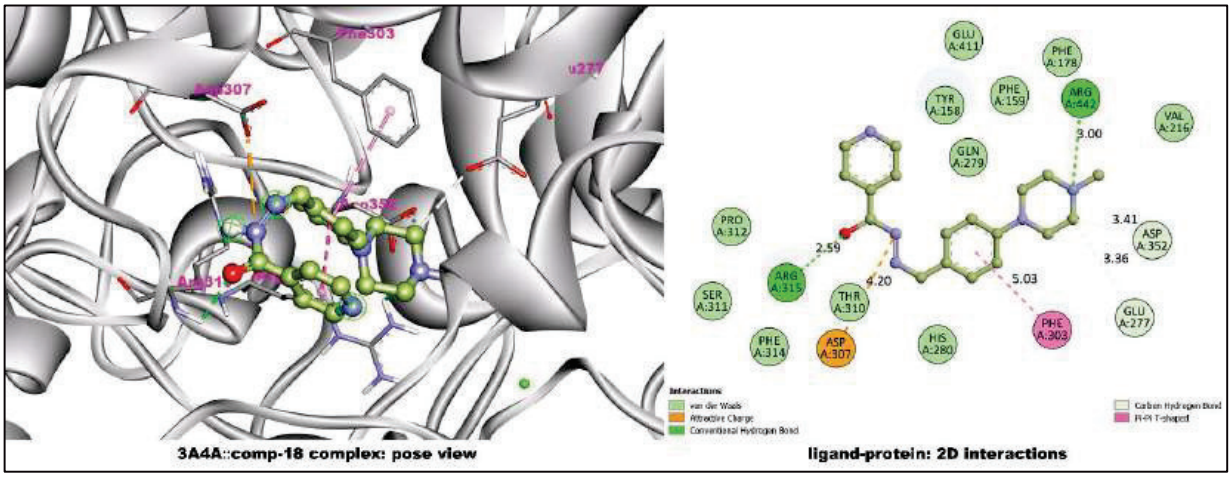

Fig-5: Two & three-dimensional docking interactions of compound 18 with protein 3A4A.

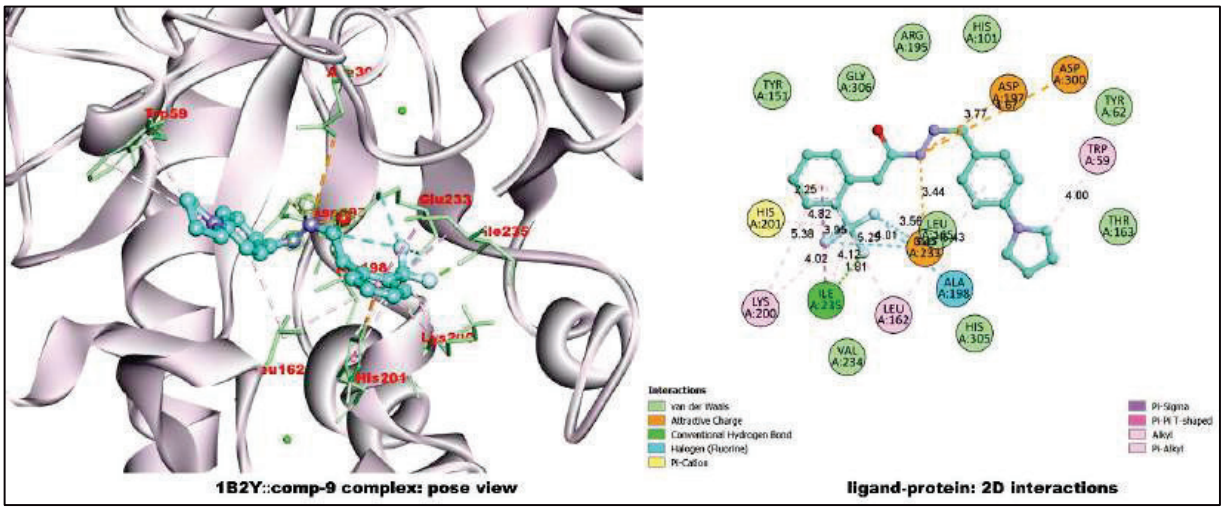

Fig-6: Two & three-dimensional docking interactions of compound 9 with protein 1B2Y.